8-1-2012

Photobiomodulation in Inherited Retinal Degeneration

Sandeep Gopalakrishnan
University of Wisconsin-Milwaukee

Recommended Citation

Gopalakrishnan, Sandeep, "Photobiomodulation in Inherited Retinal Degeneration" (2012). *Theses and Dissertations*. 4.
https://dc.uwm.edu/etd/4

PHOTOBIOMODULATION IN INHERITED RETINAL DEGENERATION

by

Sandeep Gopalakrishnan

A Dissertation Submitted in
Partial Fulfillment of the
Requirements of the Degree of

Doctor of Philosophy
in Health Sciences
at
The University of Wisconsin-Milwaukee
August 2012

ABSTRACT

PHOTOBIOMODULATION IN INHERITED RETINAL DEGENERATION

by

Sandeep Gopalakrishnan

The University of Wisconsin-Milwaukee, 2012
Under the Supervision of Professor Janis T. Eells

The retinal degenerative disease, retinitis pigmentosa (RP), is the most common cause of inherited blindness in the developed world and is caused by the progressive degeneration of rod photoreceptor cells preceding cone degeneration. Mitochondrial dysfunction and oxidative stress have been shown to play a significant role in the pathogenesis of RP and other retinal degenerative diseases. A growing body of evidence indicates that exposure of tissue to low energy photon irradiation in the far-red to near-infrared (NIR) range of the spectrum, (photobiomodulation or PBM) acts on mitochondria-mediated signaling pathways to attenuate oxidative stress and prevent cell death. These studies tested the hypothesis that PBM acts in the retina to promote mitochondrial integrity and function, prevent photoreceptor cell death and preserve retinal function in an established rodent model of retinitis pigmentosa, the P23H rhodopsin transgenic rat. Retinal function, structural integrity, surviving photoreceptors and the mitochondrial redox state were assessed using electroretinography, spectral domain optical coherence tomography, histomorphometry and cryofluorescence redox imaging. PBM did not alter the structural and functional characteristics of retina in a non-dystrophic animal strongly supporting the safety of PBM. Establishing the safety of PBM is essential to advance the therapy to clinical use. 830 nm PBM exerted a robust retinoprotective effect compared to 670 nm

PBM in the P23H transgenic rat model. 830 nm PBM during the critical period of photoreceptor degeneration in P23H transgenic rat profoundly attenuated retinal degeneration resulting in the preservation of retinal function; retinal morphology and retinal metabolic state in comparison to the sham-treated group. An *in vivo* longitudinal study corroborated the structural preservation observed in the cross-sectional study. These findings provide evidence supporting the therapeutic utility of PBM in the treatment of retinal degenerative disease. They also further our understanding of the mechanism of action of PBM by showing that it improves mitochondrial function in the retinae of RP animals. By exploiting, the cells own mechanism of self-repair, PBM has the potential for translating into clinical practice as an innovative, non-invasive stand-alone or adjunct therapy for the prevention and treatment of retinal diseases.

To my wonderful parents, lovely wife and to my little angel

Acknowledgements

Over the past seven years I had wonderful time at the graduate school because of the support and encouragement I received from a great number of individuals. I would like to thank:

- Professor Janis Eells for her unconditional support and mentoring that cultivated scientific curiosity in me and gave the strength to pursue the dream of becoming a scientist.
- My Dissertation Committee of Professors Jeri Ann Lyons, Joseph Carroll, Thomas B. Connor, Jr., Dean T. Nardelli, Wendy E. Huddleston and Mahsa Ranji for the guidance and support.
- Dean Chukuka Enwemeka and Associate Dean Paula Rhyner.
- Other UWM faculty members that I have interacted and benefitted from including Professors Mary Pat Kunert, Anthony Azenabor, Robert Burlage, Erika Sanders, Trinh Hanh, Rachel Schiffman, Ann Snyder, Cindy Brown and Kim Latwick.
- My fellow lab members-Heather Schmitt, Zahra Al Rumaih, Betsy Abroe and my past and current classmates and colleagues-Goeran Fiedler, Kamaldeen Muili, Violet Bumah, Rob Wilson, Sheerin Shabistan, Jason Rakita, David Gallegos, Priyanka Kshatriya, Daniela Mason, Vrushali Agashe, Erin Koester and Emily Siebers.
- Members of the Carroll Lab at MCW- Adam Dubis, Phyllis Summerfelt, Jungate Rha, Pooja Godara, Robert Cooper and Michelle Stoehr.
- Members of the Biophotonics Lab at UWM- Sepideh Maleki, Zahra Ghanian and Reyhaneh Sepehr.

- Dr. David Amrani for sharing his valuable time and ideas.
- Members of the Animal Resource Center at UWM- Berry Forman, Jenny Nemke and Ashley Fritsch.
- My family, friends and all well-wishers for all their love and support

TABLE OF CONTENTS

CHAPTER 1 1

LITERATURE REVIEW 1

EVOLUTION OF PHOTORECEPTORS 4

ROD OUTER SEGMENT AND RHODOPSIN 5

PHOTOTRANSDUCTION 8

High metabolic demand of photoreceptors 12

INHERITED RETINAL DEGENERATIONS 15

Retinitis Pigmentosa (RP) 15

Causal genes of Retinitis Pigmentosa 17

Therapeutic Approaches for the Treatment of RP 20

Animal Models of Retinitis Pigmentosa 22

Mitochondrial dysfunction, oxidative stress and apoptosis in retinal degenerations 24

NEAR INFRARED (NIR) PHOTOBIOMODULATION 27

The mechanism of near-infrared photobiomodulation 29

Mitochondrial retrograde signaling in NIR photobiomodulation 32

CHAPTER 2 39

PRELIMINARY DATA AND SPECIFIC AIMS 39

PRELIMINARY DATA 40

NIR PBM attenuates the loss of photoreceptors in the P23H rat during the ‘critical period’ of photoreceptor degeneration. 40

Photobiomodulation increases cytochrome oxidase concentrations in the P23H retina. 42

Photobiomodulation up-regulates cytoprotective enzymes in the P23H retina. 44

SPECIFIC AIMS, RATIONALE AND DESIGN 45

Specific Aim 1: To investigate the effect of NIR photobiomodulation in a non-dystrophic (SD) animal. 45

Specific Aim 2: To determine if NIR photobiomodulation can protect photoreceptors against damage induced by the P23H transgene and compare the efficacy of 670 nm vs. 830 nm PBM using three different treatment protocols.... 45

Specific Aim 3: To investigate the cellular changes underlying the protection provided by NIR photobiomodulation. 47

CHAPTER 3 48

MATERIALS AND METHODS 48

ANIMAL MODEL 49

NIR LIGHT EMITTING DIODE ARRAY AND TREATMENT PROTOCOL...... 50

ASSESMENT OF STATUS OF RETINA 52

Full-Field Flash Electroretinography 53

Spectral Domain Optical Coherence Tomography (SD-OCT) imaging 59

Quantitative Morphometric Analysis: Measurement of ONL thickness 64

Measurement of Surviving photoreceptors 64

Retinal metabolic state was assessed by Cryo Optical Imaging 65

Statistical Analysis 69

CHAPTER 4 70

EFFECT OF NIR PHOTOBIOMODULATION IN NON -DYSTROPHIC ANIMAL MODEL 70

CHAPTER 5 81

MITOCHONDRIAL REDOX IMAGING 81

Introduction 82

Materials and Methods 85

Statistical evaluation of data 89

Results 90

Discussion and conclusion 97

References 100

CHAPTER 6 106

COMPARISON OF 670 nm vs. 830nm PHOTOBIOMODUALTION USING THREE TREATMENT PARADIGMS 106

CHAPTER 7 116

PHOTOBIOMODUALATION ATTENUATES RETINAL DEGENERATION IN THE P23H RAT MODEL OF RETINITIS PIGMENTOSA 116

Introduction 117

Materials and Methods 120

Data Analysis 126

Results 126

Discussion 138

References 141

CHAPTER 8 148

DISCUSSION AND CONCLUSIONS 148

BIBLIOGRAPHY 154

APPENDIX 170

Conference Proceedings 170

Posters 173

Curriculum Vitae 176

LIST OF FIGURES

Figure 1 Both rod (A) and cone (B) photoreceptor consist of four distinct regions: an outer segment (OS) which contains stacks of bilipid membranous discs embedded with photopigments which are responsible for photoabsorption and initiation of phototransduction cascade, an inner segment that contains biosynthetic and metabolic functions as well as optical functions which by the phenomenon of total internal reflection confines the photons within the receptor (Hoang, Linsenmeier et al. 2002), a cilium connecting both the inner and the outer segments, and a synaptic terminal which signals to the inner retina by neurotransmitters. (Reproduced from Neuroscience. 2nd edition. Purves D, Augustine GJ, Fitzpatrick D, et al., editors. Sunderland (MA): Sinauer Associates; 2001)..3

Figure 2 Development of anatomical structures of eye from the optic vesicle. (Reproduced from Neuroscience. 2nd edition. Purves D, Augustine GJ, Fitzpatrick D, et al., editors. Sunderland (MA): Sinauer Associates; 2001)..4

Figure 3 The outer segment of the photoreceptor is a modified cilium containing numerous discs which has embedded light sensitive visual pigments. (Reproduced from Steinberg, Fisher et al. 1980)..6

Figure 4 Secondary structure of bovine Rho. The NH_2-terminal tail and extracellular domain point toward the top and the COOH-terminal tail and cytoplasmic domain is toward the bottom. Letter codes indicate amino acid residues. The structure has 7 transmembrane α-helical segments (H1 to H7). Inset: structure of the chromophore -11-*cis*- retinal. (Reproduced from Menon, Han et al. 2001). 7

Figure 5 A molecular ribbon diagram of inactive and active views of Rho from the 43 Å crystal structure coordinate. Unlike other GPCRs Rho binds to 11-*cis* retinal (ligand) covalently both in inactive as well as photo activated state-11-cis dark form (yellow) to all-trans light (magenta). (Reproduced from Bourne and Meng 2000) 8

Figure 6 Schematic representation of phototransduction cascade in rod photoreceptors. (Reproduced from Burns and Arshavsky 2005) 10

Figure 7 Schematic representation of information flow in the retina. Signals can pass both vertically and laterally. (Reproduced from Lagnado 2000) 11

Figure 8 Metabolism in photoreceptors. The high metabolic demand in photoreceptors is met by adequate supply of glucose and oxygen by the choroidal vessels through the RPE cells. Oxidative phosphorylation in the mitochondria provides photoreceptors with adequate amounts of ATP for the high energy demanding phototransduction process. Increased ROS generated as a result of mitochondrial phosphorylation is removed by the antioxidant defense mechanisms involving enzymatic (superoxide dismutase, glutathione peroxidase, and catalase) and non-enzymatic (natural antioxidant glutathione) endogenous systems. The constant recycling of the photoreceptor OS and recycling of 11-*trans*-retinal in the RPE requires rapid macromolecular synthesis and active transport mechanism. Studies have shown that activated insulin receptors can up regulate the growth factor signaling that ends up regulating glycolysis through stimulation of mTOR phosphorylation. (Reproduced from Punzo, Xiong et al. 2012). 14

Figure 9 Fundus image of a normal (left) vs. RP eye (right). (Reproduced from Farrar, Kenna et al. 2002) 16

Figure 10 Classification of rod dominated retinal and vitreoretinal diseases including RP and casual genes. (Reproduced from Berger, Kloeckener-Gruissem et al. 2010). 18

Figure 11 Loss of retinal architecture in RP demonstrated by high resolution microscopy.(Reproduced from http://www.nei.nih.gov/eyeonnei/snapshot/archive/ 0909.asp) ... 19

Figure 12 Schematic representation of photoreceptor loss in Retinitis Pigmentosa. Normal Retina (A), when rods start to die (B), extensive loss of rod photoreceptor as the disease progresses (C) and eventually retina will lose all the rod photoreceptors which results in reduced nutrient flow, which leads to the death of remaining photoreceptors and the loss of retinal architecture. (Reproduced from Punzo, Xiong et al. 2012). 20

Figure 13 Hypothesized cell signaling events following photoabsorption/photoexcitation of cytochrome *c* oxidase by NIR photons 31

Figure 14 Activity of Neuronal Cytochrome Oxidase and Cellular ATP Correlates with Cytochrome Oxidase Action Spectrum. Reproduced from (Wong-Riley, Liang et al. 2005) 31

Figure 15 Putative mitochondrial retrograde signaling and other associated cellular events following photoabsorption by cytochrome *c* oxidase. (Reproduced from Karu 2008). 33

Figure 16 Comparison of degeneration rates of ONL in three different lines of P23H rhodopsin transgenic rat strains with control animal. (Reproduced and modified from http://www.ucsfeye.net/mlavailRDratmodels.shtml to highlight the ‘critical period’). 40

Figure 17 Photoreceptor cell death by apoptosis is demonstrated in P23H retina by TUNEL+ cells and following NIR PBM there is a significant reduction (greater than 70%) in the number of TUNEL+ cells in the ONL 41

Figure 18 A significant up regulation of cytochrome oxidase activity in the inner segments of photoreceptor cells following NIR PBM is demonstrated by density profiling ($n = 6$, $p < 0.001$) 43

Figure 19 NIR PBM upregulates mitochondrial form of superoxide dismutase, MnSOD, in the inner segments, which can protect the degenerating retina from oxidative damage. 44

Figure 20 LED arrays used for delivering NIR photons. WARP 75 LED Unit (Left); λ = 670 ± 20 nm; Surface Energy: 60mW/cm^2; Fluence ~5.4J /cm^2. 51

Figure 21 Exposure of animals to NIR photons. Animals were habituated to the restraint apparatus and handling from p5. Monochromatic LED source is placed directly over the animal's head at a distance of 2 cm exposing both eyes. 52

Figure 22 Animals were dark-adapted, anesthetized, pupils dilated and placed on a thermoregulated heating pad at 37°C during recordings. 55

Figure 23 Full-field ERGs were obtained in a Mini-Ganzfeld half-sphere bowl. Flash intensities are generated with white LEDs and duration of the each flash is test dependent. 55

Figure 24 A normal biphasic ERG waveform showing a-wave and b-wave amplitude and corresponding implicit times. Reproduced from www.webvision.med.utah.edu. The a-wave reflects the physiological activity in the photoreceptors of the outer retina and the b-wave corresponds to the electrical responses from the inner retinal layers including the ON bipolar cells and the Muller cells (Miller and Dowling 1970). 56

Figure 25 Comparison of a-wave and b-wave amplitude obtained from a normal subject (left) and from a patient with RP. Reproduced from www.webvision.med.utah.edu.................................. 56

Figure 26 Set up of an OCT system for retinal imaging. The light source is typically a broad band source and the light (λ~ 800nm) is split into half by a beam splitter and sent to a reference arm and the sample arm. The backscattered light is reflected back from the sample arm and reference arm combines forming an interference pattern. This spectrum is detected via a spectrometer placed as the detector and an algorithm is used to reconstruct an A –scan which represents the anatomical features of retina. Multiple A-scans are used to generate B-scan and multiple B-scans are used to generate 3D volume scans. (Reproduced and modified from Frohman, Fujimoto et al. 2008). 59

Figure 27 Aligning the AIM-RAS to achieve the “Magic Point” for aiming (Reproduced and modified from Bioptigen’s Guide to Small Animal Imaging: Optimizing Image Quality presentation by Joseph Vance)........ 60

Figure 28 Animal Imaging Mount and Rodent Alignment System with bite bar. The bite bar helps to reproduce alignment of the rodent eye and suppress motion artifacts from breathing. 61

Figure 29 Representative image (line scans 1000x80x1samplings) centered on the ONH, showing the segmentation lines for automated segmentation for Total Retinal Thickness. 100 pixels (px) are removed at the ONH manually to account for variable thickness in this region........ 62

Figure 30 Longitudinal Reflectivity Profile (LRP) and the corresponding individual retinal layers (Nerve Fiber Layer; NFL & Ganglion Cell Layer; GCL, Outer Plexiform Layer; OPL, Outer Nuclear Layer; ONL, Inner Segment/Outer Segment; IS/OS, Retinal Pigment Epithelium; RPE and Choroid) 63

Figure 31 Method used to generate spider plots for ONL thickness from averaged OCT scans... 63

Figure 32 (a) frozen eye and b) embedding frozen eye in customized mounting medium. 66

Figure 33 Schematic representation of a Cryoimager. This device sequentially slices the tissue, imaging the surface between each successive slice, in as many as 5 channels. The images are then displayed and saved to a computer, where they can be processed to create a 3-D rendering of the tissue. 68

Figure 34 shows the comparison of mean a-wave amplitude between SD normal control (■; n=8) and 830nm treated SD normal control (▲; n=8) groups. The a-wave represents the functional electrical activity recorded from the photoreceptors and reflects the general health of the photoreceptor layer of the retina. The main effect between groups were not statistically significant ($F_{(1,14)}$ = .627, p = .442) between groups at various flash intensities. Error bars: SEM. 72

Figure 35 shows the comparison of mean b-wave amplitude between SD normal control (■; n=8) and 830nm treated SD normal control (▲; n=8) groups. The b- wave represents the functional electrical activity post synaptic to photoreceptors and reflects the health of the inner layers of the retina. The main effect between groups were not statistically significant ($F_{(1,14)}$ = .122, p = .733) between groups at various flash intensities. Error bars: SEM. 73

Figure 36 shows the mean a-wave implicit time comparing SD normal control (■; n=8) and 830nm treated SD normal control (▲; n=8) groups. The a-wave implicit time represent s the time from flash onset to the trough of the a-wave. There was no significant difference ($F_{(1,14)}$ = 1.14 , p = .302) between groups at various flash intensities. Error bars: SEM 74

Figure 37 shows the mean b-wave implicit time comparing SD normal control (■; n=8) and 830nm treated SD normal control (▲; n=8) groups. The b-wave implicit time represents the time from flash onset to the peak of the b-wave. There was no significant difference ($F_{(1,14)}$ = 4 .12, p = .062) between groups at various flash intensities. Error bars: SEM 74

Figure 38 shows the comparison of mean a-wave amplitude between SD normal control (■; n=6) and 670 nm treated SD normal control (▲; n=8) groups. The a-wave represents the functional electrical activity recorded from the photoreceptors and reflects the general health of the photoreceptor layer of the retina. The main effect between groups were not statistically significant ($F_{(1,10)}$ = .039, p = .848) between groups at various flash intensities. Error bars: SEM 76

Figure 39 shows the comparison of mean b-wave amplitude between SD normal control (■; n=8) and 670 nm treated SD normal control (▲; n=6) groups. The b- wave represents the functional electrical activity post synaptic to photoreceptors and reflects the health of the inner layers of the retina. The main effect between groups were not statistically significant ($F_{(1,12)} = .147$, $p = .708$) between groups at various flash intensities. Error bars: SEM. 77

Figure 40 shows the mean a-wave implicit tine comparing SD normal control (■; n=8) and 670 nm treated SD normal control (▲; n=8) groups. The a-wave implicit time represent s the time from flash onset to the trough of the a-wave. The main effect between groups were not statistically significant ($F_{(1,14)} = .103.$, $p = .752$) at various flash intensities. Error bars: SEM. ... 78

Figure 41 shows the mean b-wave implicit time comparing SD normal control (■; n=8) and 670 nm treated SD normal control (▲; n=8) groups. The b-wave implicit time represents the time from flash onset to the peak of the b-wave. There was no significant difference ($F_{(1,14)} = 2.31$, $p = .151$) between groups at various flash intensities. Error bars: SEM 78

Figure 42 shows the average total retinal thickness (upper panel) generated from SD-OCT linear scans (n=4) between non-dystrophic SD animals and 670 nm treated SD animals. Lower panel shows the representative linear scans at the same location on the retina (ONH used as the landmark) comparing non-dystrophic SD animal and 670 nm treated SD animal and there was no significant difference in the retinal morphology or structural integrity of retina following 670 nm NIR-PBM. Error bars: SEM 80

Figure 43 Representative max projected NADH, FAD and RR images for eyes from normal and disease groups. 92

Figure 44 A representative histogram for eyes from normal and diseased groups comparing Redox Ratio intensity between P23H transgenic retina vs. SD Normal retina. Oxidative stress causes more oxidation in the NADH redox histogram 93

Figure 45 Bar graph plot comparing the mean values of the histograms of max projected images from SD and P23H transgenic rat eyes. The results show a significant difference between normal and diseased eyes (***$p<.001$). Error bars: SEM; p values were obtained from Unpaired Student's t- test. 94

Figure 46 A) The mean a-wave amplitude assessed by the scotopic intensity series protocol comparing P23H transgenic (■; n=8) and SD normal control (▲; n=8) groups B) The mean b-wave amplitude comparing P23H transgenic (■; n=6) and SD normal control (▲; n=6) groups. P23H transgene caused a significant decrease in both a-wave ($F_{(1, 14)} = 161.0$, $p < .001$; Fig. 46A) and b-wave ($F_{(1, 10)} = 35.4$, $p < .001$; Fig. 46B) amplitudes at all flash intensities compared to the normal SD controls. Error bars: SEM. 95

Figure 47 shows the a-wave implicit time as well as b- wave implicit time assessed at 100mcd.s/m2. The implicit times reflecting peak latencies of a- and b- waves were significantly (**$p<.01$) different between P23H transgenic and normal SD retina. Error bars: SEM; p values were obtained from Unpaired Student's t- test. 96

Figure 48 compares the functional and structural changes in P23H transgenic retina following NIR PBM by 830 and 670 nm photons during the critical period of photoreceptor degeneration (p10-p25). Panel A compares the a-wave amplitude and panel B compares the b-wave amplitude between P23H (■) and 830 nm treated group (▲, left), P23H (■) and 670 nm treated group (▲, right) respectively. The main effect for a-wave and b-wave between the groups are significantly different [a-wave: ($F_{(1,14)} = 16.32$, $p < .001$); b-wave: ($F_{(1,22)} = 23.57$, $p < .001$)] in 830 nm treated group when compared to that of the 670 nm treated group [a-wave: ($F_{(1,22)} = .396$, $p = .536$); b-wave: ($F_{(1,11)} = 2.11$, $p = .173$)]. Panel C compares the implicit time for a-wave and b-wave at 100mcd.s/m^2. 830 nm treatment caused a significant difference in a-wave ($p<.01$) and b-wave ($p<.05$) when compared to the 670 nm group even though a trend was observed in the later.

Panel D shows total retinal thickness measured by SD-OCT demonstrating retinal structural integrity which was significantly different ($p<.01$) in 830 nm treated group at both 0 degree and 90 degree linear scans when compared to P23H group but 670 nm treatment demonstrated a trend without a statistically significant result. Error bars: SEM. 110

Figure 49 compares the functional and structural changes in P23H transgenic retina following NIR PBM by 830 and 670 nm photons during the onset of the critical period of photoreceptor cell death to young adulthood (p10-p 40). Panel A compares the a-wave amplitude and panel B compares the b-wave amplitude between P23H (■) and 830 nm treated group (▲, left), P23H (■) and 670 nm treated group (▲, right) respectively. The main effect for a-wave and b-wave between the groups are significantly different [a-wave: ($F_{(1,14)} = 16.63$, $p < .01$); b-wave: ($F_{(1,14)} = 14.6$, $p < .01$)] in 830 nm treated group when compared to that of the 670 nm treated [a-wave: ($F_{(1,10)} = .279$, $p =.609$); b-wave: ($F_{(1,11)} = 2.01$, $p =.172$)]. Panel C compares the implicit time for a-wave and b-wave at 100mcd.s/m^2 and there was no statistically significant difference between P23H and both treatment groups. Panel D shows total retinal thickness measured by SD-OCT linear scans representing retinal structural integrity which was not statistically significant between P23H and 830 nm treated group. Error bars: SEM. 112

Figure 50 compares the functional and structural changes in P23H transgenic retina following NIR PBM by 830 and 670 nm photons during the later stage (p20-p 40) to rescue remaining photoreceptors. Panel A compares the a-wave amplitude and panel B compares the b-wave amplitude between P23H (■) and 830 nm treated group (▲, left), P23H (■) and 670 nm treated group (▲, right) respectively. The main effect for a-wave and b-wave between the groups are significantly study [a-wave: ($F_{(1,22)} = 4.60$, $p < .05$); b-wave: ($F_{(1,20)} = 5.85$, $p < .05$)] in 830 nm treated group when compared to that of the 670 nm treated [a-wave: ($F_{(1,10)} = .00$, $p =.99$); b-wave: ($F_{(1,10)} = 0.28$, $p =.608$)]. Panel C compares the implicit time for a-wave and b-wave at

100mcd.s/m^2 and there was no statistically significant difference between P23H and both treatment groups. Panel D shows total retinal thickness measured by SD-OCT linear scans representing retinal structural integrity. 90 degree linear scans were statistically significant between P23H and 830 nm treated group ($p < .05$) but in contrast 0 degree scans were not statistically significant ($p =.05$). Error bars: SEM. 114

Figure 51 a and 51 b shows the ONH landmark used for SDOCT imaging. Figure 51c shows the difference in the reflectivity of retinal layers from which Longitudinal Reflectivity Profile (LRP) is generated. Low reflecting layers in the linear scan correspond to nuclear layers and high reflecting layers correspond to synaptic layers in the retina[31, 53]. NFL, nerve fibre layer; GCL, ganglion cell layer; OPL, outer plexiform layer; ONL, outer nuclear layer; IS/OS, inner segment/outer segment junction; BM, Bruch's membrane. Figure 51 d represents the LRP lines 50Px apart on either side of the ONH (100Px width) used for characterizing the ONL thickness. 123

Figure 52a shows the mean a-wave amplitude and figure 52b shows the mean b-wave amplitude assessed by the scotopic intensity series protocol comparing P23H transgenic retina (■) and 830 nm treated P23H retina (▲). 830 nm caused a significant increase in both a-wave ($F_{(1, 14)} = 16.32$, $p < .001$; n=8, Fig. 52a) and b-wave amplitudes ($F_{(1, 22)} = 23.57$, $p < .001$; n=12, Fig. 52b) at all flash intensities compared to the P23H group. Figure 52c shows the ISCEV protocol for Rod only response (a wave; flash strength -10mcds/m^2) which was significantly ($p<.05$)and Figure 52d shows ISCEV protocol for Standard Rod and Cone response (a wave; flash strength -3000 mcds/m^2). Error bars: SEM. 128

Figure 53a and b compares the total retinal thickness and ONL thickness respectively from SD-OCT linear scans (1000 A-scans/B-scan, 80 B-scans). Total retinal thickness was significantly ($p < .05$; Fig. 53a) higher in NIR-PBM treated group when compared to the P23H group. The ONL thickness of NIR-PBM treated group (▲) derived from Longitudinal Reflectivity Profile (LRP) was significantly greater ($F_{(1, 8)} = 12.23$, $p < .01$; Fig.53b) compared to the sham-treated group (●) across the entire scan. 130

Figure 54 compares the representative images of retinal sections stained with toluidine blue between sham-treated group and the NIR-PBM treated group. The ONL in the NIR-PBM treated group is more organized and symmetrically packed when compared to the sham-treated which was highly disrupted and disorganized. 131

Figure 55 shows quantitative analyses of the ONL thickness sampled across the retina from the superior to inferior edge (n = 4). ONL thickness in NIR-PBM treated group is significantly greater compared to the P23H group. Error bars: SEM. 132

Figure 56 compares the total retinal thickness between NIR-PBM treated group and sham-treated group monitored in a longitudinal study using SD-OCT. The retinoprotective effects of NIR PBM diminishes as the animal matures and statistically significant difference (p<.01) with the non-treated group was found only at the time period, p25. Error bars: SEM. 133

Figure 57 compares representative linear scans at p18, p25, p32, p39 and p80 134

Figure 58 Upper panel shows a representative max projected NADH (upper panel), FAD (middle panel) and RR images (lower panel) for normal (SD), P23H transgenic and 830 nm treated transgenic eyes. Lower panel shows a representative NADH redox histogram for eyes comparing normal (SD), P23H transgenic and 830 nm treated transgenic eyes 136

Figure 59 represents bar graph plot comparing the mean values of the histograms of max projected images from SD, P23H transgenic and 830 nm treated P23H transgenic rat eyes. The results show a significant decrease in the ratio between normal and diseased eyes (***p*<.01) which is reversed to normal by 830 nm treatment (**p* <.01). Error bars: SEM. 137

LIST OF TABLES

Table 1 Protocol for Scotopic Intensity series electroretinography (Reproduced and modified from HMsERG user manual).. 57

Table 2 ISCEV protocol for electroretinography. The animals are dark dapated atleast for 20 Minutes before the procedure. The ISCEV protocol includes 7 standardized individual tests as recommended by the ISCEV. (Reproduced and modified from HMsERG user manual). 58

CHAPTER 1

LITERATURE REVIEW

The vertebrate retina, is involved in generating visual perception in the visible range of the electromagnetic spectrum (400-760nm). Photoreceptors are key elements of the outer sensory retina that are activated by light. The first neuroanatomical studies revealing the complexity of the retinal structure were described in avian retinae by Santiago Ramon Cajal in 1888 (Piccolino, Strettoi et al. 1989). Light enters the vertebrate eye by the refraction at the corneal air interface. The lens focuses the light rays into the thin neural tissue-retina, which processes and extracts information from the inverted image. The vertebrate retina has a layered structure. The outermost layer contains the photoreceptors. There are two distinct types of photoreceptors, rods and cones, which can be differentiated morphologically (Figure 1). Cones (~5% of total photoreceptors) are small cone-shaped cells whereas rods (~95% of the total photoreceptors) are larger rod-shaped cells. Rod cells, containing rhodopsin pigment, are highly sensitive to low light intensity and have a low photon saturation threshold which enables night vision, whereas cone cells are for high resolution and color vision. Photoreceptors have specialized structures called outer segments that are considered to be modified cilia and contain the enzymes and the proteins responsible for phototransduction. The outer segments discs are continuously replenished by the phagocytic function of retinal pigment epithelium (RPE). The RPE also reduces the backscattering of light that enters the eye. The photoreceptors have a distinct distribution in the retina. In the peripheral retina the rod photoreceptors are abundant. In the central retina-fovea, the cone density is at a maximum. The second layer of the retina has intervening neurons including bipolar cells, horizontal cells and amacrine cells and the third layer, the ganglion cell layer, is the final output layer to the visual cortex.

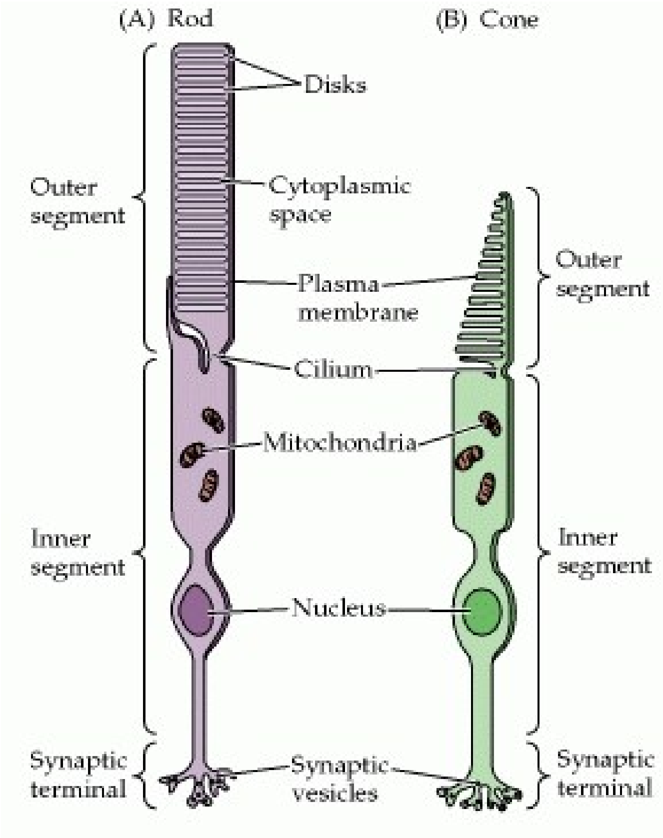

Figure 1 Both rod (A) and cone (B) photoreceptor consist of four distinct regions: an outer segment (OS) which contains stacks of bilipid membranous discs embedded with photopigments which are responsible for photoabsorption and initiation of phototransduction cascade, an inner segment that contains biosynthetic and metabolic functions as well as optical functions which by the phenomenon of total internal reflection confines the photons within the receptor (Hoang, Linsenmeier et al. 2002), a cilium connecting both the inner and the outer segments, and a synaptic terminal which signals to the inner retina by neurotransmitters. (Reproduced from Neuroscience. 2nd edition. Purves D, Augustine GJ, Fitzpatrick D, et al., editors. Sunderland (MA): Sinauer Associates; 2001).

EVOLUTION OF PHOTORECEPTORS

Historically it has been shown that the vertebrate retina evolved as two independent systems based on the nature and function of photoreceptors which enabled vision for both nocturnal and diurnal animals in the ancient visual landscape (Collin, Davies et al. 2009). The photoreceptor cell and the associated pigment cells enabled primitive life forms to move in the direction of light for phototaxis (Arendt 2003). Additional cell types including lens cells, various supporting cells and muscle cells were added as the eye evolved and cell diversity is at a maximum in the vertebrate eye. Retinal tissue in vertebrates evolved during the development from the embryonic forebrain as an out-pocketing of the diencephalon, referred as the optic vesicle which further undergoes invagination to form the optic cup (Figure 2). The inner wall of the optic cup develops into retina and the outer wall develops into RPE.

.

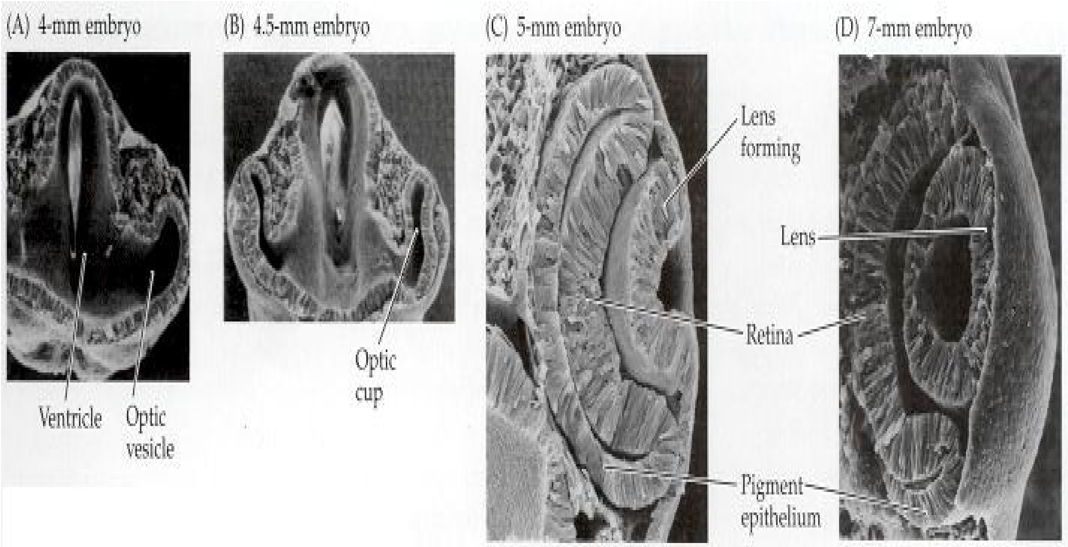

Figure 2 Development of anatomical structures of eye from the optic vesicle. (Reproduced from Neuroscience. 2nd edition. Purves D, Augustine GJ, Fitzpatrick D, et al., editors. Sunderland (MA): Sinauer Associates; 2001).

ROD OUTER SEGMENT AND RHODOPSIN

The shape of the outer segment of photoreceptors has been used to characterize its morphology and function. The photoreceptor has evolved unique structural, functional and biochemical specializations that enable the process of photoabsorption. The photoreceptor outer segment is a modified cilium that connects to the inner segment via a connecting cilium (Figure 1) which maintains the cytoplasmic connectivity. The outer segment has hundreds of stacked membranous disks surrounded by plasma membrane (Figure 3). The evagination and invagination of membranes form the base of the cilium results in the generation of outer segment. In rods the expanding membranes get detached and remain as free floating discs whereas in cones they remain attached to the outer segment membrane (Steinberg, Fisher et al. 1980).

The outer segment of the photoreceptor is a dynamic structure and the length is maintained constant by shedding the distal end followed by its phagocytosis by the retinal pigment epithelium, while nascent membrane biogenesis occurs at the base of the outer segment (Young and Bok 1969). The process of rod outer segment shedding and renewal is better understood than the cones and it follows a circadian pattern; there is increased shedding in presence of light and decreased shedding in dark (Goldman, Teirstein et al. 1980). Complete outer segment turnover period is approximately 10 days in normal Sprague-Dawley rats but it alters when an animal is moved to a new intensity of light. The rod outer segment shortens during the first three days in a new intensity and later it lengthens, after which the outer segment length, as well as the rhodopsin content, is inversely related to the light intensity in the environment. This phenomenon is described as photostasis and it is believed to have evolved to adapt to variations in day-light intensity and duration

(Schremser and Williams 1995). The exact reason for outer segment renewal is unclear, but studies suggest that it confers plasticity to the rod photoreceptor and protects against damaging effects of constant light exposure (Penn, Tolman et al. 1992).

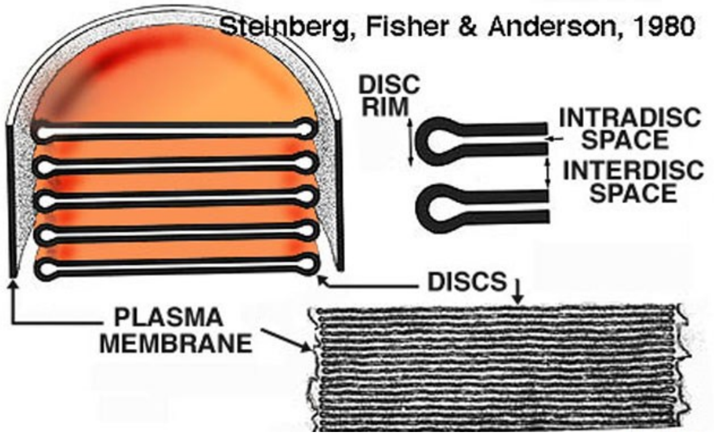

Figure 3 The outer segment of the photoreceptor is a modified cilium containing numerous discs which has embedded light sensitive visual pigments. (Reproduced from Steinberg, Fisher et al. 1980)

Rod photoreceptors are highly specialized neurons that have low spatial resolution, but high sensitivity and can detect a single photon. Conversely, cone photoreceptors are relatively insensitive to light with high spatial resolution and are therefore, responsible for visual acuity (Lamb, Baylor et al. 1979). The visual pigment Rhodopsin (Rho) is the predominant integral membrane protein (~ 50% of the disc surface area) in rods which occupies the membranes of the outer segment (Ridge and Palczewski 2007). Vertebral rhodopsin is a highly specialized G protein-coupled receptor (GPCR) which has seven transmembrane domains (H1 to H7) (Figure 4). Rho belongs to the class of A GPCRs within the superfamily and is made up of opsin apoprotein and a chromophore. The opsin molecule is synthesized in the inner segment by the Golgi apparatus and is transported to the outer segment at the area of cilium by fusion using G proteins (Papermaster, Schneider et al. 1985). The chromophore 11-*cis*-retinal is a vitamin A derivative (aldehyde of vitamin A_1) which is bound covalently to the terminal amino group of L-lysine residue embedded in the membrane (Figure 5).

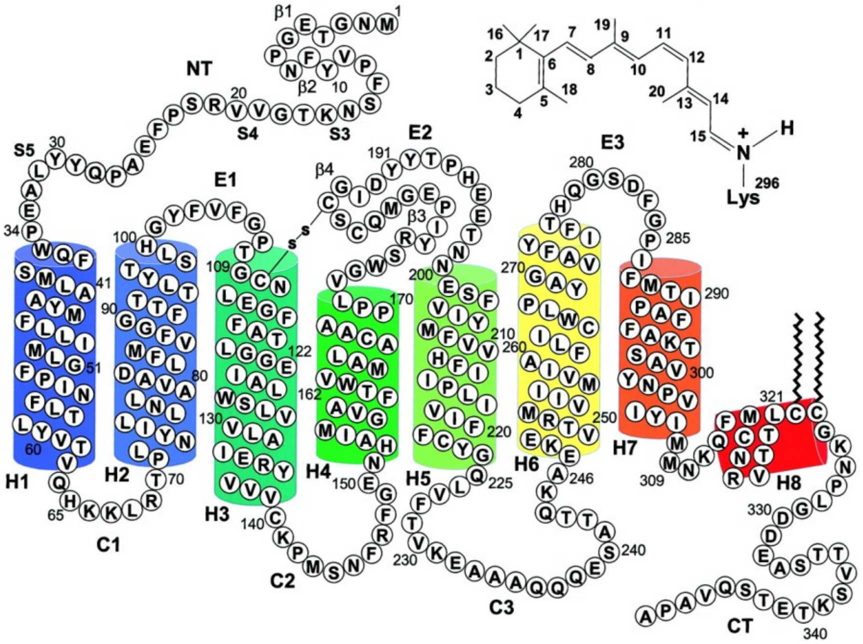

Figure 4 Secondary structure of bovine Rho. The NH_2-terminal tail and extracellular domain point toward the top and the COOH-terminal tail and cytoplasmic domain is toward the bottom. Letter codes indicate amino acid residues. The structure has 7 transmembrane α-helical segments (H1 to H7). Inset: structure of the chromophore -11-*cis*- retinal. (Reproduced from Menon, Han et al. 2001).

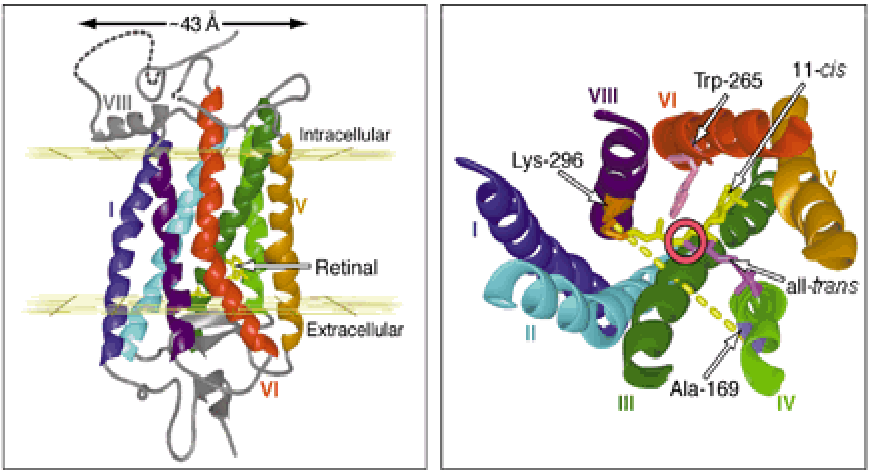

Figure 5 A molecular ribbon diagram of inactive and active views of Rho from the 43 Å crystal structure coordinate. Unlike other GPCRs Rho binds to 11-*cis* retinal (ligand) covalently both in inactive as well as photo activated state-11-cis dark form (yellow) to all-trans light (magenta). (Reproduced from Bourne and Meng 2000)

PHOTOTRANSDUCTION

The sequence of events triggered within photoreceptor cells when a single photon is absorbed is referred as phototransduction and involves the following steps: activation of Rho, activation of G-protein, activation of effector phosphodiesterase (PDE), hydrolysis of cyclic guanosine monophosphate (cGMP) and closure of ion channels. Classic studies by Wald et.al. (1950), first showed that the primary interaction of light with the bound retinal chromophore is to drive the conversion of 11-*cis*-to-*trans* isomerization at the reaction speed of 10^{-12} sec (Wald, Durell et al. 1950). The absorption of photons in the visible range (absorption maximum, λmax~500nm) by 11-*cis*-retinal is due to the extended polyene structure of the Rho molecule (Rando 1996). Photoisomerisation makes the Rho molecule active (R*) which generates spectrally distinct intermediates of Rho (bathorhodopsin, lumirhodopsin, metarhodopsin I, and metarhodopsin II) that trigger an amplifying cascade of biochemical events in the outer segment (Okada and Palczewski 2001). R* stimulates the G-protein transducin to its activated state (G*), which in turn activates the effector PDE to PDE*. Activated PDE* causes the hydrolysis of cyclic guanosine monophosphate (cGMP) to 5'-GMP. The decrease in intracellular cGMP leads to the closure of cGMP-gated channels on the plasma membrane of the photoreceptor outer segment, thereby reducing the influx of sodium ions (Na^+) through these channels, which results in membrane hyperpolarization. Hyperpolarization inhibits or decreases the release of glutamate at the synapse which is further relayed and processed as a neurochemical event by the second order retinal neurons and eventually to higher centers in brain. Following excitation by a photon of light, the photoreceptor returns to its dark state by decay of R*. The protein arrestin blocks the ability of R* to convert transducin to G* which accelerates the decay of R* (Figure 6). The all-trans chromophore dissociates from opsin and is converted back to 11-cis-retinal and is transported out of the outer segment into the RPE where 11-cis-retinal combines with opsin to regenerate new Rho (McBee, Palczewski et al. 2001).

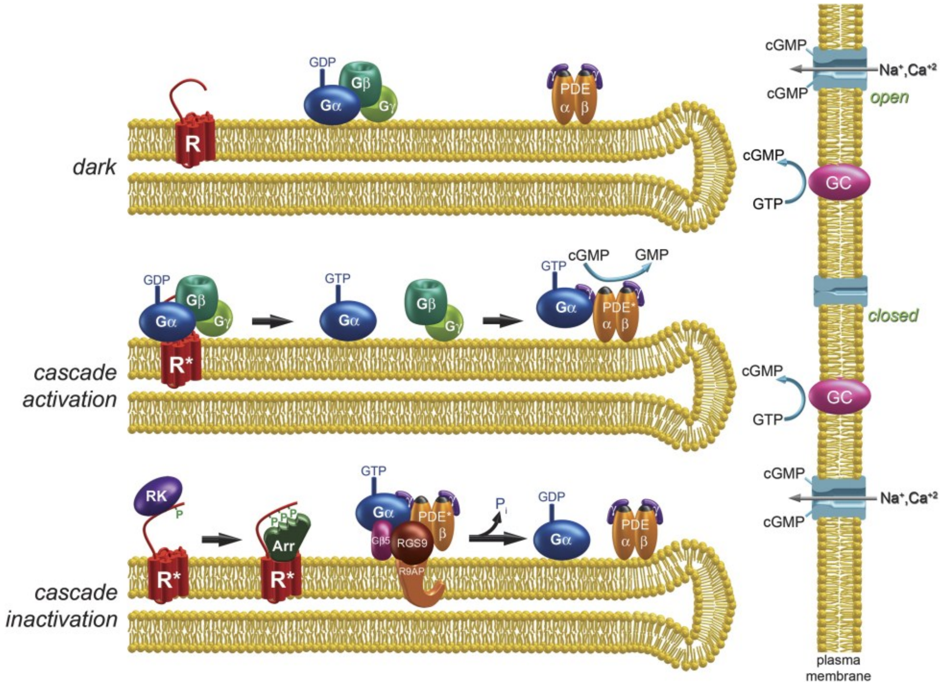

Figure 6 Schematic representation of phototransduction cascade in rod photoreceptors. (Reproduced from Burns and Arshavsky 2005)

In the dark, the photoreceptor is in a depolarized state (~ -40 mV) and a steady current known as dark current flows through the photoreceptor cell. Recovery in dark is achieved by the reopening of the cGMP-gated channel by the binding of cGMP on the cytoplasmic side of the channel. Although Ca^{2+} and Mg^{2+} ions are involved, the inward current is mediated by Na^+ influx and the outward current is carried largely by potassium ions (K^+) flowing in the photoreceptor inner segment through K^+ sensitive non-gated channels (Yau and Nakatani 1984). The photoreceptor is in a depolarized state at this stage and there is constant release of glutamate from the synaptic terminal.

The direct pathway for visual signal processing is the vertical transduction pathway which transfers neurochemical signals from photoreceptor cells, to bipolar cells, to ganglion cells, to the optic nerve by synaptic connections. Lateral inputs from horizontal cells (photoreceptor-bipolar synapse) and amacrine cells (bipolar-ganglion cell synapse) modulate this pathway in the retina and provide feedback connections (Figure 7). Glutamate is the major excitatory neurotransmitter released in the synapses. Once released from the presynaptic terminal of the photoreceptors, glutamate diffuses across the synaptic cleft and binds to the receptors (ionotropic and metabotropic glutamate receptors) located on the dendrites of the postsynaptic neurons (ON-center and OFF-center bipolar cells).

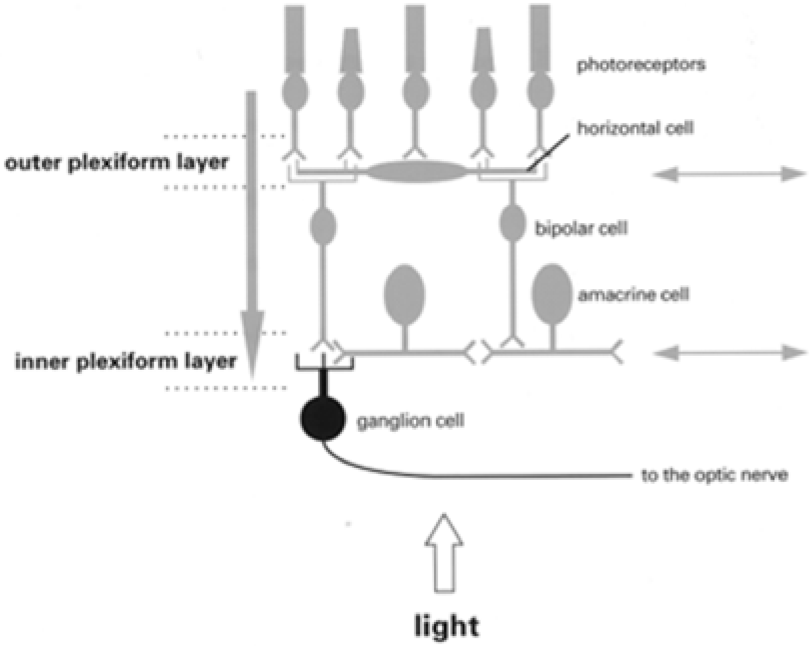

Figure 7 Schematic representation of information flow in the retina. Signals can pass both vertically and laterally. (Reproduced from Lagnado 2000)

Neurons within the OFF-pathway (horizontal cells, OFF-bipolar cells, amacrine cells, and ganglion cells) express functional ionotropic glutamate receptors and glutamate binding onto these receptors opens cation channels, depolarizing the postsynaptic cell membrane. Glutamate binding onto metabotropic glutamate receptors (APB receptor, present in ON-bipolar cells) can have a variety of effects depending on the second messenger cascade to which the receptor is linked. Thus, postsynaptic responses to glutamate are determined by the distribution of receptors and transporters (to prevent glutamate induced toxicity) which in turn determine the signal conductance mechanisms underlying visual information processing within the ON and OFF-pathways.

High metabolic demand of photoreceptors

Phototransduction is a highly energy demanding process and the energy metabolism is a critical function that determines photoreceptor function and survival. Like other neurons of the central nervous system, photoreceptors use ATP generated from glucose as their energy source and a decrease in the availability of glucose has been shown to accelerate photoreceptor death and subsequent loss of vision (Umino, Everhart et al. 2006). Vision is lost when blood supply to the eye is blocked for only 10 seconds (Linsenmeier 1990). Energy demand of photoreceptors resembles that of rapidly dividing cancer cells (Vander Heiden, Cantley et al. 2009). Oxygen microelectrode studies have shown that photoreceptors consume approximately three to four times more oxygen than any other cell in the central nervous system (Braun, Linsenmeier et al. 1995). Photoreceptors metabolize glucose either anaerobically by glycolysis or aerobically by oxidative phosphorylation. Both rod dominated and cone dominated retinae use >80% of glucose for anaerobic glycolysis even in the presence of oxygen (Chertov, Holzhausen et al. 2011). Glucose enters the photoreceptors through the Glut-1 transporters present in the inner segment which is the site for high oxidative activity (Figure 8). Glucose is then phosphorylated by hexokinase 2 and transported to the other parts of the photoreceptor cell (Gospe, Baker et al. 2010).

Dense aggregates of mitochondria fill the apical region of photoreceptor inner segments and intraretinal oxygen profiles show a deep trough in the oxygen partial pressure at this site. A high concentration of oxidative enzymes indicates the unusually large amount of oxidative energy generated (Yu, Cringle et al. 2004) (Lowry, Roberts et al. 1956). Na^+/K^+ ATPase activity, which is essential for the Na^+ transport and the maintenance of the photoreceptor dark current is by far the most energy demanding process in phototransduction (Winkler 1981). Synthesis of high energy phosphate bonds for the rapid turnover of photoreceptor cGMP also requires an appreciable amount of energy (Ames, Li et al. 1992).

Winkler investigated the ability of superfused rat retina to utilize substrates other than glucose for generating ATP and showed that pyruvate maintained the amplitude of Fast PIII (Intra retinal photoreceptor potential) and maintained the concentration of ATP in the absence of glucose (Winkler 1981). These results demonstrate that ATP generated by photoreceptor mitochondrial activity is capable of supporting cellular electrical activity when glycolytic production of ATP is blocked. Interestingly, when pyruvate was superfused at higher concentrations (20 mM) it did not completely substitute for glucose as a substrate in generating functional electrical responsiveness thus providing evidence that either glycolysis alone or Krebs cycle activity alone can maintain retinae at an optimal functioning level (Winkler 1981).

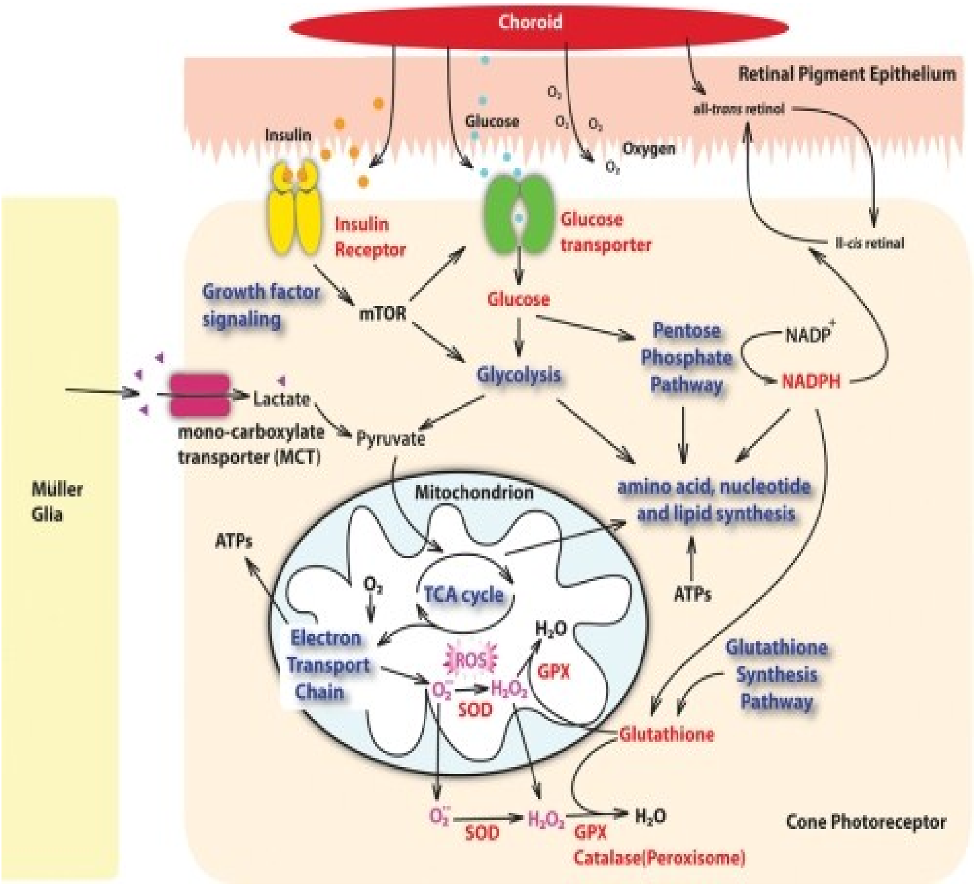

Figure 8 Metabolism in photoreceptors. The high metabolic demand in photoreceptors is met by adequate supply of glucose and oxygen by the choroidal vessels through the RPE cells. Oxidative phosphorylation in the mitochondria provides photoreceptors with adequate amounts of ATP for the high energy demanding phototransduction process. Increased ROS generated as a result of mitochondrial phosphorylation is removed by the antioxidant defense mechanisms involving enzymatic (superoxide dismutase, glutathione peroxidase, and catalase) and non-enzymatic (natural antioxidant glutathione) endogenous systems. The constant recycling of the photoreceptor OS and recycling of 11-*trans*-retinal in the RPE requires rapid macromolecular synthesis and active transport mechanism. Studies have shown that activated insulin receptors can up regulate the growth factor signaling that ends up regulating glycolysis through stimulation of mTOR phosphorylation. (Reproduced from Punzo, Xiong et al. 2012).

INHERITED RETINAL DEGENERATIONS

Retinal degeneration is described as a class of human eye diseases characterized by the loss of photoreceptors leading to severe visual impairment and blindness. Inherited retinal degenerations (IRDs) are a genotypically and phenotypically diverse category of inherited diseases characterized by the loss or premature death of rod and cone photoreceptor cells leading to severe visual impairment and blindness in all ages and racial backgrounds. In most inherited retinal degenerations both the rod and cone photoreceptors die, but the degree to which the two cell types are affected differs with different disorders. Over the years, knowledge of gene mutations associated with IRDs has quickly grown and many disease related gene abnormalities have been mapped and identified. 148 genes and 186 loci have been identified with various IRDs (www.sph.uth.tmc.edu/RetNet/disease.htm;www.retina-international.com). Due to the heterogeneous nature of retinal degenerations many associated mutations have yet to be identified, emphasizing the need for additional research and the development of additional animal models.

Retinitis Pigmentosa (RP)

Retinitis Pigmentosa (RP) is a large genetically heterogeneous group of IRD and the most common cause of inherited blindness in the developed world. RP affects about one in 5000 individuals worldwide (Hartong, Berson et al. 2006). The age at which the individuals show symptoms ranges from 30 to 60 years of age and even varies significantly between individuals in the same family. Molecular genetic techniques have revealed that 30-40% of RP cases are autosomal-dominant, 50-60% are autosomal-recessive and 5-15% are an X-linked trait. Individuals with an autosomal dominant trait generally retain vision longer than those with autosomal recessive or X-linked traits (Dryja, McGee et al. 1990) (Berger, Kloeckener-Gruissem et al. 2010). Non Mendelian inheritance patterns such as mitochondrial inheritance (maternal) are reported in a small proportion of cases (Kajiwara, Berson et al. 1994). The symptoms of RP are well characterized and affected individuals report impaired dark adaptation, night blindness and loss of peripheral vision. Characteristic clinical features in RP include thinning of pigment epithelium and retinal vasculature, optic disc pallor and classic pigmentary deposits referred as 'bone spicule' (Figure 9). There is an exponential loss of visual field area (2.6–13.5% loss annually) and electroretinogram amplitude (8.7–18.5%) in affected individuals. In 20-30% of the individuals affected by RP, the disease is associated with non-ocular diseases including Usher’s syndrome (type I and II), Bardet-Biedl syndrome and Refum’s disease (Hartong, Berson et al. 2006). Mutations in many rod photoreceptor specific genes including rhodopsin, arrestin and rod outer segment membrane proteins result in photoreceptor degeneration (Phelan and Bok 2000). In addition mutations within the RPE - *CRALBP* mutations and *RDH5* mutations result in photoreceptor degeneration.

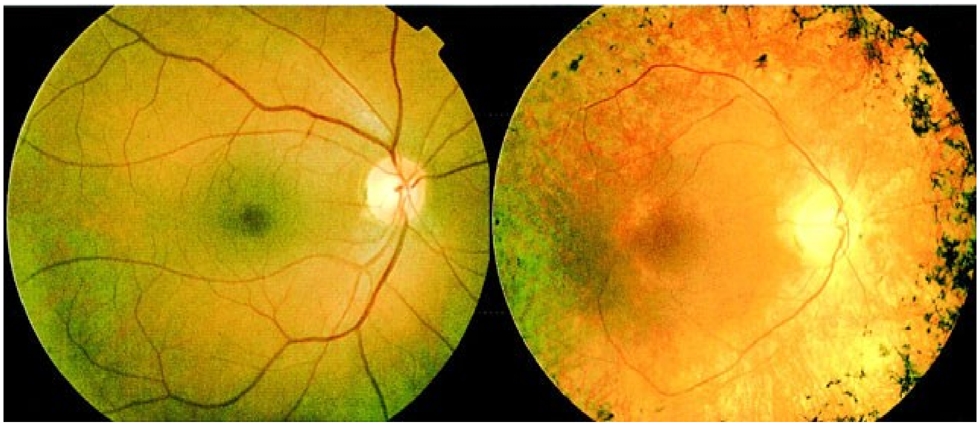

Figure 9 Fundus image of a normal (left) vs. RP eye (right). (Reproduced from Farrar, Kenna et al. 2002)

Causal genes of Retinitis Pigmentosa

Although the majority of RP cases are monogenic, the disease is characterized by its genetic heterogeneity. Researchers have identified mutations in 45 gene loci which cause RP (Berger, Kloeckener-Gruissem et al. 2010). The first gene abnormality in RP was reported in 1984 and was associated with gene for X-linked RP (Bhattacharya, Wright et al. 1984). In 1989, first autosomal RP (adRP) gene was localized to 3q. This mutation was a single-base substitution in codon 23 of rhodopsin gene (*RHO*) and it accounts for 12% of autosomal dominant RP in US (Dryja, McGee et al. 1990). This mutation within the rhodopsin gene at codon 23 in one allele causes a change from proline to histidine in the 23rd amino acid (P23H) of the rhodopsin molecule, which results in misfolding and mislocalization of the protein. This mutation results in an autosomal dominant RP phenotype characterized by night blindness (nyctalopia) during adolescence resulting from the initial loss of rod photoreceptors that carries the mutation followed by progressive loss of vision in adulthood resulting from the secondary degeneration of cones, loss of retinal vasculature and optic disc pallor (Berson, Rosner et al. 1991). The second most observed adRP locus was on 6p and coded for mutations in retinal degeneration slow (RDS) gene encoding a vital component of OS disc membrane glycoprotein- Peripherin. Mutations in the peripherin/RDS gene are often associated with less progressive disorders and sometimes with atypical findings, including early macular involvement.

The other common gene mutations seen in rod dominated retinal and vitreoretinal diseases including RP are classified in Figure 10. This includes *ABCA4, USH2A, arrestin, MERTK, PRKCG, ROM-1, RPE 65, PDE6A* etc., highlights functional diversity and investigators still believe that about 40% of RP cases are due to genes that are yet undiscovered. In summary, the linkage studies done in early 1990s investigating mutations revealed the genetic complexity and heterogeneity associated with retinal degeneration.

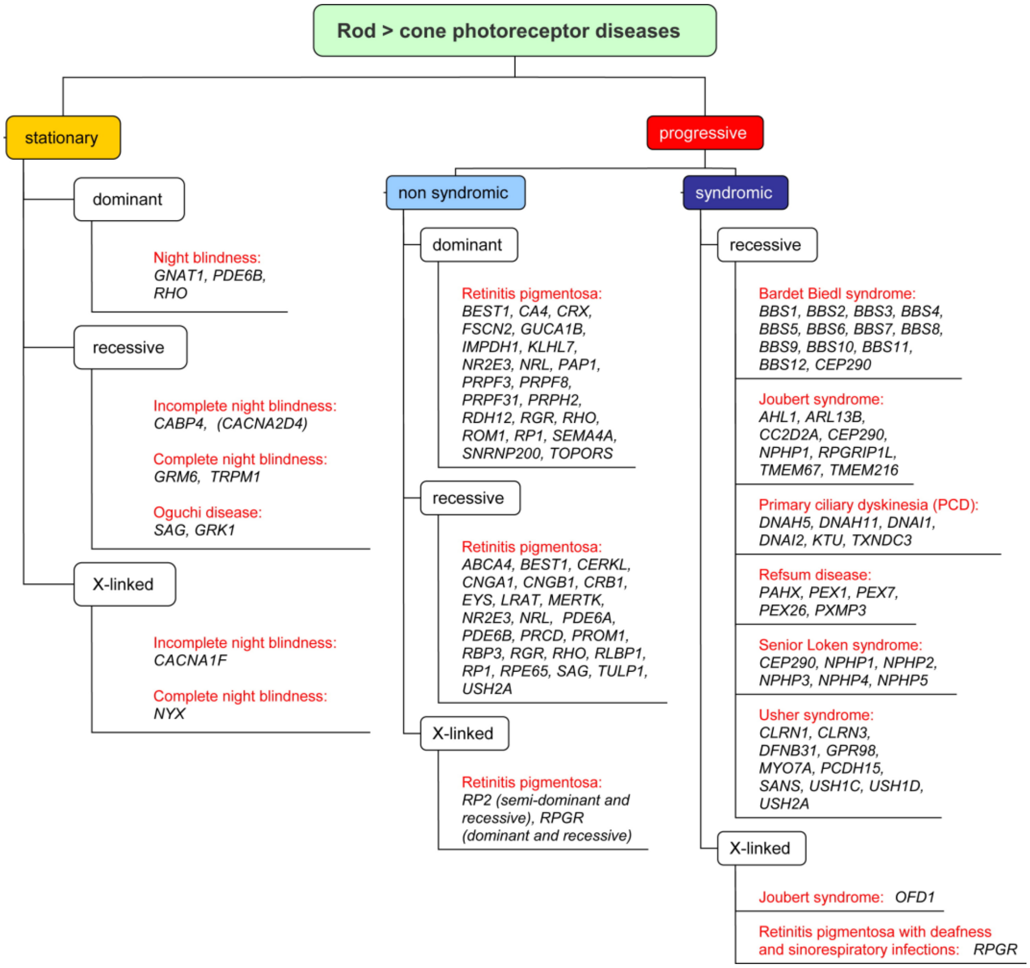

Figure 10 Classification of rod dominated retinal and vitreoretinal diseases including RP and casual genes. (Reproduced from Berger, Kloeckener-Gruissem et al. 2010).

Identified genes in RP normally encode for proteins that are essential for phototransduction cascade (RHO, PDE6A), vitamin A metabolism (ABCA4, PRE65), rod outer segment protein (ROM1), cell signaling (SEMA4A), cell-cell interaction (CDH23), RNA intron-splicing factors (PRPF31), intracellular trafficking proteins (MYO7A), phagocytosis (MERTK) and proteins for pH regulation (CA4) (Hartong, Berson et al. 2006). Loss of rod photoreceptors leading to altered retinal architecture (Figure 11 and Figure 12) is the outcome of abnormal physiology associated with mutated or absent gene products. Biochemical interaction between rods and cones and the mechanisms of secondary death of cones following rod mutations and the role of rod derived cone viability factors (RdCVF) in the degeneration process are still not clearly understood.

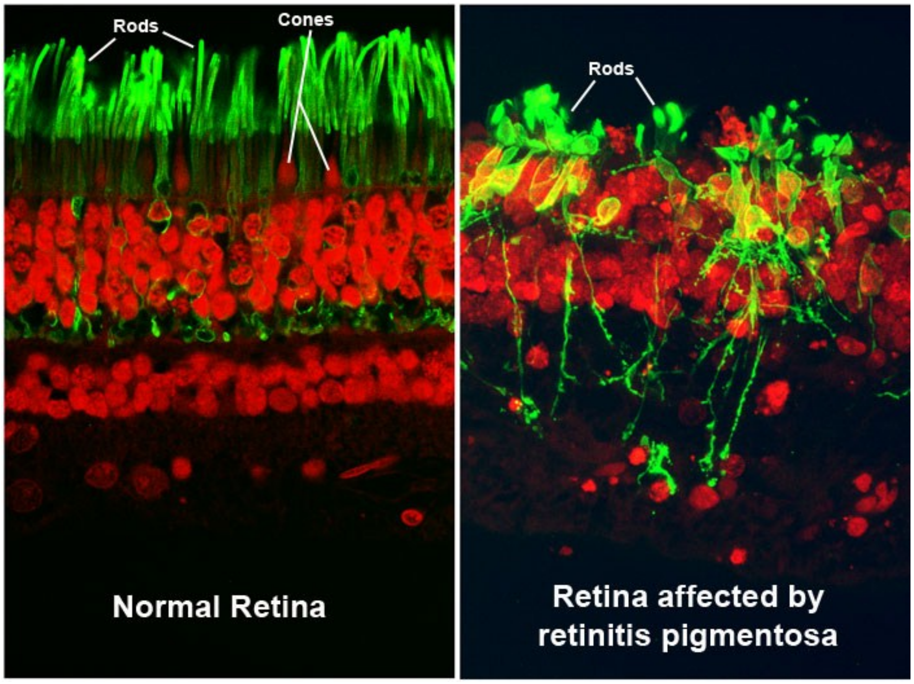

Figure 11 Loss of retinal architecture in RP demonstrated by high resolution microscopy.(Reproduced from http://www.nei.nih.gov/eyeonnei/snapshot/archive/0909.asp)

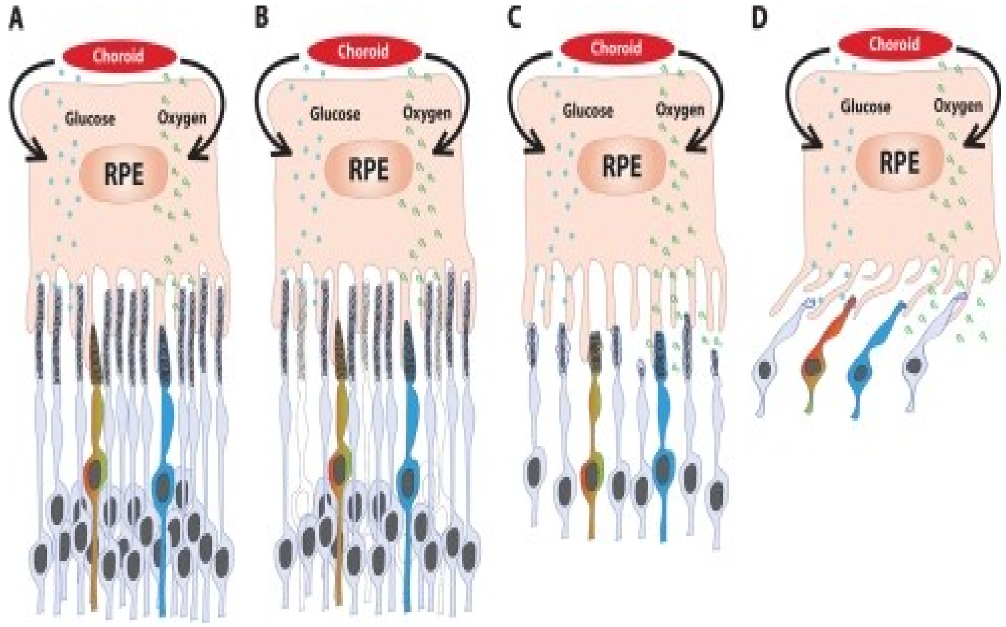

Figure 12 Schematic representation of photoreceptor loss in Retinitis Pigmentosa. Normal Retina (A), when rods start to die (B), extensive loss of rod photoreceptor as the disease progresses (C) and eventually retina will lose all the rod photoreceptors which results in reduced nutrient flow, which leads to the death of remaining photoreceptors and the loss of retinal architecture. (Reproduced from Punzo, Xiong et al. 2012).

Therapeutic Approaches for the Treatment of RP

There is presently no effective treatment for RP. A three year follow-up study on the natural course of RP has shown that patients with dominant, recessive, and X-linked RP taking vitamin A, Vitamin E or both showed slower decline in electroretinography amplitudes compared to those not taking any supplements but the visual-field area and visual acuity was not significantly different between groups (Berson, Sandberg et al. 1985). A study investigating the role of docosahexaenoic acid (DHA), an omega-3 fatty acid, did not show a clear benefit (Hoffman, Locke et al. 2004). Based on the findings in two animal models of RP it is postulated that reduction in the exposure to light can slow down the rate of degeneration (Naash, Peachey et al. 1996). Use of pharmacological agents including carbonic anhydrase inhibitors has been shown to decrease the secondary pathology associated with RP including edema of the macula (Fishman, Gilbert et al. 1989). Valproic acid is an inhibitor of histone deacetylase and is identified as a pharmacologic chaperone for treating RP and an active clinical trial is currently going on (Clemson, Tzekov et al. 2011).

The recent advances in finding a cure for RP are based on gene specific therapies, transplantation of lost retinal tissue by tissue engineered grafts/encapsulated cell technologies, regeneration by pluripotent stem cells and the use of retinal prosthetic devices. Gene specific therapies are based on the type of mutation and substantial improvement towards clinical trials is made on experiments in animal model targeting RPE65 gene (Bennett, Tanabe et al. 1996). Gene silencing and interference RNA(RNAi)-based gene therapy is being developed for dominantly inherited mutations (Cashman, Binkley et al. 2005). The potential use of transplanting RPE, photoreceptors or pluripotent stem cells is being widely investigated and studies have shown beneficial effects (Whiteley, Litchfield et al. 1996). Prosthetic devices that can electrically stimulate the optic nerve, optic nerve head and the visual cortex and being tested in patients (Rizzo, Wyatt et al. 2003; Roessler, Laube et al. 2009). A clinical trial with second-generation electronic retinal implant-Argus II Retinal Stimulation System is ongoing and the implant is designed to take the place of degenerated photoreceptors in RP (www.clinicaltrials.gov).

One difficulty in the treatment of RP is that many patients have already lost all or nearly all rod photoreceptors when they complain about compromised vision thus strategies should be developed that can rescue the few remaining cone photoreceptors. Despite the advances mentioned above there is a clear need for a neuroprotective therapy that has the potential to attenuate photoreceptor cell loss during the course of the disease. Photobiomodulation holds the promise to be a retinoprotective non-invasive therapy for the prevention and treatment of retinal diseases.

Animal Models of Retinitis Pigmentosa

In most inherited retinal degenerations both the rod and cone photoreceptors die, but the degree to which the cell types are affected differs with different disorders and this heterogeneity is the biggest barrier and challenge in designing and developing therapeutics. Due to the heterogeneous nature of RP many associated mutations have yet to be identified which calls for additional research and better animal models. Both transgenic mice ($Pde6b^{rd10}$, rd11, $Crb1^{rd8}$, nr, Tub^{tub}, $Rpe65^{rd12}$) and rat (P23H, S334ter) have been extensively used to understand the molecular mechanisms involved in inherited retinal degeneration.

The first retinal degeneration animal model was the $Pde6b^{rd1}$ mouse model discovered by Keeler in 1924, which demonstrated early-onset severe degeneration due to the lack of PDE 6 activity in the rod photoreceptors. This same phenotypic resemblance is found in patients suffering from adRP (Keeler 1924). The $Pde6b^{rd1}$ mouse model was successfully used in developing novel therapeutic strategies to rescue rod degeneration by gene therapy. Cone degeneration has been prevented by introducing autologous bone marrow derived hematopoietic stem cells into the degenerating retinal vasculature (Takahashi, Miyoshi et al. 1999) (Otani, Dorrell et al. 2004). The $Pde6b^{rd10}$ (rd 10) mouse model displays retinal degeneration with sclerotic retinal vessels by p28 and resembles a model of autosomal recessive mutation that maps to the chromosome 5. Pde6b^{rd10} is considered to be a better model than Pde6b^{rd1} for developing pharmaceutical therapies and testing neuroprotective approaches for RP because of its later onset and mild degeneration phenotype. The shape and size of mouse eyes are challenging for surgical procedures and this led to the development of rhodopsin transgenic rat models which have larger eyes.

The P23H transgenic rat is a model of autosomal dominant RP in which the rhodopsin transgene mimics a human form of RP common in North America (Dryja, McGee et al. 1990). The transgene induces an autosomal dominant photoreceptor degeneration phenotype that renders the outer retina hyperoxic from early postnatal life (Wellard, Lee et al. 2005). As photoreceptors degenerate in P23H model, oxygen consumption decreases and oxygen tension increases in the outer retina. Choroid capillaries have been shown to auto regulate poorly to the changing hyperoxic environment and this is known to cause constriction of retinal vessels in P23H transgenic rats, the RCS rat model and in the Abyssinian cat model of retinal degeneration (Yu, Cringle et al. 2004). Hyperoxia induced oxidative stress and reduced levels of antioxidant systems includin catalase render the retina particularly vulnerable to progressive degenerative processes. Increased oxidative stress activates fibroblast growth factor (FGF) and ciliary neurotrophic factor (CNTF) which results in a slower degeneration process that continues throughout life (Machida, Kondo et al. 2000).

Mechanisms of retinal degeneration have also been studied using induced degeneration models. In induced models physical (e.g., light) or chemical (e.g. nitrosourea) exposure to wild type or genetically engineered animals results in the induction of photoreceptor degeneration leading to different phenotypes of retinal degeneration from mild to severe. Induced models have the advantage of control over disease severity and onset. Many toxic agents (alkylating agent; *N*-Nitroso-*N*-methylurea) and strategies including iron overload and autoantibody treatments have been reported in the literature to induce the photoreceptor degeneration process in rodents (Yuge, Nambu et al. 1996), (Nambu, Yuge et al. 1997), (He, Poblenz et al. 2000). The most widely accepted induced rodent model is the light induced retinal degeneration model (LIRD) (Noell, Walker et al. 1966). The advantage of the induced model is that the severity of retinal damage can be adjusted according to the experimental needs.

Mitochondrial dysfunction, oxidative stress and apoptosis in retinal degenerations

Photoreceptors are the most metabolically active cells in the body. They have a dense concentration of mitochondria in their inner segments to provide ATP for the energy-intensive processes of outer segment renewal and maintenance of the dark current (Bramall, Wright et al. 2010). Considerable evidence supports a key role for mitochondrial dysfunction and oxidative damage in the pathogenesis of photoreceptor cell death in RP and other retinal degenerative disorders (Campian, Qian et al. 2004). Human retinal dystrophies and degenerations and light-induced retinal degeneration have been associated with profound loss of retinal antioxidant systems and cytoprotective factors thus compromising the ability of retinal neurons and glia to protect against oxidative damage leading to apoptotic cell death (Carmody and Cotter 2000).

Mitochondrial dysfunction is also reported in a broad spectrum of pathologies including Parkinson's disease, Alzheimer's disease, Huntington's disease, amyotrophic lateral sclerosis and many other neurodegenerative diseases

Reactive oxygen species (ROS) are formed as the by-product of oxidative phosphorylation in the electron transport chain (ETC) of the mitochondria. There are important antioxidant systems including mitochondrial superoxide dismutase (MnSOD), glutathione (GSH) and thioredoxin to keep the concentrations of free radicals at a minimum and to prevent conversion to stronger oxidants. The inability of the antioxidant systems in the cell to quench the increased production of free radicals creates a biochemical imbalance referred as oxidative stress (Ceriello and Motz 2004). The production of reactive oxygen species and oxidative damage is increased under conditions of mitochondrial dysfunction (Shen, Yang et al. 2005). The ROS generated attack lipids, proteins and nucleic acids and disrupt their functions. The metabolic products generated by ROS interactions with these cellular components also disrupt major functions including energy metabolism, signal transduction, intracellular transport and various other functions. A key ROS molecule, superoxide ($O_2^{-\cdot}$), becomes highly reactive when combined with NO to form peroxynitrite ($ONOO^-$) and these potent oxidant molecules can oxidize chemical moieties including lipids, proteins and DNA and causing irreversible damage to them. These toxic reactions often result in cell death by apoptosis or necrosis (Butterfield, Reed et al. 2007). There is strong evidence regarding the link between oxidative stress and photoreceptor damage in various *in vivo* and *in vitro* experimental models (Vlachantoni, Bramall et al. 2011).

In many IRDs the defective gene is present in the rod photoreceptor, rod cell death precedes the cone cell death, and the mechanisms by which cone cells undergo apoptosis are still not clear. IRDs characterized by common rhodopsin mutations cause protein misfolding and retention in the endoplasmic reticulum (ER) which causes ER stress. ER stress activates sensor proteins that results in unfolded protein response (UPR) and activation of signaling pathways including ATF6 and PERK. These pathways reduce the translation and accelerate misfolding of protein. These abnormal proteins accumulate in the rods as opsin aggresomes. Similar proteinacious inclusions are reported in many forms of neurodegeneration, including amyotrophic lateral sclerosis, Alzheimer's disease and Parkinson's disease (Saliba, Munro et al. 2002). Oxidative stress is also generated in IRDs due to reduced oxygen utilization by inactive mutant rod photoreceptors resulting in outer retinal hyperoxia which generates ROS and this is confirmed in *Mertk*$^{RCS/RCS}$ rats, Tg. *Rho*$^{\mathrm{Pro23His}}$ (P23H) rats, and *CEP290* mutant cats (Yu, Cringle et al. 2004) (Padnick-Silver, Kang Derwent et al. 2006). ROS thus generated can cause post translational modification of thiol groups of enzymes and transcription factors leading to the activation of proapoptotic pathways thus decreasing photoreceptor survival (Janssen-Heininger, Mossman et al. 2008).

Accumulation of mitochondrial ROS influences both retrograde (mitochondria to nucleus) and anterograde (nucleus to mitochondria) redox sensitive signaling pathways which are capable of initiating the process of apoptosis. Potential redox sensitive signaling components that cause photoreceptor cell death in IRDs are p53 (Ali, Reichel et al. 1998) and HDAC4 (Chen and Cepko 2009), but based on the nature of the photoreceptor stress many other pro and antiapoptotic factors are involved. Cell death by apoptosis (both caspase dependent and caspase independent) is a unifying feature in various forms of inherited photoreceptor degenerations (Bramall, Wright et al. 2010). In several different rodent models of inherited retinal degenerations, aberrant photoreceptor apoptosis is demonstrated during the critical period of photoreceptor development in the retina.

NEAR INFRARED (NIR) PHOTOBIOMODULATION

Treatment of tissue with monochromatic photons in the far-red to near-infrared (NIR) region of the spectrum (λ=630-1000 nm), also known as photobiomodulation (PBM), improves mitochondrial function and promotes cell survival in cultured cells and animal models of disease (Liang, Whelan et al. 2006) (Desmet, Paz et al. 2006). PBM has been used clinically to treat soft-tissue injuries and stimulate wound healing for more than 40 years (Eells, Henry et al. 2003). Photobiomodulation at wavelengths between 630-830 nm at doses ranging from 3-6 J/cm^2 has been shown to reverse harmful effects of neuro and developmental toxins, accelerate wound healing in murine diabetic models of wound healing, improve recovery from ischemic reperfusion injury in the heart, prevent oral mucositis in pediatric bone marrow transplant patients and attenuate retinotoxic effects of methanol-derived formic acid in rodents (Wong-Riley, Liang et al. 2005), (Lim, Sanders et al. 2010), (Eells, Henry et al. 2003), (de Sousa, Santos et al. 2010).

Recent studies have demonstrated that 670nm NIR photons delivered transcranially to the injury site in an *in vivo* model of partial optic nerve transection, a model of traumatic injury in the central nervous system, resulted in a decrease in secondary oxidative stress in astrocytes, an increase in NG-2 immunopositive oligodendrocyte precursor cells (OPCs) and restored visual function (Fitzgerald, Bartlett et al. 2010). NIR photons have also been shown to induce neuroprotection and stimulate neural maturation *in vitro* in a rat pheochromocytoma cell line 12 (PC12) following oxidative stress and prevent rotenone-induced decreases in visual function *in vivo* by increasing cytochrome *c* oxidase and superoxide dismutase activity (Giuliani, Lorenzini et al. 2009) (Rojas, Lee et al. 2008).

Studies in rodent models of Parkinson's disease and multiple sclerosis demonstrated that treatment with PBM reduced the severity of disease and decreased concentrations of cytotoxic and pro-apoptotic factors (Liang, Whelan et al. 2006). The prolonged effect of brief PBM treatment is consistent with the induction of signaling cascades that initiate gene expression, protein synthesis, and oxidative metabolism in damaged cells (Karu, Pyatibrat et al. 2004). In a model of toxin induced retinal dysfunction, microarray analysis showed that gene expression pathways involved in mitochondrial metabolism and cytoprotection were up regulated whereas pathways involved in cell death were down regulated. Studies to identify the genes and noncoding RNAs (ncRNAs) involved in the neuroprotective actions of NIR-PBM in light induced retinal degeneration model demonstrated 44 known genes and 6 ncRNAs whose expression was significantly increased in light damage, was reduced below criterion when the retina was conditioned by PBM (Natoli, Zhu et al. 2010). Thus, existing data demonstrate the efficacy and therapeutic potential of NIR PBM.

The mechanism of near-infrared photobiomodulation

Mechanistically, light in the spectrum of 630-1000 nm is hypothesized to interact with the mitochondrial enzyme cytochrome *c* oxidase, triggering signaling mechanisms (Figure 13) that result in improved mitochondrial energy metabolism, antioxidant production and cell survival (Liang, Whelan et al. 2006) (Desmet, Paz et al. 2006) (Wong-Riley, Liang et al. 2005). The cytoprotective action spectrum of NIR light corresponds with the cytochrome *c* oxidase absorption spectrum (Figure 14). Comparative spectral analysis for transition metals and their complexes and the biomolecules associated with cellular metabolism suggests that multinuclear enzyme containing Cu(II) complexes are involved in the cellular mechanisms of action of NIR (Karu 1999). Comparing d-d transitions and charge transfer complexes of Cu with the action spectrum have revealed that the photoacceptor molecule is the terminal enzyme of the electron transport chain- cytochrome *c* oxidase. Mixed valence copper components of cytochrome *c* oxidase, Cu_A and Cu_B are believed to be the photoacceptor center of the molecule. Cytochrome *c* oxidase plays a central role in the bioenergetics of the cell and it can also initiate secondary cell signaling pathways that activate transcription factors, alter gene transcription and enhance protein synthesis of antioxidants and other proteins creating a stable microenvironment for cell survival (Figure 13) (Karu 2010), (Desmet, Paz et al. 2006).

Two pathways are widely accepted as the starting point of cellular signaling inside the cell following the interaction of NIR photons with the catalytic center of the cytochrome *c* oxidase. One of them is the photodissociation of NO from the binding sites on the heme iron and copper centers of cytochrome oxidase allowing oxygen to rebind to these sites and restore normal mitochondrial respiration (Sarti, Giuffre et al. 2003) (Huang, Chen et al. 2009). Based on the presence or absence of the NO in the catalytic center, $Cu_{A\ reduced}$ and $Cu_{B\ oxidized}$ are assumed to be associated with the charge-transfer channels and $Cu_{A\ oxidized}$ and $Cu_{B\ reduced}$ of the chromophore are associated with the d-d transition of the catalytic center which is thought to regulate the downstream signaling effects involved (Karu 2010). The other pathway associated with the NIR interaction on mitochondria is the ATP extra synthesis. Excess generation of ATP in the cell is shown to significantly alter cellular metabolism in tetrodotoxin (TTX) treated primary cultured neurons (Wong-Riley, Liang et al. 2005) (Figure 14). TTX, a voltage dependant sodium channel blocker, decreases ATP demand, impedes neuronal impulses and down-regulates cytochrome *c* oxidase in primary cultured neurons. ATP thus acts not only as the energy currency of the cell but also as a critical molecule that can initiate downstream cell signaling. Specific receptor family that is directly activated by ATP – P2 family and the breakdown product adenosine-P1 family are identified (Burnstock 2009). These receptors and their subtypes (P2X, P2Y, P2Y2, P2Y11) are shown to mediate the beneficial effects of NIR PBM and low level light therapy (Karu 2010). ATP when binds to P2Y receptors initiates a cascade of molecular evens in the cell, increasing the intracellular Ca^{2+} ions which can in turn act as a positive effector molecule for mitochondrial function. The postulated molecular interaction of NIR photons with cytochrome oxidase initiates a cascade of secondary cell signaling pathways that activates transcription factors, alters gene transcription and enhances protein synthesis of antioxidants and other proteins creating a stable microenvironment for cell survival (Figure 13) (Desmet, Paz et al. 2006) (Whelan, Buchmann et al. 2003).

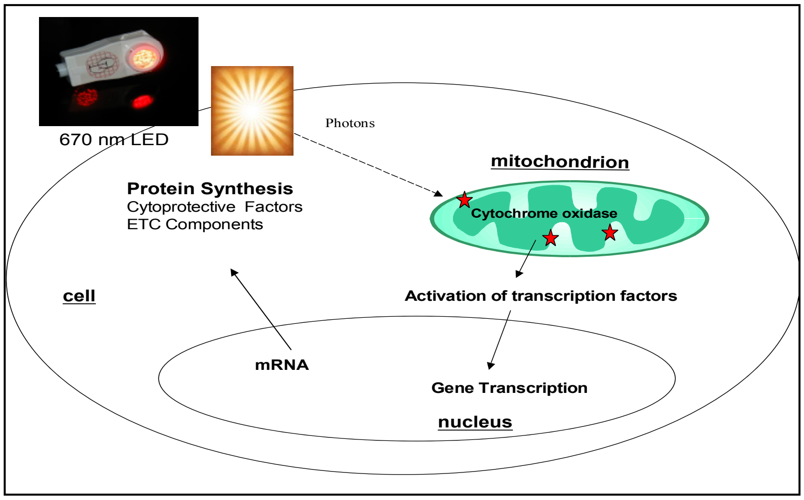

Figure 13 Hypothesized cell signaling events following photoabsorption/photoexcitation of cytochrome *c* oxidase by NIR photons

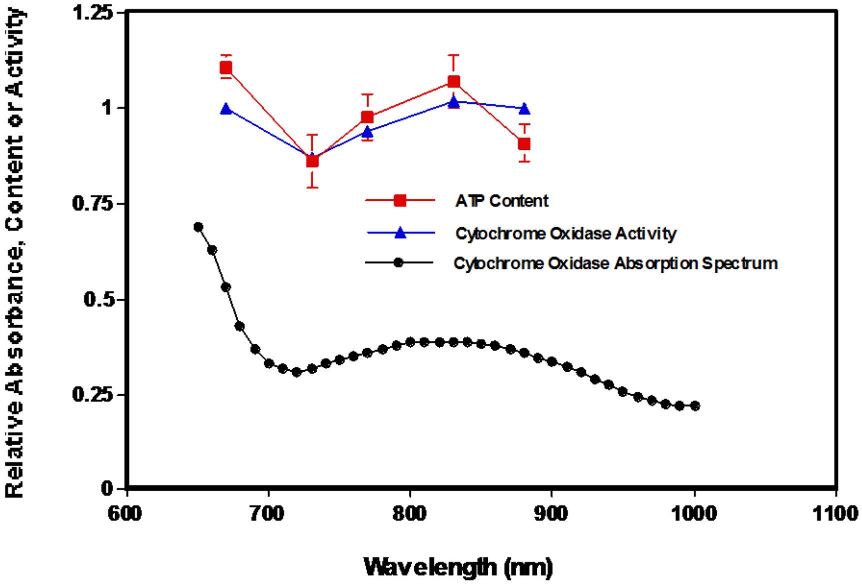

Figure 14 Activity of Neuronal Cytochrome Oxidase and Cellular ATP Correlates with Cytochrome Oxidase Action Spectrum. Reproduced from (Wong-Riley, Liang et al. 2005)

Mitochondrial retrograde signaling in NIR photobiomodulation

The mitochondrion plays a central role in the cell by mediating diverse cellular functions and integrating signals between the nucleus and the organelle. Mitochondrial retrograde signaling is defined as the one way communication between mitochondria and the nucleus that regulates many cellular functions in both normal as well as diseased states (Butow and Avadhani 2004). The possibility of retrograde mitochondrial signaling was established with NIR photobiomodulation when studies showed an increase in DNA and RNA synthesis in cultured cells when irradiated with a range of λ from 300 - 860nm, without a known chromophore in the nucleus that absorbs this range of λ.

The above possibility was reconfirmed by many investigators using cell proliferation as the model system because proliferation increases the adhesion of cells to a matrix, as well as the DNA and RNA synthesis rate (Ryan and Hoogenraad 2007). Current knowledge about mitochondrial retrograde signaling in NIR photobiomodulation (Figure 15) demonstrates that it is mediated via mitochondrial membrane potential ($\Delta\Psi m$), generation of ROS, altering the [Ca^{2+}] dynamics in the cell, and influencing NO binding to cytochrome *c* oxidase (Karu 2008). cDNA microarray study on fibroblasts irradiated with 628 nm light revealed that 111 genes of 10 functional categories were upregulated of which seven were directly or indirectly associated with the cell proliferation. The three other genes upregulated were associated with transcription factors, inflammation and cytokines (Zhang, Song et al. 2003). Mitochondrial retrograde signaling in general is considered to be both a stress response and an adaptive response of the cell. Investigators largely agree that the action associated with near-IR radiation on mammalian cells and tissues is mostly adaptive in nature. Changes in the dose and intensity of irradiation cause cyclic changes in the mitochondrial metabolic activity and the repose is characterized a bell shaped curve generalized in the Arndt-Schulz law.

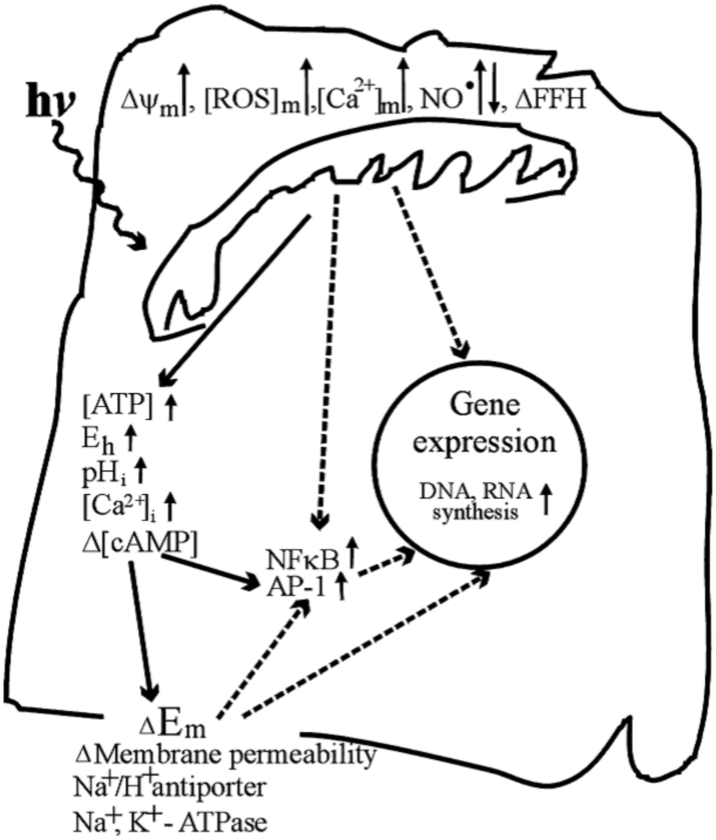

Figure 15 Putative mitochondrial retrograde signaling and other associated cellular events following photoabsorption by cytochrome *c* oxidase. (Reproduced from Karu 2008).

Experimental models using isolated mitochondria and whole cells irradiated with monochromatic radiation in the NIR range has been shown to affect $\Delta\Psi_m$ and stimulate ATP synthesis. Studies using He-Ne laser irradiation of melanoma cells induced a sudden increase in $\Delta\Psi_m$ and ATP concentration which was mediated via increased cytochrome *c* oxidase activity which in turn promoted the phosphorylation of Jun N-terminal kinase

(JNK) and activator protein-1 (AP-1) expression resulting in an increase in cell proliferation (Hu, Wang et al. 2007). Superoxide anion ($O_2^{\bullet -}$) generated in mitochondria as a result of oxidative phosphorylation is the primary ROS molecule that is capable of altering the retrograde signaling pathway which is established by its relevance in the up regulation of matrix metalloproteinase-1 (MMP-1) (Schroeder, Pohl et al. 2007). ROS generation was monitored at the single cell level in real time along with changes in $\Delta\Psi_m$, intracellular pH and [Ca^{2+}] after irradiation with 647 nm NIR photons (Alexandratou, Yova et al. 2002). Mitochondria are at the center of the crosstalk between Ca^{2+}, $\Delta\Psi_m$ and ROS which is referred as the love–hate triangle. An increase in intracellular [Ca^{2+}] is reported following irradiation with light of various wavelengths in mast cells, hepatocytes, isolated mitochondria and sperm cells (Karu 2008). This increase in intracellular [Ca^{2+}] is part of mitochondrial retrograde signaling leading to activation of calcineurin, which in turn leads to the activation of transcription factor NF-κB (Butow and Avadhani 2004).

Nitric oxide ($NO^{\bullet}$) is an important intramitochondrial signaling molecule and is generated in biological systems by nitric oxide synthases. NO directly binds to cytochrome *c* oxidase, modulates mitochondrial respiration (Cooper 2002) and is believed to induce mitochondrial retrograde signaling through altered $\Delta\Psi_m$. By inhibiting cytochrome *c* oxidase, NO not only interferes with the oxygen consuming ability of the cell but also alters the redox status of the respiratory chain and thus generates $O_2^{\bullet -}$ (Brookes, Levonen et al. 2002).

Coherent light sources like lasers are limited in their ability to deliver far-red to near-infrared light without producing thermal effects at the tissue interface. Moreover the narrow beam width makes it difficult to treat large areas using a laser. Non coherent sources like LED arrays were initially developed by NASA for experimental protocols in outer space. LED arrays can be tuned to generate light in the far-red to near-infrared range of the spectrum at optimal wavelengths and energy densities without producing any thermal effects. Light emitted by LED arrays at optimal wavelengths can penetrate skin and tissue to a depth of approximately 23 cm (Beauvoit, Kitai et al. 1994). Optimal wavelengths and energy densities necessary for therapeutic interventions have been characterized with NIR-LEDs. An energy density of 4 J/cm^2 has been shown to be effective at stimulating biological processes. Further, NIR-LED light therapy has been deemed a nonsignificant risk by the FDA and has been approved for use in humans (Desmet, Paz et al. 2006).

Mitochondrial dysfunction and oxidative stress is attributed to the pathogenesis of many retinal and optic nerve diseases including age-related macular degeneration, diabetic retinopathy and Leber's hereditary optic neuropathy (Barron, Johnson et al. 2001). Oxidative stress plays a central role in laser burn injury, methanol induced retinal toxicity and many other retinal degenerative diseases (Seme, Summerfelt et al. 1999). Our understanding of the genetic and molecular mechanisms of retinal degenerations and retinal injury are incomplete and no efficient therapeutic strategy to prevent or manage the degenerations does exist. The long term goal should improve mitochondrial function and attenuate oxidative stress. Although the majority of investigators agree that cytochrome *c* oxidase is the major mediator for the beneficial effects of NIR PBM, the role played by other cellular photoacceptors including cytochrome *b*, cytochrome *c*, catalase, nitric-oxide synthase and heme-containing proteins including neuroglobin require additional investigation.

Pilot experiments conducted in collaboration with other investigators have demonstrated that NIR-PBM administered during the critical period (P10-25) of photoreceptor cell loss in an established rodent model of retinitis pigmentosa, the P23H-3 rat, increases retinal mitochondrial cytochrome oxidase activity and protects against apoptotic photoreceptor cell death. These findings demonstrate the promise of NIR-PBM as a potential non-invasive therapy for the treatment of RP. These preliminary findings also call for a more thorough understanding of both the efficacy and mechanism of this therapeutic approach over the disease course. Studies proposed in this dissertation will test the therapeutic benefit of NIR PBM in the treatment of RP using this established and well-studied animal model of disease which are essential before NIR PBM can be translated to clinical trials for the treatment of RP and other retinal dystrophies.

Rationale for the Comparison of 670nm vs. 830 nm light

The optical window for effective tissue penetration of red to near infrared radiation allows researchers to postulate that possible specific biological effects of irradiation happens between λ=600 and λ=1000nm. Results from our lab demonstrated that the irradiation of retinae and optic nerve *in vitro* at λ=670 nm provided retinoprotection by increasing the survival and functional recovery of photoreceptors after an acute injury (Eells, Henry et al. 2003). Following our study many investigators demonstrated similar retinoprotective and neuroprotective effects with λ=670 nm in both *in vivo* animal models and *in vitro* culture systems (Wong-Riley, Liang et al. 2005) (Rojas, Lee et al. 2008). Karu's laboratory, among others, has shown that the mitochondrion is the target organelle in photobiomodulation and comparative spectral analysis revealed that cytochrome oxidase acts as a photoacceptor molecule. In many *in vitro* models studied, two peaks in the action spectrum of cytochrome oxidase following photon irradiation were observed at 670 nm and at 830 nm which prompted many researchers to focus on these two wavelengths to identify the cellular mechanisms involved in PBM (Karu 2008).

There is a growing interest in the use and safety of low level light and laser for traumatic brain injury and neurodegenerative diseases (Zivin, Albers et al. 2009). A non-invasive transcranial application of 808-nm low level light therapy given 4 h following traumatic brain injury in a rodent model significantly decreased the lesion volume and preserved neurobehavioral function (Oron, Oron et al. 2012). Using similar light sources, investigators have shown an increase in cortical tissue ATP content following embolic strokes in rabbits (Lapchak and De Taboada 2010). A recently published study compared the efficacy of both λ=670 nm and λ=810-nm laser treatment in a traumatic brain injury model and showed that the neurologic severity score decreased by 21% in 670nm and 32% in 810nm treated group when compared to that of the controls (Qiuhe Wu et. al, Proc. of SPIE Vol. 7552 755206-1).

The above findings led us to conduct a pilot experiment using both 670 nm and 830 nm in rodent model of inherited retinal degeneration, P23H transgenic rat. The findings from this experiment demonstrated that 830 PBM treatments using LED monochromatic light source produced a more robust retinoprotective effect in the P23H rats treated from p10-p25 when tested at p30 than the 670 nm treatment for the same intensity. Based on these data we propose to examine the retinoprotective efficacy of both 670 nm and 830 nm LED treatment in P23H transgenic rat.

CHAPTER 2

PRELIMINARY DATA AND SPECIFIC AIMS

PRELIMINARY DATA

Mechanistic studies from our lab and other investigators have demonstrated that NIR photons interact with cytochrome oxidase, in mitochondria, triggering signaling mechanisms which result in increased efficiency of the electron transport chain (ETC), improved mitochondrial energy metabolism, up regulation of cytoprotective genes and improved cell survival in various *in vitro* and *in vivo* disease models (Eells, Wong-Riley et al. 2004).

NIR PBM attenuates the loss of photoreceptors in the P23H rat during the 'critical period' of photoreceptor degeneration.

Photoreceptor death in different P23H strains exhibits a specific pattern. Photoreceptor death is excessive during the early developmental stages (p10-p25) which is referred as the 'critical period' of photoreceptor degeneration in this dissertation (Figure 16).

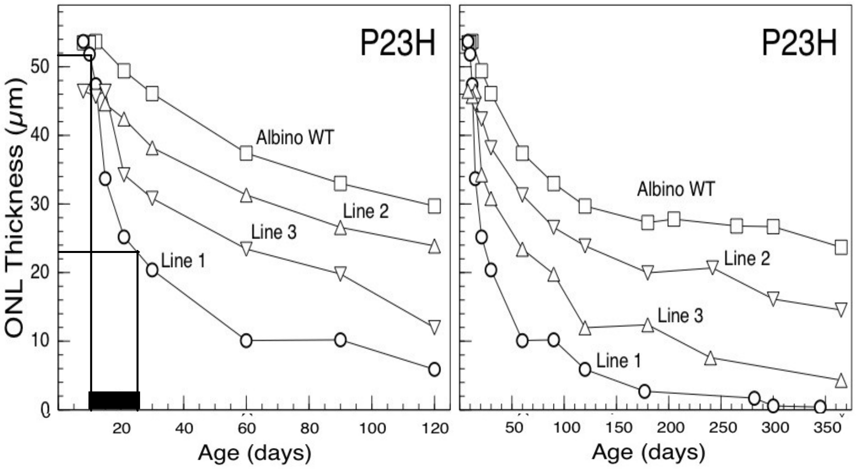

Figure 16 Comparison of degeneration rates of ONL in three different lines of P23H rhodopsin transgenic rat strains with control animal. (Reproduced and modified from http://www.ucsfeye.net/mlavailRDratmodels.shtml to highlight the 'critical period').

Published work from our lab has shown that NIR PBM is retinoprotective against toxin-induced damage, and recent studies have demonstrated that NIR PBM can attenuate photoreceptor cell death by 70% during the critical period of photoreceptor development (Figure 17) in the P23H-3 rat indicating that NIR PBM can alter the underlying pathology during the developmental stages of the retina (Eells, Wong-Riley et al. 2004). Our hypothesis is that oxidative stress is generated in P23H photoreceptors due to reduced oxygen utilization by inactive mutant rod photoreceptors resulting in outer retinal hyperoxia which generates ROS (Stone, Maslim et al. 1999; Yu, Cringle et al. 2004).

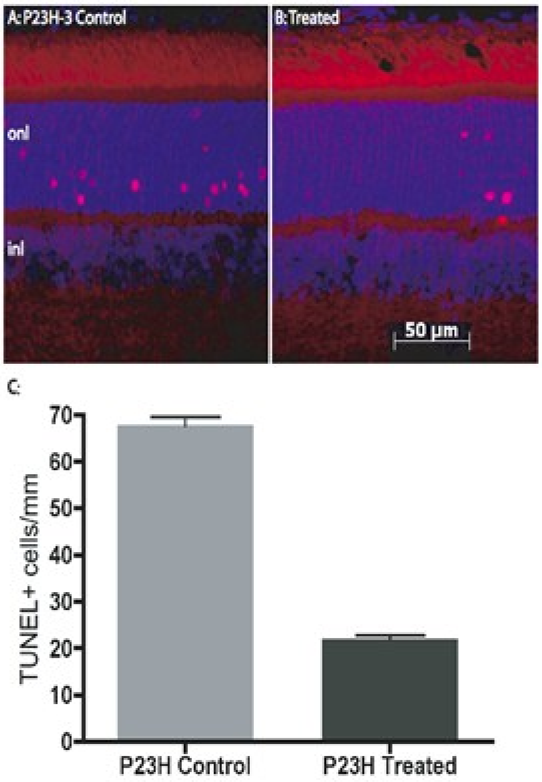

Figure 17 Photoreceptor cell death by apoptosis is demonstrated in P23H retina by TUNEL+ cells and following NIR PBM there is a significant reduction (greater than 70%) in the number of TUNEL+ cells in the ONL.

ROS thus generated can cause posttranslational modification of thiol groups of enzymes and transcription factors, leading to the activation of proapoptotic pathways, thus affecting the photoreceptor survival particularly during early development. PBM acts to improve mitochondrial function and to increase antioxidant protection (Geller, Krowka et al. 2006). PBM-induced improvement of mitochondrial function would increase oxygen consumption in the P23H retina and reduce oxygen tension and thus reduce oxygen toxicity (Stone, Maslim et al. 1999). Secondly, it is thought that the PBM-induced increased production of cytoprotective factors and antioxidants would act in concert to protect the retina from apoptotic photoreceptor cell death. NIR-PBM administered during the critical period of photoreceptor development in the P23H-3 rat is neuroprotective.

Photobiomodulation increases cytochrome oxidase concentrations in the P23H retina.

In vitro studies in our laboratory and by other investigators have shown that NIR PBM improves photoreceptor oxidative metabolism by increasing mitochondrial cytochrome oxidase activity and upregulating key antioxidant protective enzymes, cofactors and neurotrophic factors in the retina, culminating in a significant attenuation of apoptotic photoreceptor cell death (Karu 1999; Eells, Wong-Riley et al. 2004; Ying, Liang et al. 2008). As shown in Figure 18, NIR PBM significantly increased the concentration of cytochrome oxidase in the retina of the P23H-3 rat. Density profiling of retinal layers for specific cytochrome oxidase immunolabeling shows increased labeling density in the inner segments of the photoreceptor cells, which is consistent with the higher mitochondrial density in the inner segments of photoreceptors. These findings are consistent with the *in vitro* observations and support our hypothesis that upregulation of cytochrome oxidase activity is a critical component in the neuroprotective actions of NIR PBM. Our hypothesis is further supported by studies showing that increased cytochrome oxidase activity improves respiratory efficiency under conditions of oxidative stress, thus attenuating the production of reactive oxygen species (Campian, Qian et al. 2004).

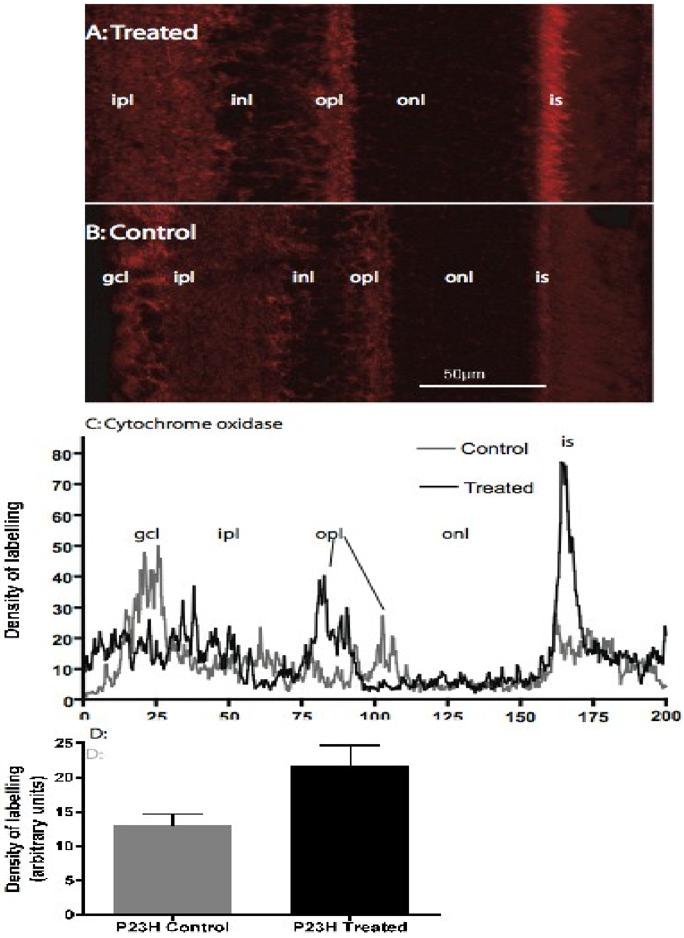

Figure 18 A significant up regulation of cytochrome oxidase activity in the inner segments of photoreceptor cells following NIR PBM is demonstrated by density profiling (n = 6, p < 0. 001)

Photobiomodulation up-regulates cytoprotective enzymes in the P23H retina. Photoreceptor cell death by mitochondrial dysfunction, generation of reactive oxygen species and apoptosis are common in human retinal dystrophies and degenerations and light-induced retinal degeneration in animal models (Carmody and Cotter 2000). (Stone, Maslim et al. 1999). NIR-PBM not only increases cytochrome oxidase activity and oxidative capacity in the photoreceptors but also increases the concentrations of a critical neuroprotective factor in the retina, the mitochondrial form of superoxide dismutase, MnSOD (Figure 19). Overexpression of MnSOD in the retina has been shown to protect the retina against oxidative damage (Kanwar, Chan et al. 2007). Early AMD like characteristics are manifested in animal models with reduced retinal expression of MnSOD.

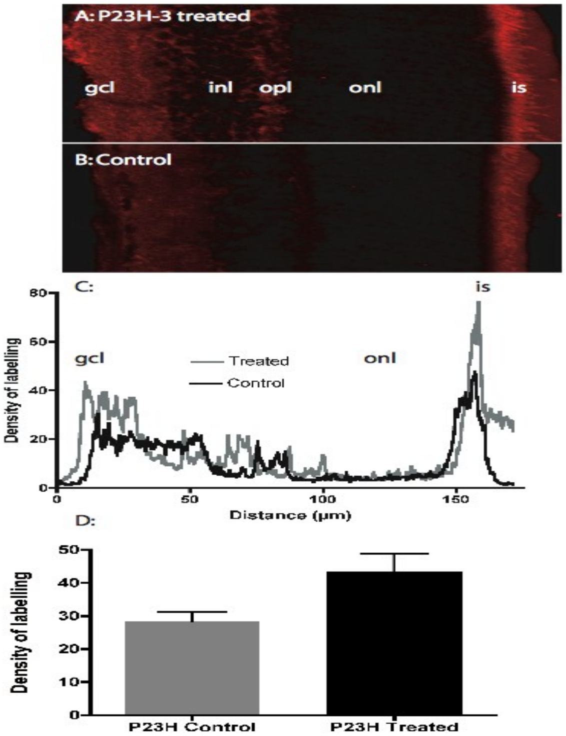

Figure 19 NIR PBM upregulates mitochondrial form of superoxide dismutase, MnSOD, in the inner segments, which can protect the degenerating retina from oxidative damage.

In summary, these preliminary data demonstrated that NIR-PBM treatment administered once per day for 5 days during the critical period of photoreceptor cell loss (p10-p25) in the P23H-3 rat increases retinal mitochondrial cytochrome oxidase activity, up regulates the production of antioxidant protective enzymes and attenuates apoptotic photoreceptor cell death.

These preliminary data obtained in collaboration with Diana Kirk, Krisztina Valter, Ph.D, and Jonathan Stone, Ph.D. (Australian National University and Sydney University) support our hypothesis and set the stage for more detailed studies described below.

SPECIFIC AIMS, RATIONALE AND DESIGN

Specific Aim 1: To investigate the effect of NIR photobiomodulation in a non-dystrophic (SD) animal.

Specific Aim 2: To determine if NIR photobiomodulation can protect photoreceptors against damage induced by the P23H transgene and compare the efficacy of 670 nm vs. 830 nm PBM using three different treatment protocols.

Three NIR-LED treatment paradigms will be tested.

a) The first treatment protocol will determine if NIR PBM can rescue photoreceptor function during the critical period of photoreceptor development. In these studies, immature P23H rats will be treated once per day with 670 nm-LED or 830 nm-LED (4 J/cm^2) during the critical period (p10-25). Retinal function (mixed and cone electroretinography responses), *in vivo* retinal imaging and histomorphometric analysis will be determined at p30.

b) In the second treatment protocol, immature P23H rats will be treated once per day with 670 nm or 830 nm -LED (4 J/cm^2) from the onset of the critical period of photoreceptor cell death to young adulthood (p10-p40). The efficacy of NIR PBM will be assessed at p45 by measurement of retinal function, *in vivo* retinal imaging and photoreceptor cell loss as above. These studies will determine if a longer treatment protocol will improve photoreceptor protection and retinal function compared with a limited treatment protocol.

c) In the third treatment protocol, we will determine if photobiomodulation can rescue remaining photoreceptors and preserve retinal function in young adult rats in which the majority of rods have degenerated. For these studies young adult P23H rats (P20) will be treated once per day with 670 or 830 nm nm-LED (4 J/cm^2) from p20 to p40 and we will examine the efficacy of photobiomodulation at p50 as described above.

Rationale and design for Specific aim 2: The P23H rhodopsin transgenic rat is a model of autosomal dominant retinitis pigmentosa in which photoreceptor degeneration especially the rod degeneration begins as early as p10. The ONL thickness decreases from approximately 46µm from p10 to 22µm by p25 which is considered as the critical period of photoreceptor degeneration in this model (Yu, Cringle et al. 2004). Rod degeneration is nearly complete by p60. The first two experimental designs will investigate the therapeutic potential of NIR-PBM during the critical period (p10-p25) and from critical period to young adulthood (p10-p40). The third design will investigate the potential of NIR-PBM to rescue remaining photoreceptors and preserve retinal function after the majority of rods have degenerated.

Specific Aim 3: To investigate the cellular changes underlying the protection provided by NIR photobiomodulation.

These studies will test the hypothesis that NIR-PBM will stimulate photoreceptor bioenergetics by up regulating retinal cytochrome oxidase expression and will also up regulate antioxidant protective pathways and neuroprotective factor production.

The experiments described in specific aim 2 will characterize the effects of NIR-PBM on RP. The functional biochemical and molecular studies will provide information on the mechanism(s) by which NIR-PBM protects retinal function. These experiments are fundamental in determining the potential of NIR-PBM as a therapeutic approach in the prevention and treatment of retinal dystrophies and retinal degenerative disease. The results of this research may provide the essential information required to initiate an investigation into the clinical use of NIR-PBM as an innovative and noninvasive therapeutic approach.

Rationale and design for specific aim 3: Oxidative stress and mitochondrial dysfunction play vital roles in the pathogenesis of photoreceptor cell death in retinal degeneration. These studies will test the hypothesis that NIR-PBM will improve mitochondrial function and attenuate oxidative stress in the P23H rat.

CHAPTER 3

MATERIALS AND METHODS

ANIMAL MODEL

All animal experiments have been approved by the Institutional Animal Care and Use Committee (IACUC) and were conducted in accordance with the ARVO (The Association for Research in Vision and Ophthalmology) statement for the use of animals in ophthalmic and vision research and with the National Institutes of Health regulations.

Heterozygous P23H transgenic rats, the offspring of P23H homozygotes and Sprague-Dawley (SD) albino rats (Harlan Sprague Dawley, Madison, WI) were used as the model of retinal degeneration. The original P23H homozygotes were obtained from Retinal Degeneration Rat Model Resource at University of California, San Francisco.

This model was selected for the following reasons:

(1) It is a widely studied model of retinal dystrophy, allowing us to integrate and compare our findings with those of other investigators (Walsh, van Driel et al. 2004) (Yu, Cringle et al. 2004) (Machida, Kondo et al. 2000).

(2) Several neuroprotective strategies have been investigated in the P23H rat, facilitating a comparison with the efficacy of PBM (Leonard, Petrin et al. 2007) (LaVail, Yasumura et al. 2000)

(3) The time course of photoreceptor degeneration in the P23H rat is relatively short, enabling us to evaluate the efficacy of photobiomodulation within a few months and to modify treatment protocols depending on our findings.

Housing conditions and light management

All animals were bred and housed in an American Association for Accreditation of Laboratory Animal Care (AAALAC) approved animal facility at the University of

Wisconsin-Milwaukee. Animals were supplied food and water ad libitum and maintained in a temperature and humidity-controlled environment under dim cyclic light, 12-hour light/12-hour dark cycle, with an average illuminance of 5 to 10 lux inside the cage.

NIR LIGHT EMITTING DIODE ARRAY AND TREATMENT PROTOCOL

A monolithic array of custom fabricated (λ=670nm and λ=830nm) Light Emitting Diodes (LED) engineered to eliminate heat (Hybrid GaAlAs, Quantum Devices, Inc., Barneveld, WI) and designed to emit diffused monochromatic light at specific wavelength of photon energy were used to deliver light at a desired energy density. The LEDs are shielded by a glass barrier and are unlensed, allowing for even dispersion of light over a 180° viewing angle (Figure 20). This allows each LED chip to act as a point source, providing a high degree of illumination uniformity. The hybrid lamp housing contains the ceramic substrates on which LED arrays are assembled, acting as a heat sink. A fan is mounted on the opposite side of the light source to keep the monolithic system running cool. The LED arrays are factory calibrated for proper LED wavelength and intensity before use.

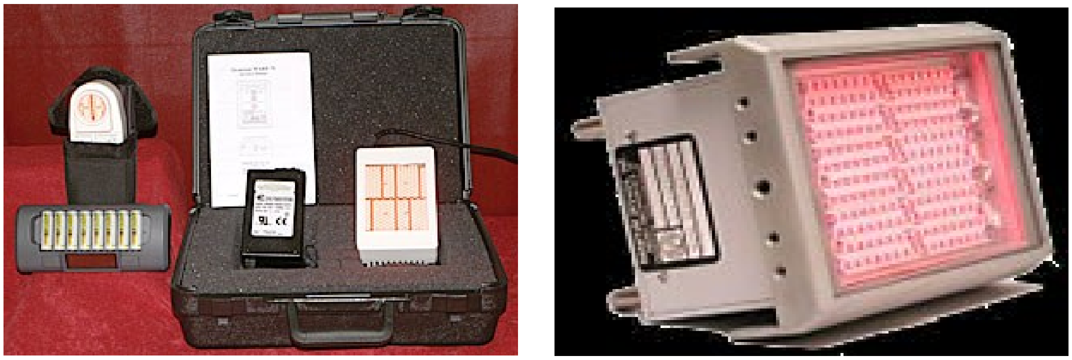

Figure 20 LED arrays used for delivering NIR photons. WARP 75 LED Unit (Left); $\lambda = 670 \pm 20$ nm; Surface Energy: 60mW/cm^2; Fluence ~5.4J /cm^2. SpectraLife LED Hybrid Lamp (Right); λ=830nm ± 10 nm; Surface Energy: 50mW/ cm^2; Fluence ~4.5 J/cm^2

Immature and young adult P23H-1 transgenic rats were hand-held by the investigator or placed in a plexiglass restraint device and the WARP 75 or SpectraLife LED Hybrid Lamp were positioned directly over the animal's head at a distance of 2 cm exposing both eyes (Figure 21). Sham-treated SD rats were handled in the same way, except that they were not exposed to the LED array. These treatment protocols have been used with both immature and adult rodents and are well tolerated by the animals. Treatment consisted of irradiation at 670 nm for 90 sec at a power intensity of 50mW/cm^2, resulting in an energy density of 4.5 joules/cm^2 at the surface of the cornea or irradiation at 830 nm for 180 sec at a power intensity of 25mW/cm^2, resulting in an energy density of 4.5 joules/cm^2 at the surface of the cornea. These stimulation parameters have been previously demonstrated to stimulate cell survival and cytochrome oxidase activity in cultured neurons, to promote wound healing clinically and in experimental animal models to promote the survival and functional recovery of the retina and optic nerve *in vivo* after acute injury by a mitochondrial toxin and to exhibit neuroprotective actions in the retinae of P23H rats

(Liang, Whelan et al. 2006) (Ying, Liang et al. 2008) (Desmet, Paz et al. 2006) (Whelan, Buchmann et al. 2003) (Eells, Henry et al. 2003).

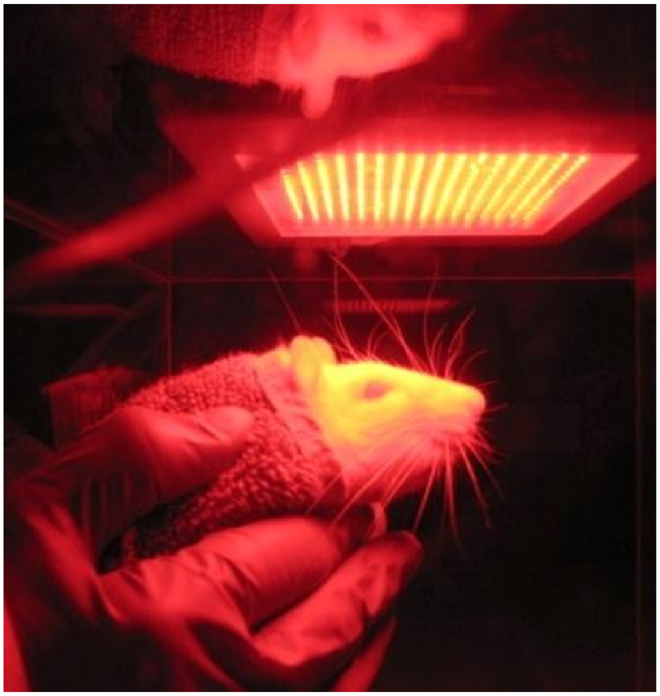

Figure 21 Exposure of animals to NIR photons. Animals were habituated to the restraint apparatus and handling from p5. Monochromatic LED source is placed directly over the animal's head at a distance of 2 cm exposing both eyes.

ASSESMENT OF STATUS OF RETINA

To evaluate the therapeutic efficacy of 670 nm and 830 nm PBM, the status of the retinae was assessed by measuring well established indices of photoreceptor function, photoreceptor morphology and by a new measurement of retinal oxidative metabolism

Photoreceptor function will be assessed by

Full-Field Flash Electroretinography

Animal preparation

The function of the retina was monitored using full-field flash electroretinography (ERG), which measures the electrical impulses emitted by the retina in response to flashes of light. Animals were dark adapted for at least 2 hours prior to recording and were prepared under red dim light. Animals were anesthetized with an intraperitoneal injection of xylazine- ketamine hydrochloride cocktail (5 mg/kg and 100 mg/kg respectively). Pupils were dilated with 0.1% atropine and mild topical anesthesia was applied on the eyes. Animals were placed on a heating pad to maintain the body temperature at 37°C during the entire recording time. Full-field ERGs were obtained using Handheld Multi-species ElectroRetinoGraph (HMsERG) Instrument (Retvet Corp, MO).

Photostimulator

The Mini-Ganzfeld half-sphere bowl is 76 mm in diameter, and has a 55 mm circular aperture (Figure 23). This is illuminated with white LEDs, which have a rated color temperature of around 7000^0 K and flash intensities ranging from 10 mcd.s/m^2 to 30 cd.s/m^2. Flash intensity is set by a combination of flash time (from 5 microseconds to 5 milliseconds) and LED peak current. The white light flash intensity in the Ganzfeld dome is protocol dependent. The individual tests set the flash intensity from 10 mcd.s/m^2 to 25000 cd.s/m^2 and the flash duration runs from 0.005 to 5 msec. Any required background illumination can also be set. The photostimulator is intended to be used close to the animal's eye (between 1 and 2cm).

Placement of electrodes and ERG recording

A nylon coated gold thread electrode was placed on the corneal surface, overlaid with 1% methylcellulose and a small drop of methylcellulose was placed into the concave side of the contact lens before it was placed over the thread electrode. The corneal contact lens will be adjusted so that it was centered on the retina. Stainless steel needle ground electrode was inserted on top of the head (midline). Stainless steel needle reference electrodes were inserted subcutaneously on either side of the base of the ear. Needle electrodes were secured with surgical tape (Figure 22). Signals obtained from the corneal surface were amplified, digitized and averaged using ERG view 2.5 software (Retvet Corp, MO). This software allows for low pass filtering of the final ERG test waveforms before they are graphed on the unit. This filter can be used to remove environmental and unit generated noise from the observed ERG. A custom designed Faraday cage was employed block 60 cycle electrical noise. The amplitudes and latencies of the a-waves (photoreceptor responses,) and b-waves (bipolar cell and Muller cell responses) were fit to a computational model to determine transduction parameters for photoreceptor responses(Figure 24 & 25).

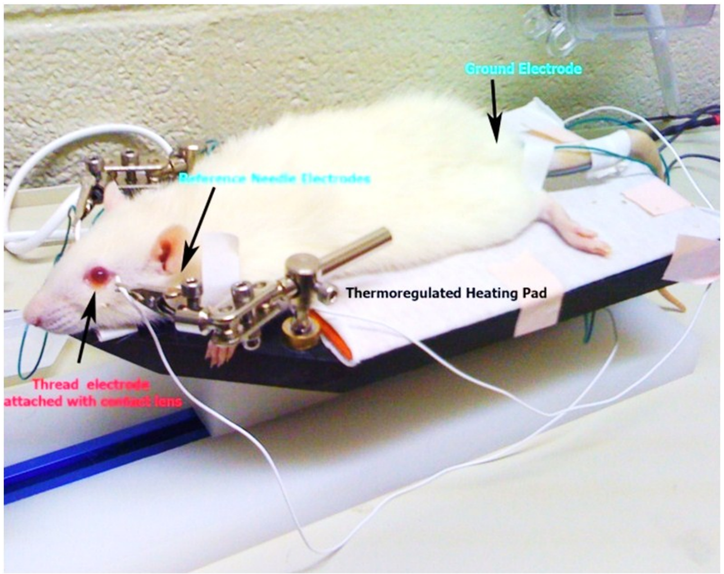

Figure 22 Animals were dark-adapted, anesthetized, pupils dilated and placed on a thermoregulated heating pad at 37°C during recordings.

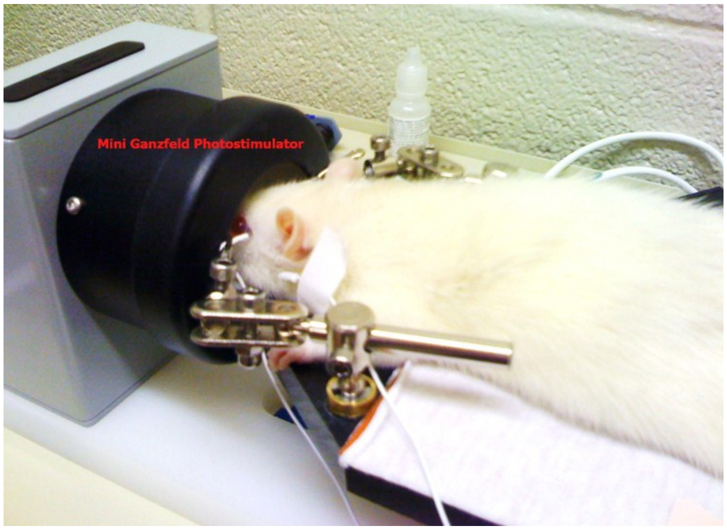

Figure 23 Full-field ERGs were obtained in a Mini-Ganzfeld half-sphere bowl. Flash intensities are generated with white LEDs and duration of the each flash is test dependent.

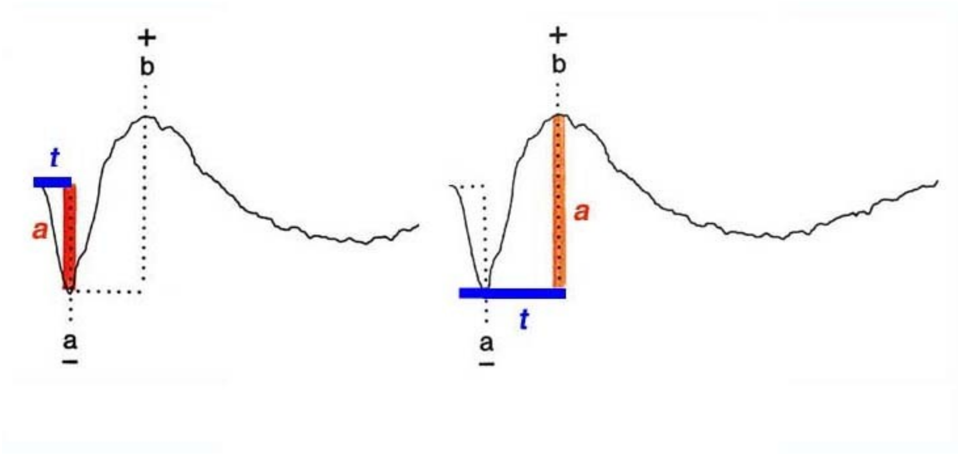

Figure 24 A normal biphasic ERG waveform showing a-wave and b-wave amplitude and corresponding implicit times. Reproduced from www.webvision.med.utah.edu. The a-wave reflects the physiological activity in the photoreceptors of the outer retina and the b-wave corresponds to the electrical responses from the inner retinal layers including the ON bipolar cells and the Muller cells (Miller and Dowling 1970).

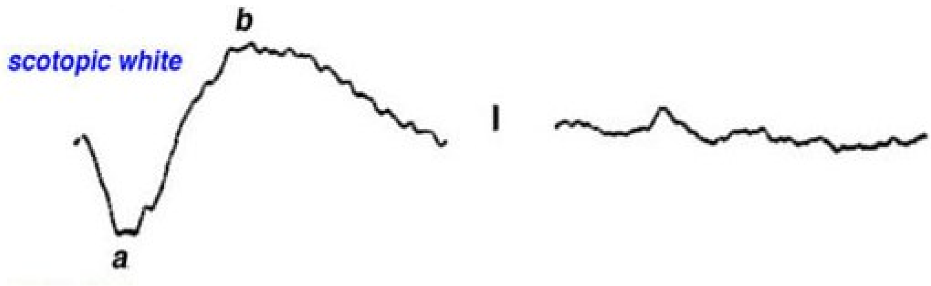

Figure 25 Comparison of a-wave and b-wave amplitude obtained from a normal subject (left) and from a patient with RP. Reproduced from www.webvision.med.utah.edu

Due to the high number of rods in the rodent retina compared to cones, the ERG response following a white flash of light is predominantly the rod photoreceptor response. The flash intensity, number of flashes and its rate and the exposure time can be manipulated so that the rod and cone photoreceptor function can be isolated. Two well established protocols are used in this dissertation.

Scotopic intensity series protocol

This protocol gives the best estimate of the functional status of the retina using increasing flash intensities over a fixed time period (Table 1). The resulting scotopic intensity response curves were plotted and compared between treated and sham control animals.

Action	Flash intensity		Number of flashes Avg'd	Interval seconds	Action time Seconds	Elapsed Time Seconds
	Log	mcd.s/m2				
Test 1	-1.5	100	4	10	40	40
Delay					60	100
Test 2	-1	300	4	10	40	140
Delay					60	200
Test 3	-0.5	1000	4	10	40	240
Delay					60	300
Test 4	0	3000	4	10	40	340
Delay					60	400
Test 5	0.5	10000	1			400
Delay					60	460
Test 6	~1.0	25000	1			460
Delay						
	Total Time Elapsed in Minutes					7.7

Table 1 Protocol for scotopic intensity series electroretinography (Reproduced and modified from HMsERG user manual).

International Society for Clinical Electrophysiology of Vision (ISCEV) protocol

To tease out individual and combination of photoreceptor response, ISCEV recommended protocol is used (Table 2). Varying the flash intensity, duration and rate of stimulation after dark adaptation and background adaptation (with 30000 mcd.s/m^2 intensity for 10 minutes) will help to isolate rod response as well as cone photoreceptor response.

ERG test Session	Flash intensity		Number of flashes Avg'd	Interval seconds	Action time Seconds	Elapsed Time Seconds
	Log	mcd.s/m2				
Dark Adaptation	ISCEV recommends 20 Minutes					
Rods	-2.5	10	10	2	18	18
Delay			4	2	2	20
Std.Rods & Cones	0	3000		10	30	50
Delay			4		30	80
Hi.Int.Rods & Cones	0.5	10000		20	60	140
BG adaptation	1	30000			600	740
Cones with BG	0	3000	32	0.5	15.5	755.5
Delay w/BG					2	757.5
Hi Cones with BG	0.5	10000	32	0.5	15.5	771
Delay with BG					2	773
Std.Flicker w/BG	0	3000	128	0.032	4.192	777.2
Delay with BG					2	779.2
Hi.Int. Flicker w/BG	0.5	10000	128	0.032	4.192	783.4
Total time elapsed in Minutes						13.06

Table 2 ISCEV protocol for electroretinography. The animals are dark adapted for 20 minutes before the procedure. The ISCEV protocol includes 7 standardized individual tests as recommended by the ISCEV (Reproduced and modified from HMsERG user manual).

Retinal Morphology will be assessed by Spectral Domain Optical Coherence Tomography (SD-OCT) imaging

Optical coherence tomography is a non-invasive optical imaging technique that uses low coherence interferometry to create high resolution, cross-sectional, two and three dimensional tomograms of biological tissue *in vivo* (Drexler, Morgner et al. 2001). OCT is extensively used in ophthalmology to understand retinal and corneal morphology to help early diagnosis and detection of ocular pathologies, when treatment is most promising. Specific advantages of OCT include excellent depth (axial) and lateral resolution, which allows finer anatomical details of the retina to be observed (Figure 26).

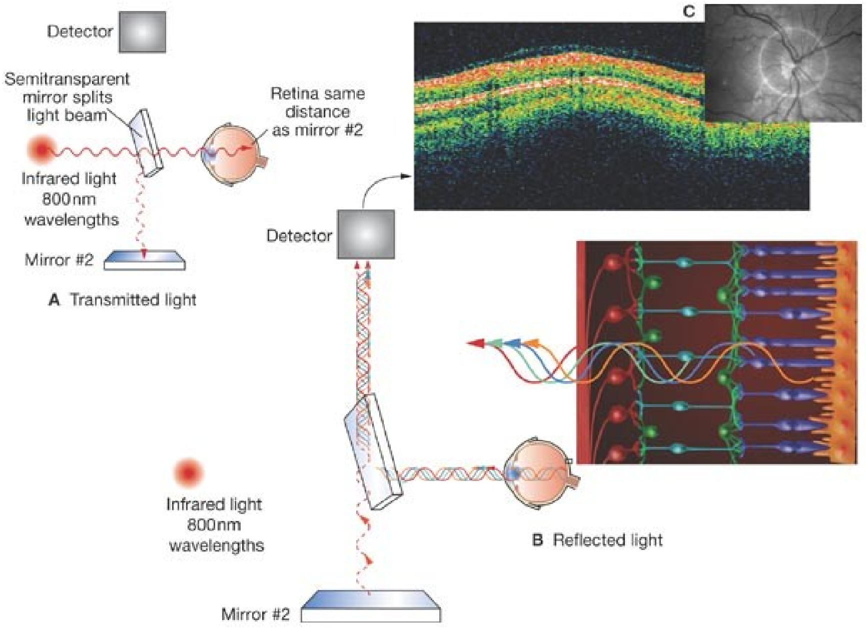

Figure 26 Set up of an OCT system for retinal imaging. The light source is typically a broad band source and the light (λ~ 800nm) is split into half by a beam splitter and sent to a reference arm and the sample arm. The backscattered light is reflected back from the sample arm and reference arm combines forming an interference pattern. This spectrum is detected via a spectrometer placed as the detector and an algorithm is used to reconstruct an A –scan which represents the anatomical features of retina. Multiple A-scans are used to generate B-scan and

multiple B-scans are used to generate 3D volume scans. (Reproduced and modified from Frohman, Fujimoto et al. 2008).

Animal Imaging Mount and Rodent Alignment System

Before the animal is anesthetized for imaging, the Animal Imaging Mount (AIM) and Rodent Alignment System (RAS) are aligned with the long axis of animal cassette with laser. Once the long axis of the laser and the cassette are along the same z-axis, an aiming tip is placed at the end of the bore and adjustments are made to achieve the "Magic Point" for aiming. The "Magic Point" is referred to as the intersection of 3 axes which are Cassette center line, Optical axis of the imaging probe and the Cassette swivel axis (Figure 27).

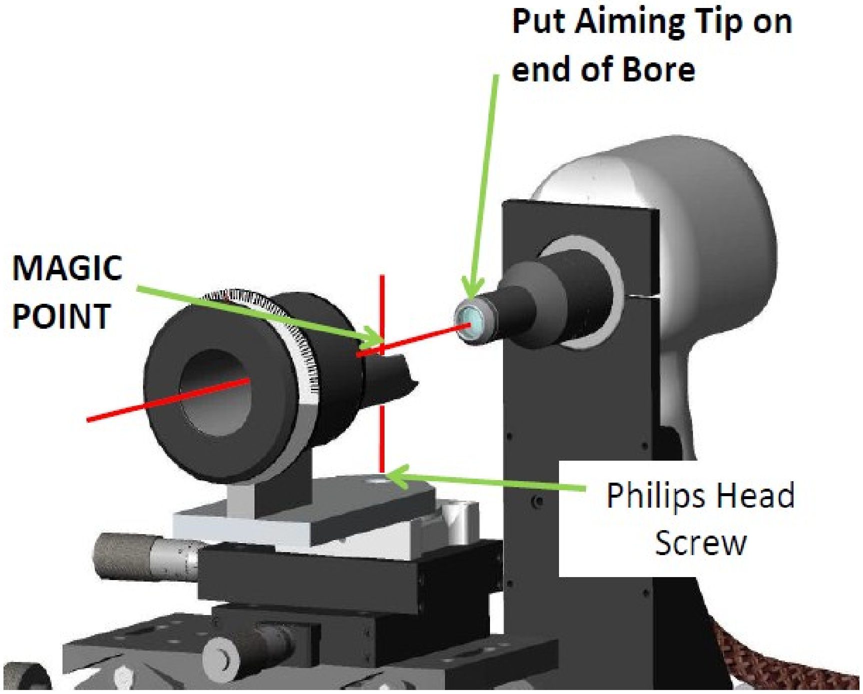

Figure 27 Aligning the AIM-RAS to achieve the "Magic Point" for aiming (Reproduced and modified from Bioptigen's Guide to Small Animal Imaging: Optimizing Image Quality presentation by Joseph Vance).

Animal preparation

Animals were anesthetized by an intraperitoneal injection with a ketamine and xylazine mixture (50:5 mg/kg body weight) and the pupils are dialated with 1% atropine sulphate ophthalmic solution. After one minute hydrate the cornea with sterile Systane Ultra Lubricant Eye Drops (Polyethylene Glycol 400, 0.4% and Propylene Glycol 0.3%; Alcon Labs). Systane Ultra offers the right balance of viscosity and optical properties, and the corneal surface is hydrated every 2 minutes during the entire period of anesthesia to prevent dryness and opacities arising from exposure keratopathy. Lubricant is wicked away before acquiring an image to have high image quality. Both eyes were imaged in a single session by mounting the animal with a bite bar on a custom made six-axis rodent alignment system. The bite bar is laterally and ventrally adjusted to align the animal eye with the "Magic Point" for aiming (Figure 28).

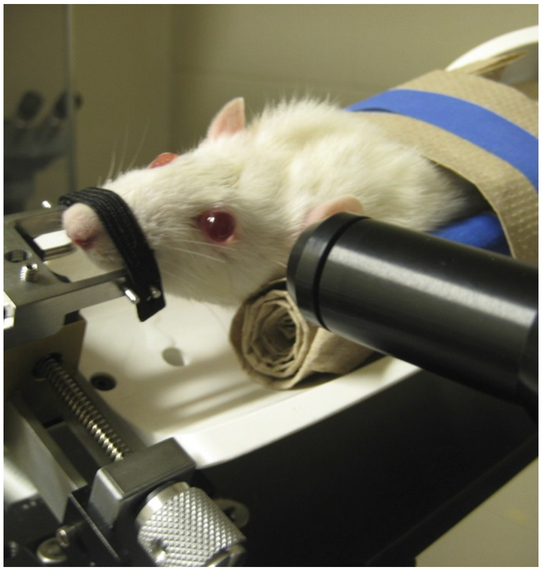

Figure 28 Animal Imaging Mount and Rodent Alignment System with bite bar. The bite bar helps to reproduce alignment of the rodent eye and suppress motion artifacts from breathing.

The fundus imaging camera in the animal imaging mount provided initial alignment for the light source during the real time aiming. The Optic Nerve Head (ONH) will be used as a landmark and the alignment of the OCT optics with the retina usually is done with a 'Fast Fundus' scan (200x100x1.6x1.6x1x1). This scanning allows the user to get real-time feedback on the location from volume intensity projection (VIP) as user adjusts the cassette. After positioning the ONH, aiming mode was used to adjust the image brightness and contrast. Two linear scans at1000x80x1 (0 degree and 90 degree) and 2 volume scans at 750x250x1x1 (0 degree and 90 degree) per eye were captured and saved using the Bioptigen's InVivoVue^{TM} software. The linear scans were exported from the OCT machine and read into ImageJ (http://www.rsb.info.nih.gov/ij/) for processing. A rigid body registration is performed using the ImageJ plug-in "StackReg". The frames that have motion artifacts were removed subjectively before averaging to prevent surrounding frames from causing distortion. Averaging also removes large amount of speckle noise contained in individual OCT scans. The averaged scans from P23H and SD animals were used for segmentation of retinal layers for total retinal thickness (Figure 29) using algorithm generated in MATLAB (Mathworks, Natick, Massachusetts, USA).

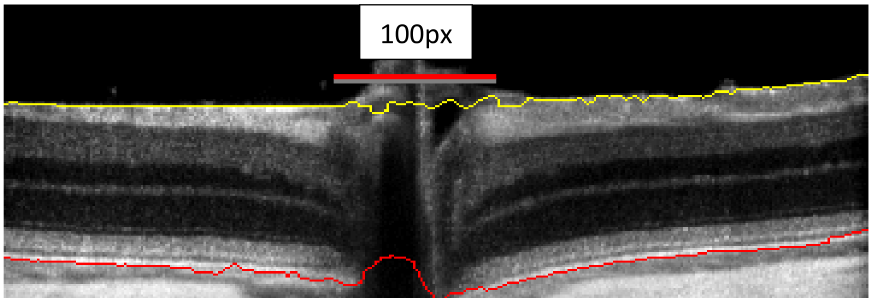

Figure 29 Representative image (line scans 1000x80x1samplings) centered on the ONH, showing the segmentation lines for automated segmentation for Total Retinal Thickness. 100 pixels (px) are removed at the ONH manually to account for variable thickness in this region.

Automated segmentation generates retinal thickness over the entire B-scan and a 100 pixel correction was used in the final average thickness to account for variable thickness in this region. The difference in reflectivity of retinal layers was explored in generating longitudinal reflectivity profiles (LRP) (Figure 30) for individual layers from the averaged scans using ImageJ at fixed locations from the 100 pixel area as demonstrated in Figure 31.

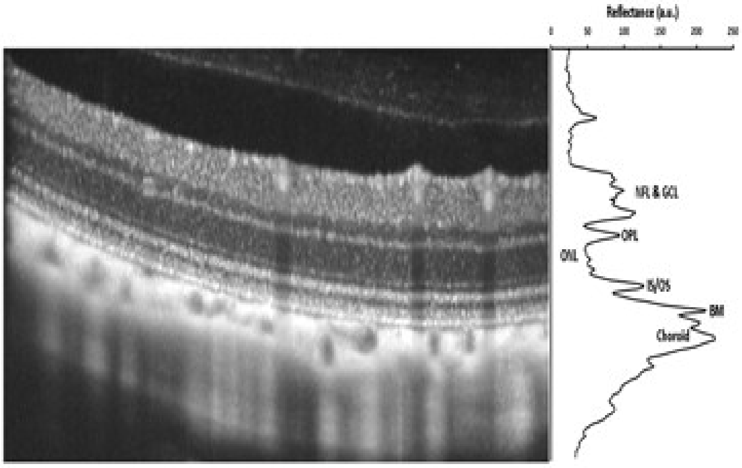

Figure 30 Longitudinal Reflectivity Profile (LRP) and the corresponding individual retinal layers (Nerve Fiber Layer; NFL & Ganglion Cell Layer; GCL, Outer Plexiform Layer; OPL, Outer Nuclear Layer; ONL, Inner Segment/Outer Segment; IS/OS, Retinal Pigment Epithelium; RPE and Choroid)

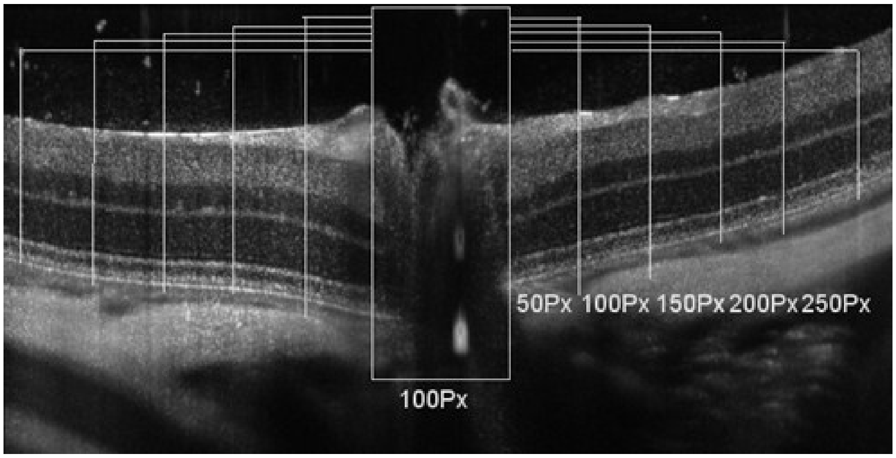

Figure 31 Method used to generate spider plots for ONL thickness from averaged OCT scans.

Quantitative Morphometric Analysis: Measurement of ONL thickness

ONL thickness was measured as previously described (Komeima, Rogers et al. 2007) . At the defined time points, animals were euthanized with an overdose of sodium pentobarbital (>60 mg/kg, intraperitoneal). One eye from each animal was prepared for histological and immunohistochemical evaluation. The retina dissected from the other eye was collected in Trizol for molecular analysis. The eyes for histology and immunohistochemistry were marked at the superior position (in the corneal limbus) using a surgical cautery and eyes were removed and embedded either in paraffin, plastic or optimal cutting temperature compound (Tissue-Tek OCT Compound ,Sakura Finetek USA , Inc.) depending upon the parameters investigated. The Ten-micrometer sections will be cut perpendicular to the 12:00 meridian through the optic nerve. The sections were stained with Harris hematoxylin and eosin (Fisher Scientific, Pittsburgh, PA), Toluidine blue and was placed in mounting medium and examined with a Olympus Axioskop microscope (40x objective). The images were digitalized and analyzed with ImageJ by outlining the ONL and then measuring the ONL thickness at three locations (100 µm, 200 µm and 300 µm) on the superior pole of the optic nerve and three locations (100 µm, 200 µm and 300 µm) on the inferior pole of the optic nerve as described (Usui, Komeima et al. 2009).

Photoreceptor protection was assessed by

Measurement of Surviving photoreceptors: The number of surviving photoreceptors was quantified by the thickness of the ONL and by counting the rows of nuclei in Toluidine blue stained resin sections, and a comparison analysis was made with the

SDOCT images at the same location. The number of cells observed in the outer nuclear layer (ONL), inner nuclear layer (INL) and ganglion cell layer (GCL) were counted and recorded separately for each 1mm distance from the ONH and a spider graph was plotted.

Experimental Design and Methodology for Aim 2: To investigate the effect of PBM on mitochondrial function in the P23H retina.

Retinal metabolic state was assessed by Cryo Optical Imaging

Fluorescence imaging provides specific information on tissue using intrinsic fluorophores or exogenous tagged proteins. Since some of the molecules in the cell act as intrinsic fluorophores and are able to fluoresce when excited with the appropriate wavelength, a growing field of fluorescence microscopy techniques relies on autofluorescent fluorophores. Fluorescence-based techniques are widely used in biomedical applications as diagnostic tools for early detection of various diseases such as cancers or heart disease (Ranji, Jaggard et al. 2006). Optical fluorescence techniques have the potential to diagnose tissue metabolic states in intact organs. These techniques are widely used in biomedical applications and have been shown to have a high sensitivity and specificity for discriminating between diseased and non-diseased tissue (Richards-Kortum, Mitchell et al. 1994) (Wagnieres, Star et al. 1998).

Oxidative phosphorylation in the mitochondria provides photoreceptors with adequate amounts of ATP for the high energy demanding phototransduction process, and mitochondrial metabolic coenzymes Nicotinamide Adenine Dinucleotide (NADH), and Flavin Adenine Dinocleotide ($FADH_2$) are the primary electron carriers in oxidative phosphorylation. NADH and FAD (the oxidized form of $FADH_2$) are autofluorescent and can be monitored without exogenous labels through the use of optical techniques. These coenzymes are beneficial in that NADH is primarily fluorescent in its reduced biochemical state, whereas FAD is only fluorescent in its oxidized form. Therefore, by imaging these two coenzymes, we can probe the oxidative state of the metabolism in tissue. The fluorescent signals of these intrinsic fluorophores have been used as indicators of tissue metabolism in injuries due to hypoxia, ischemia, and cell death (Ranji, Kanemoto et al. 2006). The normalized ratio of these fluorophores, (NADH/FAD), called the NADH redox ratio (NADH RR), acts as a novel marker of the mitochondrial redox and metabolic state of tissue ex vivo and in vivo (Maleki, Sepehr et al. 2012).

Sample Preparation: Freezing and embedding

The rats were sacrificed, and their eyes were harvested and frozen rapidly for low temperature cryoimaging. The eyes were embedded in a black mounting medium as shown in Figure 32 and scanned by the cryoimager in 500 slices each 10 µm apart through the whole eye.

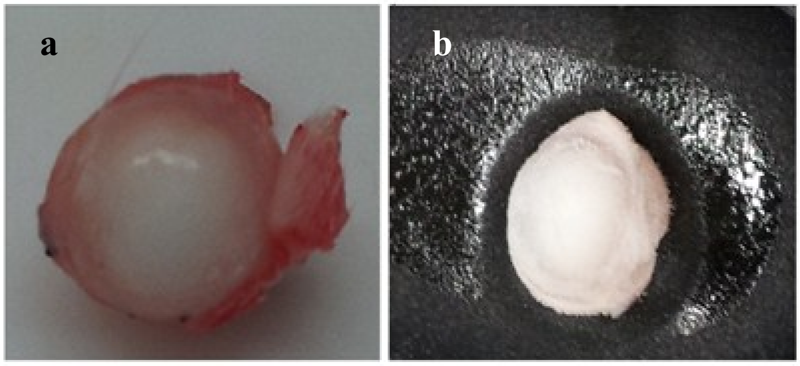

Figure 32 (a) frozen eye and b) embedding frozen eye in customized mounting medium.

Calibration

A calibration method was designed to compensate for day-to-day variation of light intensity and non-uniformity of the illumination pattern. At the beginning of each experiment and before slicing the tissue, a uniform fluorescent flat plate was placed in the same position as tissue and imaged in all channels to acquire the illumination pattern. Since the fluorescence of the standard is in both the NADH and FAD channels, it also accounts for day-to-day light intensity and uniformity changes in all channels. All the images in each channel were then normalized by dividing each image to the flat plate image, captured in the same channel.

Cryoimager

Figure 33 shows the schematic for the 3D cryoimager used in this study. The cryoimager is an automated image acquisition and analysis system consisting of software and hardware designed to acquire fluorescence images of tissue sections. A motor-driven microtome sequentially sections frozen tissue at the desired slice thickness while filtered light from a mercury arc lamp excites up to five distinct fluorophores in the exposed surface of the tissue block. The excitation light source is a 200W mercury arc lamp filtered at the excitation wavelengths of NADH and FAD, 336 nm and 470 nm, respectively. The emission wavelengths are 520 nm and 450 nm for FAD and NADH, respectively. At each slice, a CCD camera records fluorescence images of the tissue block in pixel dimensions of 10 μm × 10 μm to be later analyzed for fluorophore distribution. The microtome is housed in a freezer unit that maintains the sample at -80°C during sample slicing and image acquisition. The resolution in the z direction of microtome slices can be as small as 5 um. For this study, we used a resolution of 10 um in the z direction, which resulted in ~ 400 z-slices per eye.

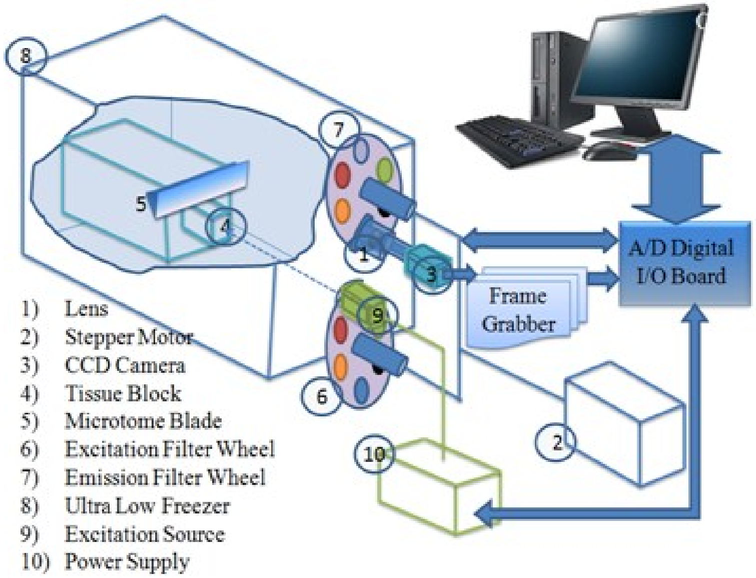

Figure 33 Schematic representation of a Cryoimager. This device sequentially slices the tissue, imaging the surface between each successive slice, in as many as 5 channels. The images are then displayed and saved to a computer, where they can be processed to create a 3-D rendering of the tissue.

Data analysis

FAD and NADH autofluorescence images (containing 250 slices per eye) from each group of eyes were processed using Matlab. The composite images were created using all the image slices for each eye, for both NADH and FAD signals. The ratio of NADH and FAD, known as the NADH redox ratio (Sepehr, Staniszewski et al. 2012), was calculated voxel by voxel, using Matlab, according to equation (1).

$$\textbf{Redox Ratio} = \textbf{RR} = \textbf{NADH} / \textbf{FAD} \qquad \textbf{(1)}$$

The 2D representation of each eye was then calculated using the maximum intensities in the z axis of the NADH redox 3D volume (max projection). In the maximum projection method, first a full 3D volume of images was obtained, including RR, and then the maximum projection on the volumetric data was performed and the histograms were plotted for this maximum projection. The maximum projection is used since the entirety of the anatomy has a significant contribution in this representation. A histogram of the max projection of RR values in each group was created, and the mean (or first moment) of this histogram was calculated according to Eq. (2).

$$Mean = \frac{1}{N_x \times N_y} \sum_{i=1}^{N_x} \sum_{j=1}^{N_y} eye\_Maxpro(i, j) \qquad \textbf{(2)}$$

Where Nx and Ny are the number of pixels in the x and y directions and the pixel size in x and y is 10µm and 10µm. The previously mentioned histograms were calculated for quantitative comparison between normal and diseased groups.

Statistical Analysis

Sample size for the experiment will be determined by power analysis. The data obtained from the study will be analyzed using SPSS. All values will be expressed as means ± SEM. A mixed model ANOVA (Greenhouse-Geisser correction was performed whenever the assumption of sphericity was violated), MANOVA, 1-way ANOVA (Kruskal-Wallis test) and Student's t-test performed, as appropriate. Statistical analysis was performed using SPSS 19.0 (SPSS Inc, Chicago, IL) and GraphPad Prism 4.0 (GraphPad, La Jolla, CA USA). The level of significance for all statistical tests was set at 0.05

CHAPTER 4

EFFECT OF NIR PHOTOBIOMODULATION IN NON - DYSTROPHIC ANIMAL MODEL

Many studies with PBM have shown that in the absence of pathology, there is no physiological action of the light. Moreover, our previous studies on methanol and light induced toxicity models of retinal degeneration demonstrated the lack of any significant effect of NIR treatment on normal, healthy and non-challenged retinal physiology. Natoli et al. (2010) demonstrated by wide-scale gene analysis that NIR treatment resulted in the up regulation of many noncoding RNAs (ncRNA) (Natoli, Zhu et al. 2010). The inability of ncRNAs to translate to a functional protein may explain the cellular effects of NIR PBM in a non-dystrophic retina. Follow up studies are needed to characterize the exact role of these ncRNAs in the mammalian retina. Albarracin et al. suggested a possible hypothesis that the up regulated ncRNAs in the above animal models following NIR PBM may not have any significant function in the healthy retinal cellular environment but may be acting as a pre-conditioning event in the retina leading to altered regulation of potentially damaging genes in the presence of stress stimuli, as seen in induced or inherited retinal degenerations (Albarracin, Eells et al. 2011).

Studies were performed to characterize the role of NIR-PBM during the early phase of photoreceptor development in non-dystrophic SD animal at both 830 nm and 670 nm.

830 nm photobiomodulation does not alter retinal function in non-dystrophic SD rats.

Figure 34 and Figure 35 summarizes the average a-wave and b-wave amplitudes measured by dark-adapted full-field flash ERG using the scotopic intensity series protocol. In agreement with the previously published data from our lab and other colleagues 830 nm PBM in a non-challenged retina does not alter retinal function.

The main effect of mean ERG amplitudes between non-dystrophic SD and 830nm treated non-dystrophic SD rats for a-wave ($F_{(1,14)}$ = .627, p = .442; Figure 34) and for b-wave ($F_{(1,14)}$ = .122, p = .733 ; Figure 35).

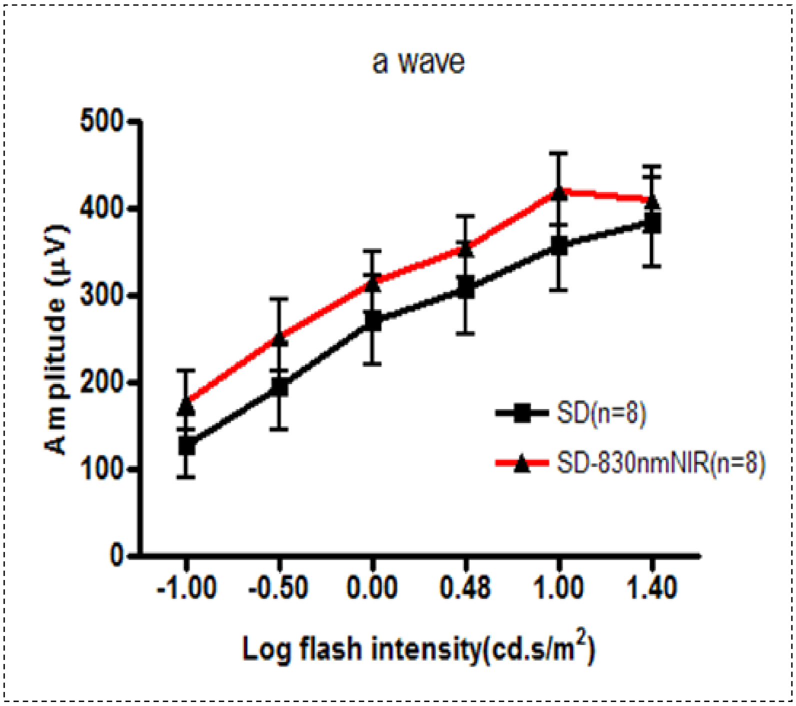

Figure 34 shows the comparison of mean a-wave amplitude between SD normal control (■; n=8) and 830nm treated SD normal control (▲; n=8) groups. The a-wave represents the functional electrical activity recorded from the photoreceptors and reflects the general health of the photoreceptor layer of the retina. The main effect between groups were not statistically significant ($F_{(1,14)}$ = .627, p = .442) between groups at various flash intensities. Error bars: SEM.

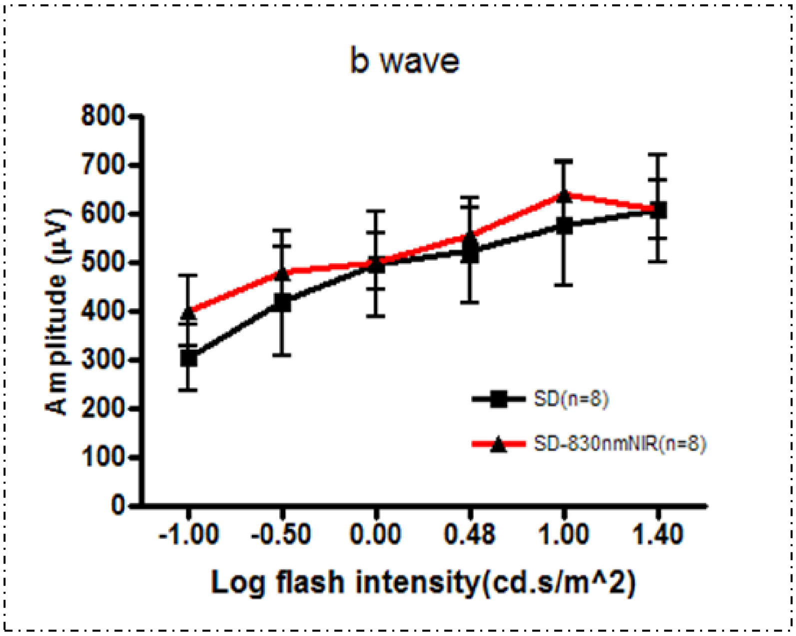

Figure 35 shows the comparison of mean b-wave amplitude between SD normal control (■; n=8) and 830nm treated SD normal control (▲; n=8) groups. The b-wave represents the functional electrical activity post synaptic to photoreceptors and reflects the health of the inner layers of the retina. The main effect between groups were not statistically significant ($F_{(1,14)} = .122$, $p = .733$) between groups at various flash intensities. Error bars: SEM.

Figure 36 and figure 37 summarize the mean a- wave and b- wave implicit times for the above scotopic intensity series protocol.

The main effect of mean ERG implicit times between non-dystrophic SD and 830nm treated non-dystrophic SD rats for a-wave ($F_{(1,14)} = 1.14$, $p = .302$; Figure 36) and for b-wave ($F_{(1,14)} = 4 .12$, $p = .062$; Figure 37).

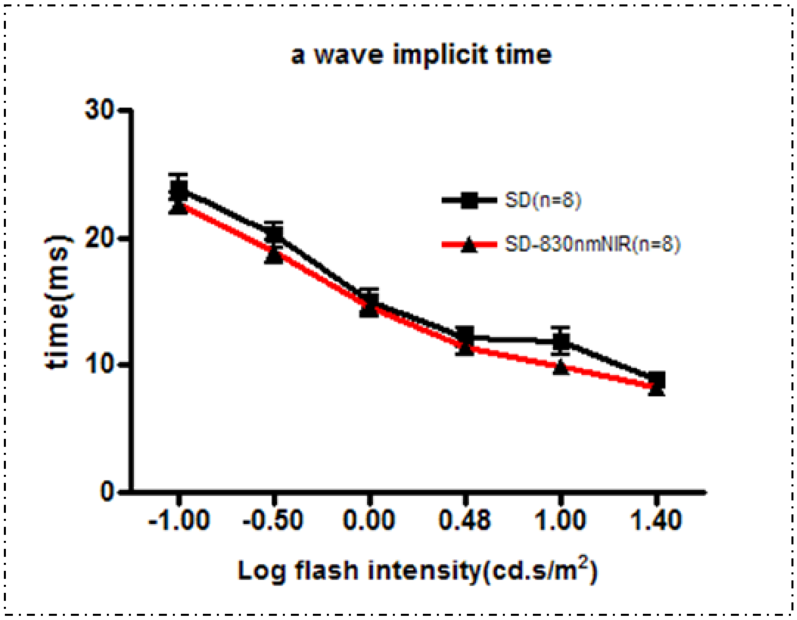

Figure 36 shows the mean a-wave implicit time comparing SD normal control (■; n=8) and 830nm treated SD normal control (▲; n=8) groups. The a-wave implicit time represent s the time from flash onset to the trough of the a-wave. There was no significant difference ($F_{(1,14)} = 1.14$, *p* = .302) between groups at various flash intensities. Error bars: SEM

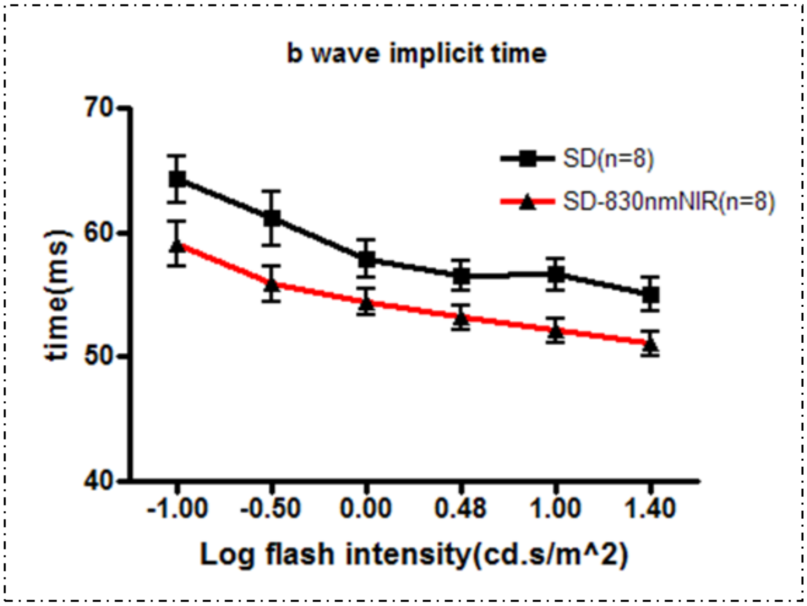

Figure 37 shows the mean b-wave implicit time comparing SD normal control (■;

n=8) and 830nm treated SD normal control (▲; n=8) groups. The b-wave implicit time represents the time from flash onset to the peak of the b-wave. There was no significant difference ($F_{(1,14)}$ = 4 .12, p = .062) between groups at various flash intensities. Error bars: SEM

670 nm photobiomodulation does not alter the retinal function and retinal morphology in non-dystrophic SD animal.

Figure 38 and figure 39 show the average a-wave and b-wave amplitudes assessed by dark-adapted full-field flash ERG using scotopic intensity series protocol comparing non-dystrophic SD and 670nm light treated non-dystrophic SD rats. Similar to our findings with 830 nm PBM, 670 nm PBM did not alter retinal function or retinal morphology in the non-dystrophic retina.

The main effect of mean ERG amplitudes between non-dystrophic SD and 670 nm treated non-dystrophic SD rats for a-wave ($F_{(1,10)}$ = .039, p = .848; Figure 38) and for b-wave ($F_{(1,12)}$ = .147, p = .708 ; Figure 39).

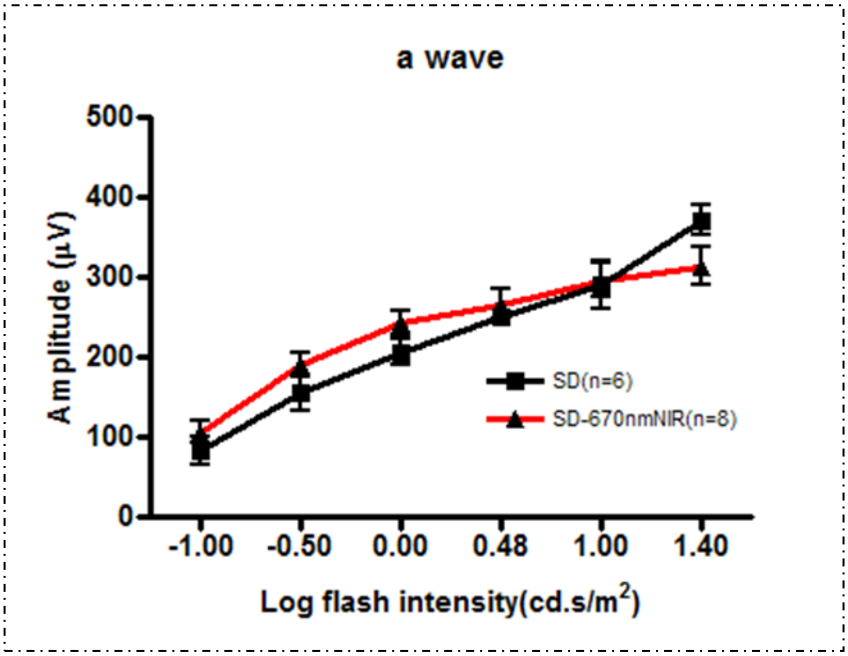

Figure 38 shows the comparison of mean a-wave amplitude between SD normal control (■; n=6) and 670 nm treated SD normal control (▲; n=8) groups. The a-wave represents the functional electrical activity recorded from the photoreceptors and reflects the general health of the photoreceptor layer of the retina. The main effect between groups were not statistically significant ($F_{(1,10)}$ = .039, *p* = .848) between groups at various flash intensities. Error bars: SEM

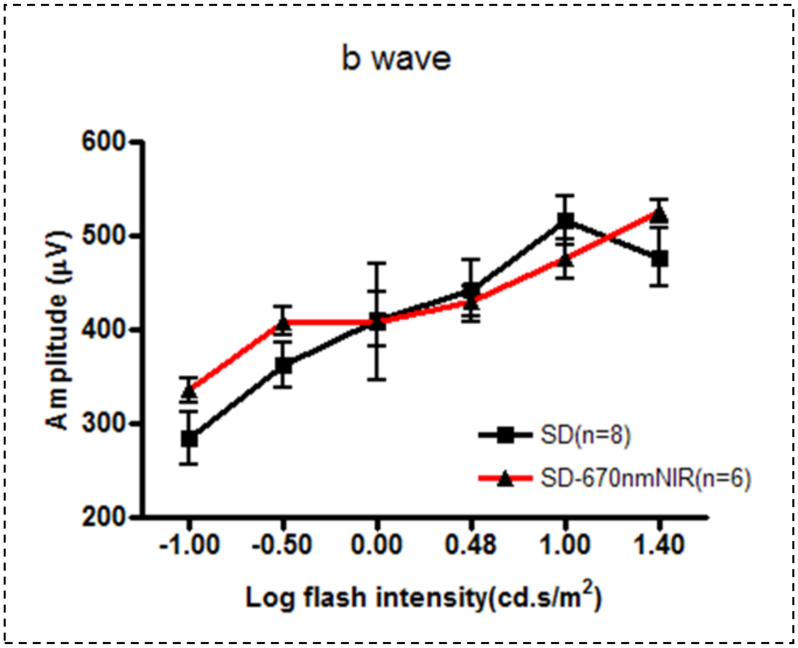

Figure 39 shows the comparison of mean b-wave amplitude between SD normal control (■; n=8) and 670 nm treated SD normal control (▲; n=6) groups. The b-wave represents the functional electrical activity post synaptic to photoreceptors and reflects the health of the inner layers of the retina. The main effect between groups were not statistically significant ($F_{(1,12)}$ = .147, *p* = .708) between groups at various flash intensities. Error bars: SEM.

Figure 40 and Figure 41 summarize the mean a- wave and b- wave implicit times for the above scotopic intensity series protocol .

The main effect of mean ERG implicit times between non-dystrophic SD and 670 nm light treated non-dystrophic SD rats for a-wave ($F_{(1,14)}$ = .103. , *p* = .752; Figure 40) and for b-wave ($F_{(1,14)}$ = 2.31, *p* = .151 ; Figure 41)

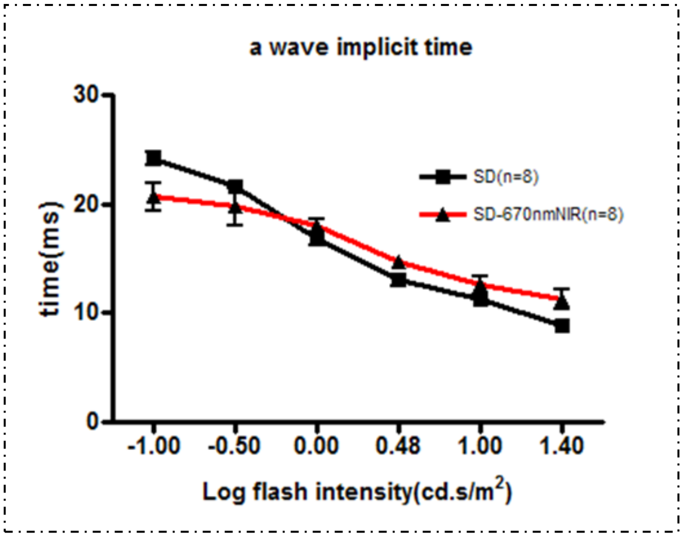

Figure 40 shows the mean a-wave implicit tine comparing SD normal control (■; n=8) and 670 nm treated SD normal control (▲; n=8) groups. The a-wave implicit time represent s the time from flash onset to the trough of the a-wave. The main effect between groups were not statistically significant ($F_{(1,14)}$ = .103. , *p* = .752) at various flash intensities. Error bars: SEM.

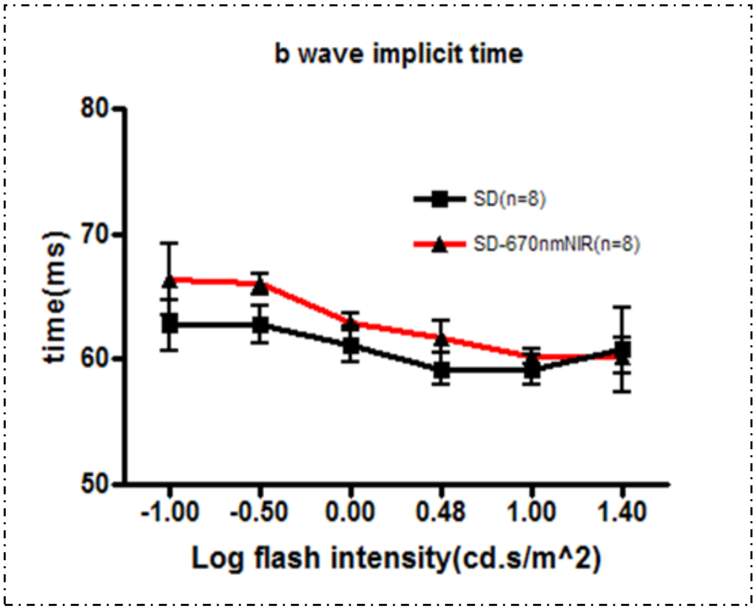

Figure 41 shows the mean b-wave implicit time comparing SD normal control (■;

n=8) and 670 nm treated SD normal control (▲; n=8) groups. The b-wave implicit time represents the time from flash onset to the peak of the b-wave. There was no significant difference ($F_{(1,14)} = 2.31$, $p = .151$) between groups at various flash intensities. Error bars: SEM

Total retinal thickness was quantified in non-dystrophic SD and 670 nm light treated non-dystrophic SD rats using SD-OCT and the mean total retinal thickness (Figure 42) was not significantly different between the groups (SD: 174.2 ± 2.3 µm, n=4 vs. SD-670: 181.0 ± 2.4 µm, $p<.05$)

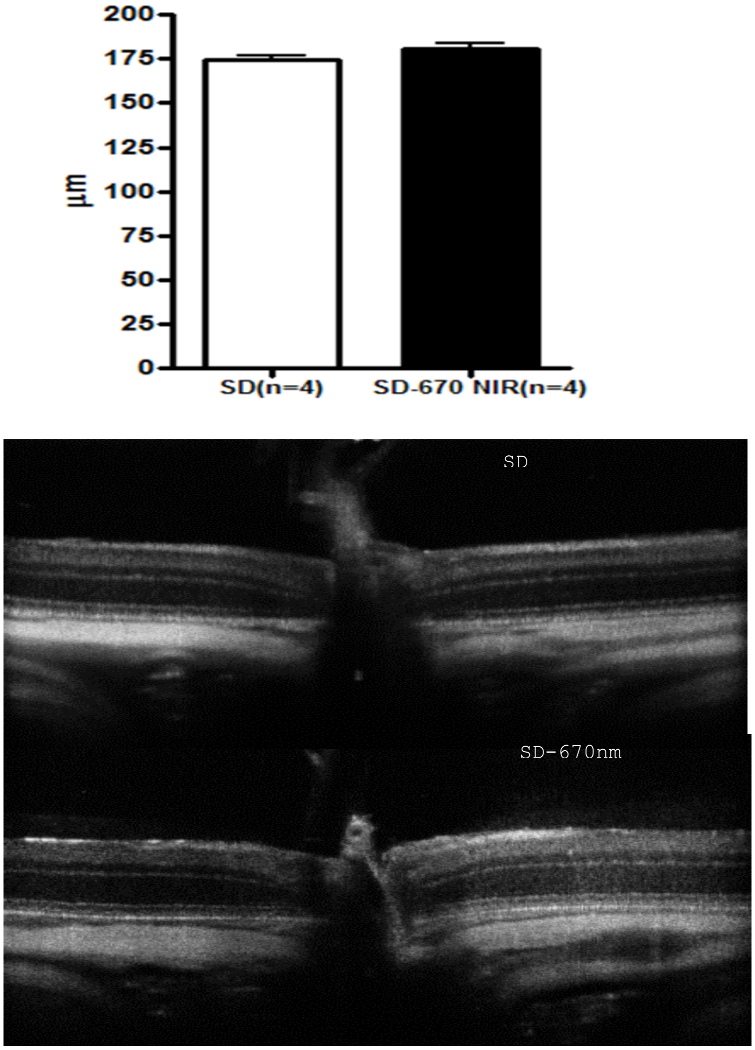

Figure 42 shows the average total retinal thickness (upper panel) generated from SD-OCT linear scans (n=4) between non-dystrophic SD animals and 670 nm treated SD animals. Lower panel shows the representative linear scans at the same location on the retina (ONH used as the landmark) comparing non-dystrophic SD animal and 670 nm treated SD animal and there was no significant difference in the retinal morphology or structural integrity of retina following 670 nm NIR-PBM. Error bars: SEM

In summary 830 nm and 670 nm photobiomodulation did not alter the functional response or the structural integrity of retina in a non-dystrophic control animal. These findings are important with respect to both animal and human safety considerations. This is a crucial piece of evidence for a comprehensive FDA approval for the use of NIR-LED devices in control populations in clinical trials for the treatment of retinal degenerative diseases.

CHAPTER 5

MITOCHONDRIAL REDOX IMAGING

[This Chapter is submitted to be considered for publication in the Journal of Biomedical Optics and the authors assign(s) to Society of Photo-Optical Instrumentation Engineers (SPIE) copyright ownership in the work presented in this Chapter, effective if and when the Paper is accepted for publication by SPIE and to the extent transferable under applicable national law]

Introduction

Irreversible loss of rod photoreceptors is the outcome of abnormal physiology associated with mutated or absent gene products and leads to blindness in many retinal degenerative disorders, including retinitis pigmentosa (RP). RP is a large genetically heterogeneous group of inherited retinal degeneration characterized by progressive and neurodegenerative photoreceptor apoptosis with subsequent degeneration of the cone photoreceptors and the retinal pigment epithelium (RPE) cells (Besch, Jagle et al. 2003; Sancho-Pelluz, Arango-Gonzalez et al. 2008). RP is the leading cause of inherited retinal degeneration-associated blindness in the developed world (Hartong, Berson et al. 2006). To date 52 genes are known to be associated with all forms of RP inheritance (Neveling, Collin et al. 2012). Although the majority of RP cases are monogenic, the disease is characterized by its genetic heterogeneity and approximately 10% of the RP cases are due to defects in rhodopsin (RHO) gene (Dryja, McGee et al. 1990). The Pro23His (P23H) rhodopsin mutation underlies the most common form of human autosomal dominant retinitis pigmentosa (adRP). The symptoms of RP are well characterized and a prominent early clinical feature of RP manifests as night blindness with peripheral visual field loss as a result of the death of rod photoreceptor cells (Shigenaga, Hagen et al. 1994; Wallace 2005; Bramall, Wright et al. 2010).

Photoreceptors are the most metabolically active cells in the body. They contain a dense concentration of mitochondria in their inner segments that provides the ATP for the energy-intensive processes of outer segment renewal and maintenance of the dark current (Bramall, Wright et al. 2010). The high metabolic demand in photoreceptors for phototransduction processes is met by mitochondrial oxidative phosphorylation

(OXPHOS). The retina is also adequately supplied with glucose and oxygen by the choroidal vessels through the RPE cells. ATP is generated as a result of the synchronized activity of tricarboxylic acid (TCA) cycle and the multi enzyme complex-electron transport chain (ETC). The coenzymes, nicotine adenine dinucleotide (Karunadharma, Nordgaard et al.) (Karunadharma, Nordgaard et al.) and flavin adenine dinucleotide ($FADH_2$) are electron carriers in the ETC. Between 0.4–4.0% of all oxygen consumed in OXPHOS is transformed to superoxide (O_2^-) radicals (Shigenaga, Hagen et al. 1994) which are converted to H_2O_2 by Mn superoxide dismutase (Wallace 2005) and finally to molecular H_2O by glutathione peroxidase (GPX) or peroxiredoxin III (PRX III) (Green, Brand et al. 2004). However, the inability of the antioxidant systems (superoxide dismutase, glutathione and thioredoxin systems) in the mitochondria to quench the increased production of reactive oxygen species (Ranji, Kanemoto et al.) (Ranji, Kanemoto et al.) creates a biochemical imbalance known as oxidative stress (OS), resulting in oxidative damage to the mitochondrial proteins, lipids and DNA. This oxidative damage initiates a cascade of events resulting in mitochondrial dysfunction and cell death (Shigenaga, Hagen et al. 1994; Wallace 2005; Vlachantoni, Bramall et al. 2011). Considerable evidence supports a key role for mitochondrial dysfunction and oxidative damage in the pathogenesis of progressive photoreceptor cell death by apoptosis in RP both *in vitro* (Sanvicens, Gomez-Vicente et al. 2004; Sanz, Johnson et al. 2007) and *in vivo* (Donovan, Carmody et al. 2001; Yamada, Yamada et al. 2001; Sanz, Johnson et al. 2007). Mitochondrial dysfunction and OS have also been documented in other retinal degenerative disorders including glaucoma, age-related macular degeneration (AMD) and diabetic retinopathy, as well as, numerous neurodegenerative disorders including Parkinson's disease and Alzheimer's disease (Lin and Beal 2006; Pieczenik and Neustadt 2007; Kong, Van Bergen et al. 2009; Karunadharma, Nordgaard et al. 2010).

Optical fluorescence techniques have been shown to posses a high sensitivity and specificity for discriminating between diseased and non-diseased tissue. Fluorescence imaging provides specific information on tissue intrinsic fluorophores as a diagnostic tool for early detection of different diseases (Ramanujam, Richards-Kortum et al. 2001; Ranji, Kanemoto et al. 2006; Ranji, Matsubara et al. 2009; Maleki, Sepehr et al. 2012; Sepehr, Staniszewski et al. 2012). Here we used optical fluorescence imaging to evaluate the redox state of the P23H transgenic and the Sprague-Dawley (SD) normal retina. Although a link between OS and photoreceptor degeneration has been proposed, a direct analysis of the redox state within the mitochondrial compartment of the rodent eye has not been performed. We hypothesized that there would be a significant difference in the optical redox ratio of dystrophic retina of the P23H rat compared to that of the non-dystrophic normal rat. We tested this hypothesis using a 3-D optical cryofluorescence imaging technique.

Mitochondrial metabolic coenzymes NADH and $FADH_2$ are two of the primary electron donors and acceptors in OXPHOS, respectively. NADH and FAD (the oxidized form of $FADH_2$) are autofluorescent and can be monitored without exogenous labels through the use of optical techniques. NADH is primarily fluorescent in its reduced biochemical state, whereas FAD is only fluorescent in its oxidized form. Therefore, by imaging these two coenzymes, we can probe the mitochondrial redox state of the tissue.

Although this ratio is not a direct measure of the concentrations of these fluorophores, the fluorescence intensity measured is a relative measure of their concentrations (Maleki, Sepehr et al. 2012). The fluorescent signals of these intrinsic fluorophores have been used as indicators of tissue metabolism in injuries due to hypoxia (Ranji, Kanemoto et al. 2006; Ranji, Matsubara et al. 2009; Maleki, Sepehr et al. 2012; Sepehr, Staniszewski et al. 2012), ischemia (Ranji, Kanemoto et al. 2006; Ranji, Matsubara et al. 2009), and diabetes (Maleki, Sepehr et al. 2012). Our studies have demonstrated that the ratio of these fluorophores, (NADH/FAD), called the NADH redox ratio (NADH RR), acts as a quantitative marker of the mitochondrial redox and metabolic state of tissue *ex vivo* (Ranji, Jaggard et al. 2006) and *in vivo* (Matsubara, Ranji et al. 2010).

We evaluated the mitochondrial redox state quantitatively in the *in situ* retina using a 3-D fluorescent optical imaging instrument called the cryoimager to detect the oxidative state of the retina in P23H transgenic (diseased) eyes as well as SD normal eyes

Materials and Methods

Animal preparation:

All animal experiments were approved by the Institutional Animal Care and Use Committee (IACUC) and were conducted in accordance with the ARVO (The Association for Research in Vision and Ophthalmology) statement for the use of animals in ophthalmic and vision research and with the National Institutes of Health regulations. All animals were housed and bred in an American Association for Accreditation of Laboratory Animal Care (AAALAC) approved animal facility at the University of Wisconsin-Milwaukee.

Albino SD normal and heterozygous P23H-1 transgenic rats, the offspring of P23H-1 homozygotes (Retinal Degeneration Rat Model Resource, UCSF) and SD normal albino rats (Harlan Laboratories, Madison) were fed *ad libitum* and maintained in a temperature and humidity-controlled environment under dim cyclic light, 12-hour light/12-hour dark cycle, with an average illuminance of 5 to 10 lux inside the cage. Once animals reached P30, they were divided into two groups. The heterozygous P23H-1 rats were the model of retinal degeneration and SD normal albino rats were used as non-dystrophic controls.

Electroretinogram Recording:

The function of the retina was monitored using full-field flash electroretinography (ERG), which measures the electrical impulses emitted by the retina in response to flashes of light. Animals were dark adapted for 2 hours prior to recording and were prepared under red dim light. Animals were anesthetized with a xylazine/ketamine cocktail (100 mg/kg and 5 mg/kg respectively, ip). Pupils were dilated with 0.1% atropine and mild topical anesthesia (proparacaine 0.5%) was applied to the eyes. Animals were placed on a heating pad to maintain the body temperature at 37°C during the entire recording period. A nylon coated gold thread electrode was placed on the corneal surface, overlaid with 1% methylcellulose and a small drop of methylcellulose was placed into the concave side of the contact lens before it was placed over the thread electrode. The corneal contact lens was adjusted so that it was centered on the retina. A stainless steel needle ground electrode was inserted on top of the head (midline). Stainless steel needle reference electrodes were inserted subcutaneously on either side of the base of the ear. Needle electrodes were secured with surgical tape. Signals obtained from the corneal surface were amplified, digitized and averaged using ERG view 2.5 software (Retvet Corp, MO). This software allows for low pass filtering of the final ERG test waveforms before they are graphed on the unit. This filter can be used to remove environmental and unit generated noise from the observed ERG. A custom designed Faraday cage was employed to block 60 cycle electrical noise. The amplitudes and latencies of the a-waves (photoreceptor responses) and b-waves (bipolar cell and Muller cell responses) were stored in a Compact Flash storage card and fit to a computational model to determine transduction parameters for photoreceptor responses.

Freezing and embedding:

SD normal and P23H-1 transgenic rats were euthanized at postnatal day 30. The eyes were enucleated and frozen rapidly on dry-ice for low temperature cryoimaging. For fluorescence imaging, the tissue was embedded in a customized black mounting medium (that is not fluorescent in the excitation wavelengths) and placed on a chilled aluminum plate to keep the tissue in place for freezing and slicing. The embedding process starts with freezing the base medium, embedding the tissue and fixing its position by adding more black medium around the tissue. After embedding, the tissue was stored in an ultralow freezer for subsequent imaging. The plate was then installed in the cryoimager where the surface of the black medium is parallel to a microtome. Figure 32 shows a frozen eye sample and an eye sample embedded in the customized black mounting medium.

Imaging calibration:

A calibration method was designed to compensate for day-to-day variation of light intensity and non-uniformity of the illumination pattern. At the beginning of each experiment and before slicing the tissue, a uniform fluorescent flat plate was placed in the same position as tissue and imaged in NADH and FAD channels to acquire the illumination pattern. Since the fluorescence of the standard is in both the NADH and FAD channels, it also accounts for day-to-day light intensity and uniformity changes in all channels. All the images in each channel were then normalized by dividing each image to the flat plate image, captured in the same channel.

Cryoimager:

The cryoimager, which is shown in Figure 33 is an automated image acquisition and analysis system consisting of software and hardware designed to acquire fluorescence images of tissue sections. A motor-driven microtome sequentially sections frozen tissue at the desired slice thickness whereas filtered light from a mercury arc lamp excites up to five fluorophores in the exposed surface of the tissue block. The excitation light source is a 200W white light filtered at the excitation and emission wavelengths of NADH and FAD. At each slice, a CCD camera records fluorescence image of the tissue block in pixel dimensions of 10 μm × 10 μm to be later analyzed for fluorophore distribution. The microtome is housed in a freezer unit that maintains the sample at -20°C during sample slicing and image acquisition. The resolution in the z direction of microtome slices can be as small as 5 um. For this study, we used a resolution of 10 um in the z direction, which resulted in ~ 500 z-slices per eye. (Bernard, Ewen et al. 2000; Sepehr, Staniszewski et al. 2012)

Image processing:

NADH and FAD autofluorescence images (containing 500 slices per eye) from each group of eyes were processed using MATLAB. Composite images were created using all the image slices for each eye, for both NADH and FAD signals. The ratio of NADH and FAD, was calculated voxel by voxel, using MATLAB, according to equation (1).

$$\text{NADH Redox Ratio} = \text{RR} = \text{NADH} / \text{FAD} \qquad (1)$$

The 2D representation of each eye was then calculated using the maximum intensities along the z axis of the NADH redox 3-D volume (maximum projection). In the maximum projection method, first a full 3D volume of images was obtained, including RR, and then the maximum projection on the volumetric data was performed and the histograms were plotted for this maximum projection. The maximum projection is used since the entirety of the anatomy has a significant contribution in this representation. A histogram of the max projection of RR values in each group was created, and the mean (or first moment) of this histogram was calculated according to Eq. (2).

$$Mean = \frac{1}{N_x \times N_y} \sum_{i=1}^{N_x} \sum_{j=1}^{N_y} eye\_Maxpro(i, j) \qquad (2)$$

Where N_x and N_y are the number of pixels in the x and y directions and the pixel size in x and y is 10µm and 10µm. The previously mentioned histograms were calculated for quantitative comparison between normal and diseased groups.

Statistical evaluation of data

Data are presented as mean ± SEM. A mixed model 2 x 6 ANOVA with animal group (P23H vs. SD) as the between-subjects factor and flash intensities of the scotopic intensity series as the within-subjects factor was used to analyze ERG data. A Greenhouse-Geisser correction (a-wave =.500; b-wave =.460) was performed as the assumption of sphericity was violated for the a-wave ($X^2 = 31.140$, $p = .006$) and b-wave ($X^2 = 28.381$, $p = .016$) data. An unpaired Student's t-test was used for comparing mean values of NADH redox ratio and a-wave and b-wave implicit times at 100mcd.s/m^2. Statistical analysis was performed using SPSS 19.0 (SPSS Inc, Chicago, IL) and GraphPad Prism 4.0 (GraphPad, La Jolla, CA USA). The level of significance for all statistical tests was set at 0.05.

Results

In the present study, we used the cryo-fluorescence redox imaging method to probe the retinal mitochondrial redox state. The method was performed on P23H transgenic eyes and SD normal eyes at postnatal day 30, to determine the effect of disease on the NADH RR. This method detects changes in the oxidation state of the mitochondrial respiratory chain. Thus, NADH RR can be used as a quantitative marker to evaluate the OS in diseased and normal eye tissue.

3-D rendering of NADH redox images is generated from representative eye sample *(not included in this dissertation as the figure is in the process of submission for the cover page of Journal of Biomedical Optics*). The optic nerve of the eye can be seen in this figure. The 3-D rendering shows the capability of the cryoimager to perform 3-D cryofluorescence imaging on intact tissue.

Figure 43 displays, maximum projection images of NADH, FAD, and NADH RR for a representative eye in transgenic and SD normal groups. The images show a significant decrease in the mean NADH RR of eyes from diseased versus SD normal eye. The eyes in the SD normal group (first column in Figure 43) show a lower concentration of FAD and a higher concentration of NADH compared to diseased group (second column in Figure 44). Thus, the NADH RR is higher (more reduced) in eyes from SD normal rat eye compared to the eyes from transgenic rats (more oxidized). Sections from the P23H transgenic rats consistently demonstrated increased OS as shown in Figure 4 by a decreased NADH RR.

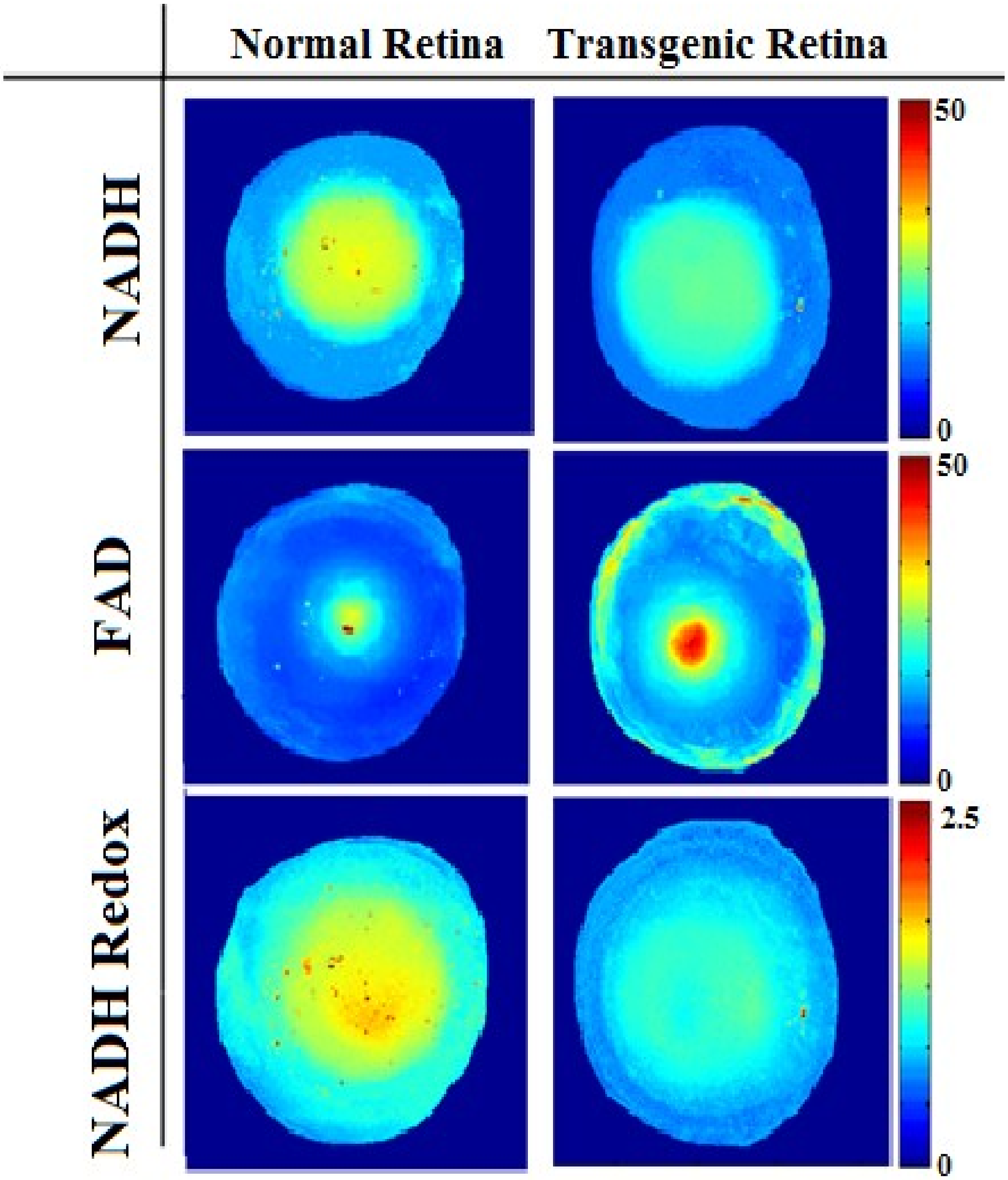

Figure 43 Representative max projected NADH, FAD and RR images for eyes from normal and disease groups.

Figure 44 shows the NADH redox histograms of a representative eye in each of the SD normal and diseased groups. In the diseased group the NADH RR indicates a more oxidized biochemical state with a mean value of 0.821 compared with a higher mean value of 1.079 in SD normal eyes. There was a blue shift in histograms from P23H transgenic eye versus the normal eye and the NADH redox histogram shows a 24% oxidation in the respiratory chain in this group.

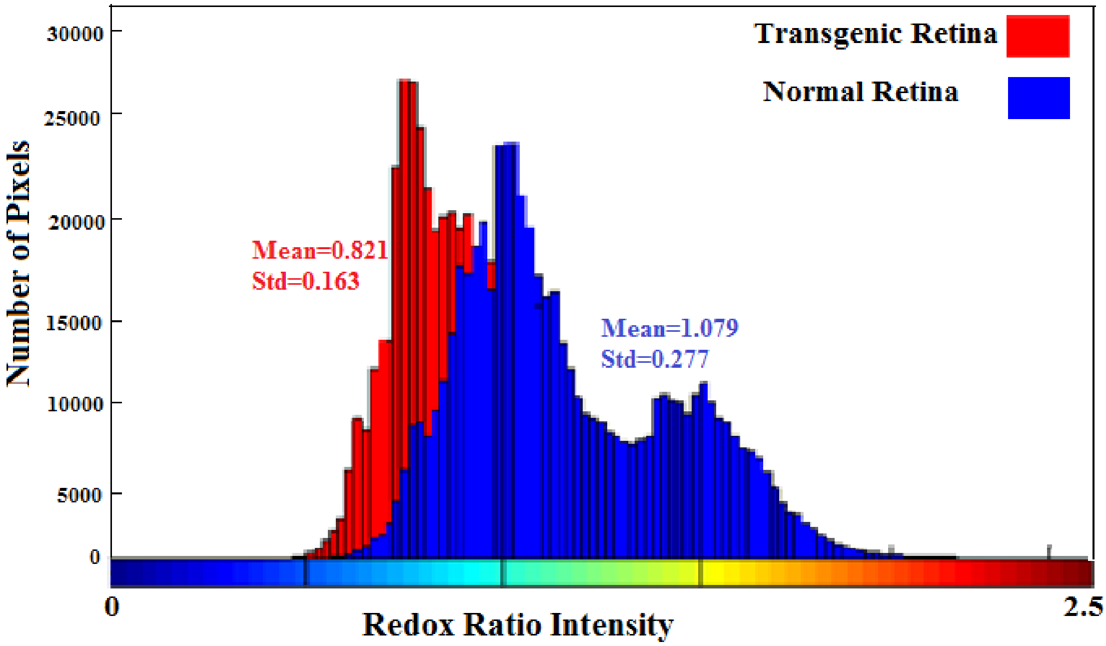

Figure 44 A representative histogram for eyes from normal and diseased groups comparing Redox Ratio intensity between P23H transgenic retina vs. SD Normal retina. Oxidative stress causes more oxidation in the NADH redox histogram

Figure 45 compares the mean values of the histograms of max projected images from SD normal and diseased groups. The results show a significant difference (*p* <.001) between P23H transgenic eyes versus the SD normal eyes (n=4 in each group).

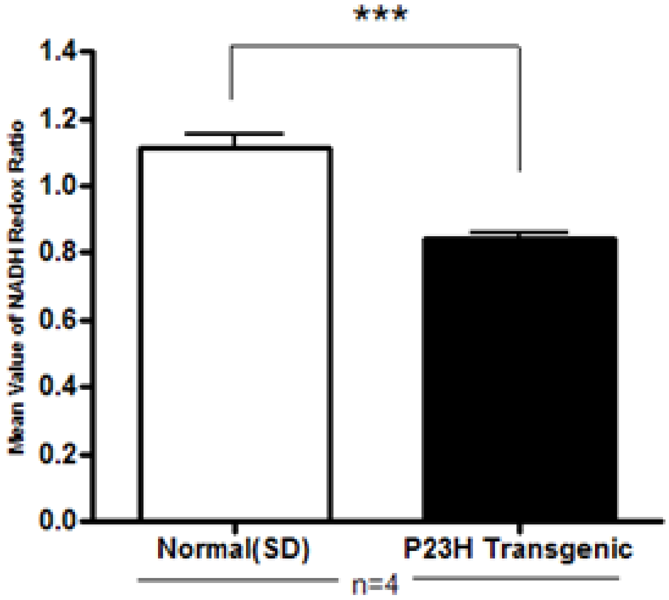

Figure 45 Bar graph plot comparing the mean values of the histograms of max projected images from SD and P23H transgenic rat eyes. The results show a significant difference between normal and diseased eyes (****p*<.001). Error bars: SEM; *p* values were obtained from Unpaired Student's t- test.

Figure 46 summarizes the differences in photoreceptor function between Sprague Dawley rats and P23H-1 transgenic rats. When the function of the photoreceptors (a-wave amplitude; Figure 46A) and inner retina (b-wave amplitude; Figure 46B) was assessed by dark-adapted, full-field flash ERG (scotopic intensity series protocol) at P30, there was a linear increase in the ERG amplitude in both non-dystrophic SD and dystrophic P23H rats ($F_{(1,14)}$ = 186.970, p <0 .001). The main effect of mean ERG amplitudes between non-dystrophic SD and dystrophic P23H rats for a-wave ($F_{(1, 14)}$ = 161.0, p <.001; Fig. 46A) and b-wave ($F_{(1, 10)}$ = 35.4, p <.001; Fig. 46B) of the scotopic intensity series protocol were significantly different. In agreement with the previous studies, P23H transgene caused a significant decrease in both a-wave and b-wave amplitudes compared to the normal SD controls.

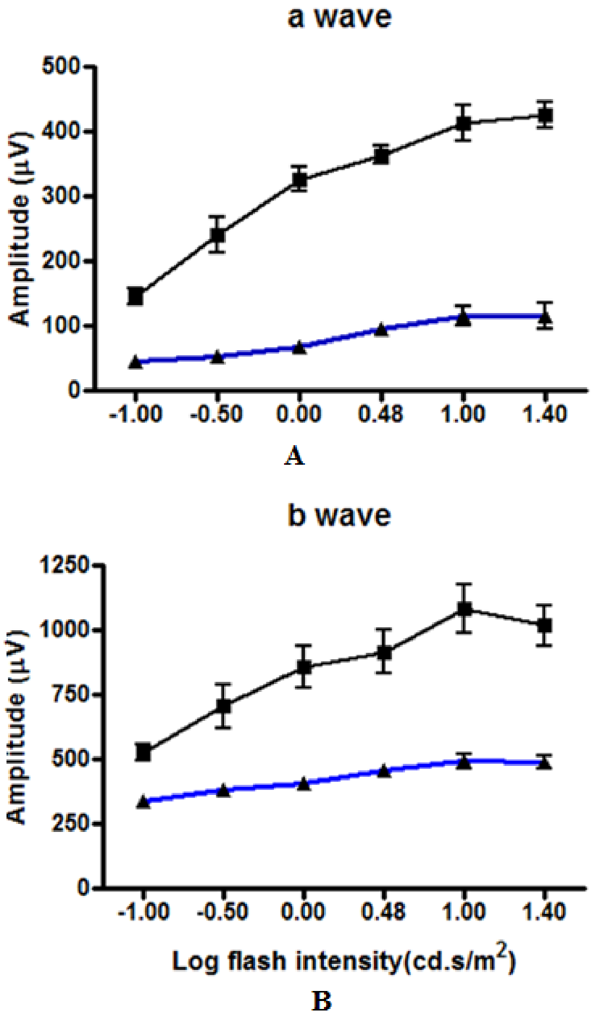

Figure 46 A) The mean a-wave amplitude assessed by the scotopic intensity series protocol comparing P23H transgenic (■; n=8) and SD normal control (▲; n=8) groups B) The mean b-wave amplitude comparing P23H transgenic (■; n=6) and SD normal control (▲; n=6) groups. P23H transgene caused a significant decrease in both a-wave ($F_{(1, 14)} = 161.0$, $p < .001$; Fig. 46A) and b-wave ($F_{(1, 10)} = 35.4$, $p < .001$; Fig. 46B) amplitudes at all flash intensities compared to the normal SD controls. Error bars: SEM.

Figure 47 compares the a-wave and b-wave peak latencies referred to as implicit times. P23H transgene caused a significant (*P*<.01) delay in both a- and b- wave implicit times in P23H retina when compared to SD normal controls. The delay and deviations of the implicit time topography in retinitis pigmentosa when compared to normal subjects is a characteristic diagnostic tool.

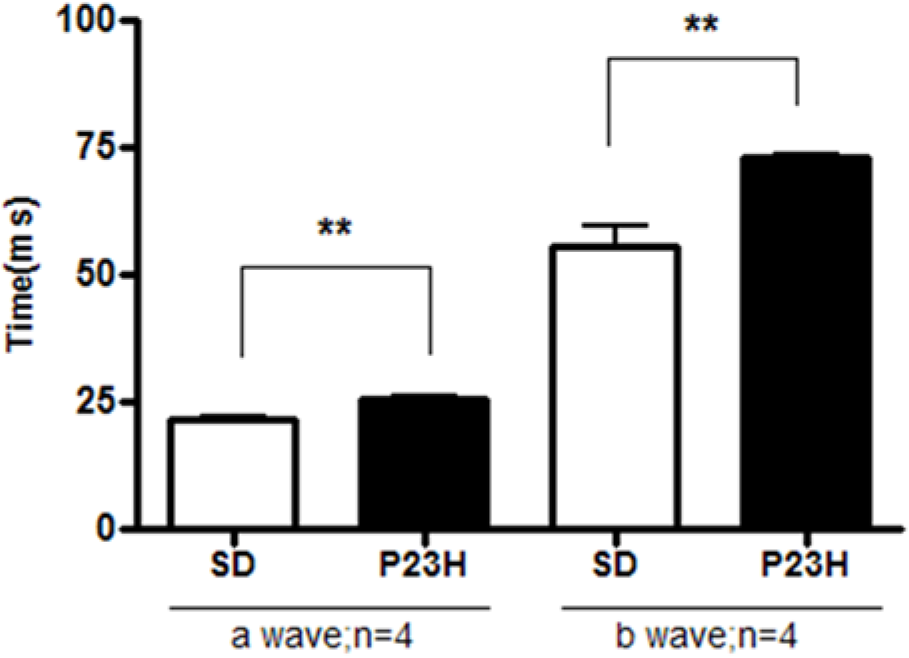

Figure 47 shows the a-wave implicit time as well as b- wave implicit time assessed at 100mcd.s/m2. The implicit times reflecting peak latencies of a- and b- waves were significantly (***p*<.01) different between P23H transgenic and normal SD retina. Error bars: SEM; *p* values were obtained from Unpaired Student's t- test.

Discussion and conclusion

Rod specific mutations, which are genetically heterogeneous trigger photoreceptor cell death by apoptosis in various forms of RP and other inherited retinal degenerations. Recent studies suggest that death of cone photoreceptors subsequent to rod cell death are due to increased oxidative and nitrosative stress (Shen, Yang et al. 2005; Usui, Komeima et al. 2009). The retina is particularly vulnerable to oxidative damage since it is one of the highest oxygen consuming tissues of the body and about 90% of tissue oxygen is metabolized within the mitochondria (Yu and Cringle 2001). As reported in induced and inherited retinal degeneration models, photoreceptors die due to OS, mitochondrial dysfunction and apoptosis (Dykens, Carroll et al. 2004). There are several potential sources of ROS generation in inherited retinal degenerative diseases that may be either caused or exacerbated by reduced oxygen consumption due to the loss or inactivity of mutant rod photoreceptors. Markers of oxidative damage to proteins, lipids and DNA have been detected in cone photoreceptors in the transgenic pig model of RP that suggesting that as the rod photoreceptors degenerate, there is a reduction in oxygen consumption in the outer retina resulting in hyperoxia in the photoreceptor layer with subsequent increase in oxidative stress, resulting in cone loss (Cassarino, Swerdlow et al. 1998; Yu and Cringle 2001). Understanding the biochemical mechanisms involved in cone photoreceptor degeneration is important since cone loss is the major reason for visual loss in RP. The above hypothesis is supported by the fact that photoreceptor depletion-induced hyperoxia is a factor that makes the degeneration process progressive as seen in models of retinal degeneration. Increasing evidence supports the therapeutic efficacy of mitochondrial targeted agents including MITO 4565, TUDCA (tauroursodeoxycholic acid), minocycline and cyclosporine A in various models of retinal and neurodegenerative disorders (Cassarino, Swerdlow et al. 1998; Dykens, Carroll et al. 2004; Phillips, Walker et al. 2008; Yang, Kim et al. 2009).

The metabolic state of a cell is reflected in mitochondrial oxidative function. Mitochondrial oxidative metabolism is an important biomarker for the diagnosis and treatment of many disease pathologies, including cancer, autoimmune disorders and neurodegenerative diseases (Green and Evan 2002; Todaro, Zeuner et al. 2004). In this study, we used a 3-D cryofluorescence redox imaging technique to quantify and compare the mitochondrial redox state in normal and diseased retinae.

In the presence of hyperoxia, as seen in RP and other inherited retinal degenerations, the coenzymes NADH and $FADH_2$ accumulate in their oxidized forms (NAD and FAD). We therefore anticipated higher concentrations of FAD and lower concentrations of NADH in the P23H retina compared to SD normal retina. It can be seen from the maximum projection images in Figure 4 that the FAD concentration is higher (brighter images) and NADH concentration is lower (darker images). This results in the NADH RR showing a significant decrease in the degenerating eye as compared to the SD normal. The difference in the mean values of the two histograms in Figure 5 suggests that OS caused by the disease in transgenic eyes is the reason for a shift in metabolic levels of the eye tissue and causes the mitochondrial respiratory chain to be more oxidized. The 24% oxidation in the NADH RR that we observed in the retina of P23H transgenic rat model suggests that substantial mitochondrial OS is a significant early cellular event in RP. The significant difference in the mean NADH RR of eyes from transgenic rats compared with their appropriate controls (SD normal eyes) suggests that the NADH RR can be used as a marker of retinal OS.

We observed an increase in signal intensity in the eye samples from the vitreous in both NADH and FAD channels that needs to be further investigated and explained. Changes in the biochemical composition of vitreous following pathological changes in the retina during the degeneration process may be one of the reasons for those isolated signals. Collagen, elastin, flavins and lipo-pigments (ceroid and lipofuscin) are some of the endogenous tissue fluorophores that has excitation emission spectral overlap with NADH (Wagnieres, Star et al. 1998). It has also been shown that upon binding to a protein, the quantum yield of NADH increases by four fold (Joseph 2006). Proteomic changes in the vitreous humor have been reported in micro vascular pathologies including proliferative diabetic retinopathy (Kim, Kim et al. 2007).

Our results demonstrate the quantitative capability of an optical cryoimaging technique to measure the tissue mitochondrial redox state in the normal and diseased rat retina. Our method is a direct analysis of the cellular metabolic state within the mitochondrial compartment of the retina of P23H transgenic rat model of Retinitis Pigmentosa, which has not previously been reported. Furthermore, the studies presented here set the stage for future studies, using *ex vivo* and *in vivo* fluorescence imaging of mitochondrial redox states of retina to characterize disease progression in various retinal dystrophies and to evaluate mitochondria targeted drug regimens that diminish OS.

References

1. D. Besch, H. Jagle, H. P. Scholl, M. W. Seeliger and E. Zrenner, "Inherited multifocal RPE-diseases: mechanisms for local dysfunction in global retinoid cycle gene defects," Vision Res 43(28), 3095-3108 (2003)
2. J. Sancho-Pelluz, B. Arango-Gonzalez, S. Kustermann, F. J. Romero, T. van Veen, E. Zrenner, P. Ekstrom and F. Paquet-Durand, "Photoreceptor cell death mechanisms in inherited retinal degeneration," Mol Neurobiol 38(3), 253-269 (2008)
3. D. T. Hartong, E. L. Berson and T. P. Dryja, "Retinitis pigmentosa," Lancet 368(9549), 1795-1809 (2006)
4. K. Neveling, R. W. Collin, C. Gilissen, R. A. van Huet, L. Visser, M. P. Kwint, S. J. Gijsen, M. N. Zonneveld, N. Wieskamp, J. de Ligt, A. M. Siemiatkowska, L. H. Hoefsloot, M. F. Buckley, U. Kellner, K. E. Branham, A. I. den Hollander, A. Hoischen, C. Hoyng, B. J. Klevering, L. I. van den Born, J. A. Veltman, F. P. Cremers and H. Scheffer, "Next-generation genetic testing for retinitis pigmentosa," Hum Mutat (2012)

5. T. P. Dryja, T. L. McGee, L. B. Hahn, G. S. Cowley, J. E. Olsson, E. Reichel, M. A. Sandberg and E. L. Berson, "Mutations within the rhodopsin gene in patients with autosomal dominant retinitis pigmentosa," N Engl J Med 323(19), 1302-1307 (1990)
6. A. N. Bramall, A. F. Wright, S. G. Jacobson and R. R. McInnes, "The genomic, biochemical, and cellular responses of the retina in inherited photoreceptor degenerations and prospects for the treatment of these disorders," Annu Rev Neurosci 33(441-472 (2010)

7. M. K. Shigenaga, T. M. Hagen and B. N. Ames, "Oxidative damage and mitochondrial decay in aging," Proc Natl Acad Sci U S A 91(23), 10771-10778 (1994)

8. D. C. Wallace, "A mitochondrial paradigm of metabolic and degenerative diseases, aging, and cancer: a dawn for evolutionary medicine," Annu Rev Genet 39(359-407 (2005)

9. P. P. Karunadharma, C. L. Nordgaard, T. W. Olsen and D. A. Ferrington, "Mitochondrial DNA damage as a potential mechanism for age-related macular degeneration," Invest Ophthalmol Vis Sci 51(11), 5470-5479 (2010)

10. K. Green, M. D. Brand and M. P. Murphy, "Prevention of mitochondrial oxidative damage as a therapeutic strategy in diabetes," Diabetes 53 Suppl 1(S110-118 (2004)

11. M. Ranji, S. Kanemoto, M. Matsubara, M. A. Grosso, J. H. Gorman, 3rd, R. C. Gorman, D. L. Jaggard and B. Chance, "Fluorescence spectroscopy and imaging of myocardial apoptosis," J Biomed Opt 11(6), 064036 (2006)

12. D. Vlachantoni, A. N. Bramall, M. P. Murphy, R. W. Taylor, X. Shu, B. Tulloch, T. Van Veen, D. M. Turnbull, R. R. McInnes and A. F. Wright, "Evidence of severe mitochondrial oxidative stress and a protective effect of low oxygen in mouse models of inherited photoreceptor degeneration," Hum Mol Genet 20(2), 322-335 (2011)

13. N. Sanvicens, V. Gomez-Vicente, I. Masip, A. Messeguer and T. G. Cotter, "Oxidative stress-induced apoptosis in retinal photoreceptor cells is mediated by calpains and caspases and blocked by the oxygen radical scavenger CR-6," J Biol Chem 279(38), 39268-39278 (2004)

14. M. M. Sanz, L. E. Johnson, S. Ahuja, P. A. Ekstrom, J. Romero and T. van Veen, "Significant photoreceptor rescue by treatment with a combination of antioxidants in an animal model for retinal degeneration," Neuroscience 145(3), 1120-1129 (2007)

15. M. Donovan, R. J. Carmody and T. G. Cotter, "Light-induced photoreceptor apoptosis in vivo requires neuronal nitric-oxide synthase and guanylate cyclase activity and is caspase-3-independent," J Biol Chem 276(25), 23000-23008 (2001)

16. H. Yamada, E. Yamada, A. Ando, N. Esumi, N. Bora, J. Saikia, C. H. Sung, D. J. Zack and P. A. Campochiaro, "Fibroblast growth factor-2 decreases hyperoxia-induced photoreceptor cell death in mice," Am J Pathol 159(3), 1113-1120 (2001)

17. G. Y. Kong, N. J. Van Bergen, I. A. Trounce and J. G. Crowston, "Mitochondrial dysfunction and glaucoma," J Glaucoma 18(2), 93-100 (2009)

18. S. R. Pieczenik and J. Neustadt, "Mitochondrial dysfunction and molecular pathways of disease," Exp Mol Pathol 83(1), 84-92 (2007)

19. M. T. Lin and M. F. Beal, "Mitochondrial dysfunction and oxidative stress in neurodegenerative diseases," Nature 443(7113), 787-795 (2006)

20. N. Ramanujam, R. Richards-Kortum, S. Thomsen, A. Mahadevan-Jansen, M. Follen and B. Chance, "Low Temperature Fluorescence Imaging of Freeze-trapped Human Cervical Tissues," Opt Express 8(6), 335-343 (2001)

21. S. Maleki, R. Sepehr, K. Staniszewski, N. Sheibani, C. M. Sorenson and M. Ranji, "Mitochondrial redox studies of oxidative stress in kidneys from diabetic mice," Biomed Opt Express 3(2), 273-281 (2012)

22. M. Ranji, M. Matsubara, B. G. Leshnower, R. H. Hinmon, D. L. Jaggard, B. Chance, R. C. Gorman and J. H. Gorman Iii, "Quantifying acute myocardial injury using ratiometric fluorometry," IEEE Trans Biomed Eng 56(5), 1556-1563 (2009)

23. R. Sepehr, K. Staniszewski, S. Maleki, E. R. Jacobs, S. Audi and M. Ranji, "Optical imaging of tissue mitochondrial redox state in intact rat lungs in two models of pulmonary oxidative stress," J Biomed Opt 17(4), 046010 (2012)

24. M. Ranji, D. L. Jaggard, S. V. Apreleva, S. A. Vinogradov and B. Chance, "Simultaneous fluorometry and phosphorometry of Langendorff perfused rat heart: ex vivo animal studies," Opt Lett 31(20), 2995-2997 (2006)

25. M. Matsubara, M. Ranji, B. G. Leshnower, M. Noma, S. J. Ratcliffe, B. Chance, R. C. Gorman and J. H. Gorman, 3rd, "In vivo fluorometric assessment of cyclosporine on mitochondrial function during myocardial ischemia and reperfusion," Ann Thorac Surg 89(5), 1532-1537 (2010)

26. S. L. Bernard, J. R. Ewen, C. H. Barlow, J. J. Kelly, S. McKinney, D. A. Frazer and R. W. Glenny, "High spatial resolution measurements of organ blood flow in small laboratory animals," Am J Physiol Heart Circ Physiol 279(5), H2043-2052 (2000)

27. S. Usui, K. Komeima, S. Y. Lee, Y. J. Jo, S. Ueno, B. S. Rogers, Z. Wu, J. Shen, L. Lu, B. C. Oveson, P. S. Rabinovitch and P. A. Campochiaro, "Increased expression of catalase and superoxide dismutase 2 reduces cone cell death in retinitis pigmentosa," Mol Ther 17(5), 778-786 (2009)

28. J. Shen, X. Yang, A. Dong, R. M. Petters, Y. W. Peng, F. Wong and P. A. Campochiaro, "Oxidative damage is a potential cause of cone cell death in retinitis pigmentosa," J Cell Physiol 203(3), 457-464 (2005)

29. D. Y. Yu and S. J. Cringle, "Oxygen distribution and consumption within the retina in vascularised and avascular retinas and in animal models of retinal disease," Prog Retin Eye Res 20(2), 175-208 (2001)

30. J. A. Dykens, A. K. Carroll, S. Wiley, D. F. Covey, Z. Y. Cai, L. Zhao and R. Wen, "Photoreceptor preservation in the S334ter model of retinitis pigmentosa by a novel estradiol analog," Biochem Pharmacol 68(10), 1971-1984 (2004)

31. D. S. Cassarino, R. H. Swerdlow, J. K. Parks, W. D. Parker, Jr. and J. P. Bennett, Jr., "Cyclosporin A increases resting mitochondrial membrane potential in SY5Y cells and reverses the depressed mitochondrial membrane potential of Alzheimer's disease cybrids," Biochem Biophys Res Commun 248(1), 168-173 (1998)

32. M. J. Phillips, T. A. Walker, H. Y. Choi, A. E. Faulkner, M. K. Kim, S. S. Sidney, A. P. Boyd, J. M. Nickerson, J. H. Boatright and M. T. Pardue, "Tauroursodeoxycholic acid preservation of photoreceptor structure and function in the rd10 mouse through postnatal day 30," Invest Ophthalmol Vis Sci 49(5), 2148-2155 (2008)

33. L. Yang, J. H. Kim, K. D. Kovacs, J. G. Arroyo and D. F. Chen, "Minocycline inhibition of photoreceptor degeneration," Arch Ophthalmol 127(11), 1475-1480 (2009)

34. D. R. Green and G. I. Evan, "A matter of life and death," Cancer Cell 1(1), 19-30 (2002)

35. M. Todaro, A. Zeuner and G. Stassi, "Role of apoptosis in autoimmunity," J Clin Immunol 24(1), 1-11 (2004)

36. G. A. Wagnieres, W. M. Star and B. C. Wilson, "In vivo fluorescence spectroscopy and imaging for oncological applications," Photochem Photobiol 68(5), 603-632 (1998)

37. L. R. Joseph, "*Principles of Fluorescence Spectroscopy*," Springer (2006)

38. T. Kim, S. J. Kim, K. Kim, U. B. Kang, C. Lee, K. S. Park, H. G. Yu and Y. Kim, "Profiling of vitreous proteomes from proliferative diabetic retinopathy and nondiabetic patients," Proteomics 7(22), 4203-4215 (2007)

CHAPTER 6

COMPARISON OF 670 nm vs. 830nm PHOTOBIOMODUALTION USING THREE TREATMENT PARADIGMS

To compare the efficacy of 670nm and 830nm NIR photobiomodulation in protecting photoreceptors against damage induced by the P23H transgene, three NIR-LED treatment paradigms were investigated. The first treatment protocol determined whether NIR PBM can rescue photoreceptor function during the critical period (p10-p25) of photoreceptor development. The second treatment protocol determined whether NIR PBM can mitigate the degenerative process from the onset of the critical period of photoreceptor cell death to young adulthood (p10-p 40) and the third treatment protocol determined the ability of NIR PBM to rescue remaining photoreceptors (p20-p40) and preserve retinal function in young rats in which the majority of rods have degenerated.

Figure 48 compares the a-wave amplitude (panel A), b-wave amplitude (panel B), the average implicit time for both a- and b-wave (panel C) at the initial flash intensity of the scotopic intensity series response and the mean total retinal thickness (panel D) for both 830nm (left panel) and 670nm (right panel) NIR PBM during the critical period of photoreceptor development. The main effect of mean ERG amplitudes for the a-wave response which reflect photoreceptor activity and b-wave response which originates from post-synaptic neurons was significantly different between P23H and the treated group in 830nm study [a-wave: ($F_{(1,14)} = 16.32$, $p < .001$); b-wave: ($F_{(1,22)} = 23.57$, $p < .001$)] when compared to that of the 670nm study [a-wave: ($F_{(1,22)} = .396$, $p =.536$); b-wave: ($F_{(1,11)} = 2.11$, $p =.173$)]. The implicit time at 100mcd.s/m^2 was significant for both a-wave ($p<.01$) and b-wave ($p<.05$) in the 830nm study but was not significant with the 670nm study. Total retinal thickness decreases as rod photoreceptors degenerate and disrupt the cellular architecture of the retina and our results demonstrate that 830nm study significantly attenuated ($p<.01$) the thinning of retina in SDOCT linear scans. As similar trend was observed with 670nm study but was not statistically significant.

Figure 49 compares the functional and structural changes in P23H transgenic retina following NIR PBM by 830nm (left panel) and 670nm (right panel) photons during the onset of the critical period of photoreceptor cell death to young adulthood (p10-p 40). The main effect of mean ERG amplitudes for a-wave (panel A) response and b-wave response (panel B) was significantly different between P23H and the treated group in 830nm study [a-wave: ($F_{(1,14)} = 16.63$, $p < .01$); b-wave: ($F_{(1,14)} = 14.6$, $p < .01$)] when compared to that of the 670nm study [a-wave: ($F_{(1,10)} = .279$, $p =.609$); b-wave: ($F_{(1,11)} = 2.01$, $p =.172$)]. The implicit time for a- and b-waves in both 830nm study and 670nm study was not statistically significant (panel C). As 670nm PBM did not preserve the retinal structure in the p10-p25 study, SD-OCT imaging was not conducted in p10-p40 and the p20-p40 study. 830nm PBM continued to preserve the structural integrity (panel D) of the retina in the p10-p40 study, but was not significantly different from the non-treated P23H group.

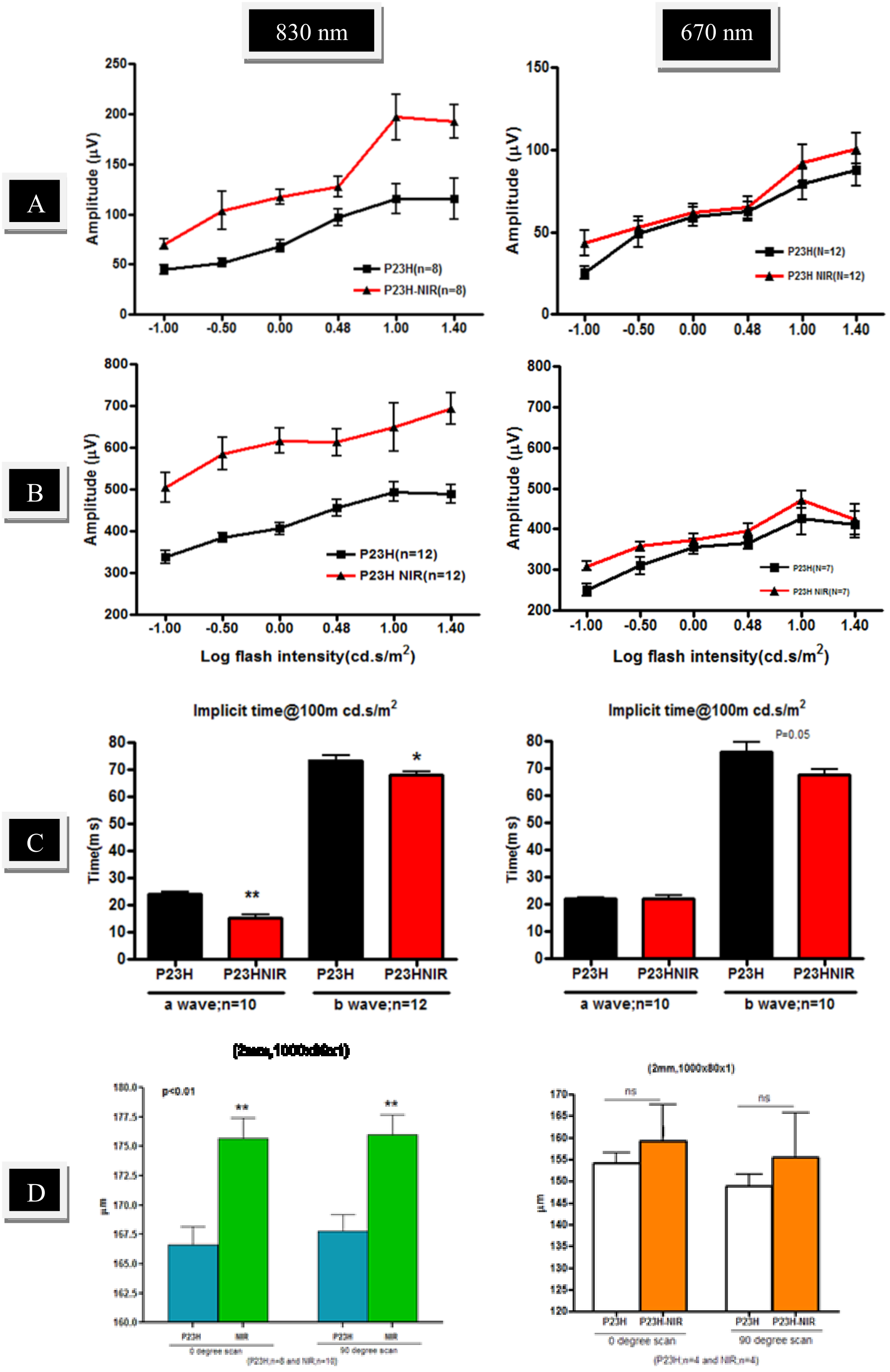
830 nm
670 nm
A
250
200
150
100
50
0
Amplitude (µV)
-1.00
-0.50
0.00
0.48
1.00
1.40
P23H(n=8)
P23H-NIR(n=8)
150
100
50
0
Amplitude (µV)
P23H(N=12)
P23H NIR(N=12)
B
800
700
600
500
400
300
200
Amplitude (µV)
P23H(n=12)
P23H NIR(n=12)
Log flash intensity(cd.s/m²)
P23H(N=7)
P23H NIR(N=7)
Log flash intensity(cd.s/m²)
C
Implicit time@100m cd.s/m²
80
70
60
50
40
30
20
10
0
Time(ms)
**
*
P23H
P23HNIR
P23H
P23HNIR
a wave;n=10
b wave;n=12
Implicit time@100m cd.s/m²
P=0.05
a wave;n=10
b wave;n=10
D
(2mm,1000x80x1)
p<0.01
180.0
177.5
175.0
172.5
170.0
167.5
165.0
162.5
160.0
µm
**
**
P23H
NIR
P23H
NIR
0 degree scan
90 degree scan
(P23H;n=8 and NIR;n=10)
(2mm,1000x80x1)
170
165
160
155
150
145
140
135
130
125
120
µm
ns
ns
P23H
P23H-NIR
P23H
P23H-NIR
0 degree scan
90 degree scan
(P23H;n=4 and NIR;n=4)

Figure 48 compares the functional and structural changes in P23H transgenic retina following NIR PBM by 830 and 670 nm photons during the critical period of photoreceptor degeneration (p10-p25). Panel A compares the a-wave amplitude and panel B compares the b-wave amplitude between P23H (■) and 830 nm treated group (▲, left), P23H (■) and 670 nm treated group (▲, right) respectively. The main effect for a-wave and b-wave between the groups are significantly different [a-wave: ($F_{(1,14)} = 16.32$, $p < .001$); b-wave: ($F_{(1,22)} = 23.57$, $p < .001$)] in 830 nm treated group when compared to that of the 670 nm treated group [a-wave: ($F_{(1,22)} = .396$, $p = .536$); b-wave: ($F_{(1,11)} = 2.11$, $p = .173$)]. Panel C compares the implicit time for a-wave and b-wave at 100mcd.s/m^2. 830 nm treatment caused a significant difference in a-wave ($p<.01$) and b-wave ($p<.05$) when compared to the 670 nm group even though a trend was observed in the later. Panel D shows total retinal thickness measured by SD-OCT demonstrating retinal structural integrity which was significantly different ($p<.01$) in 830 nm treated group at both 0 degree and 90 degree linear scans when compared to P23H group but 670 nm treatment demonstrated a trend without a statistically significant result. Error bars: SEM.

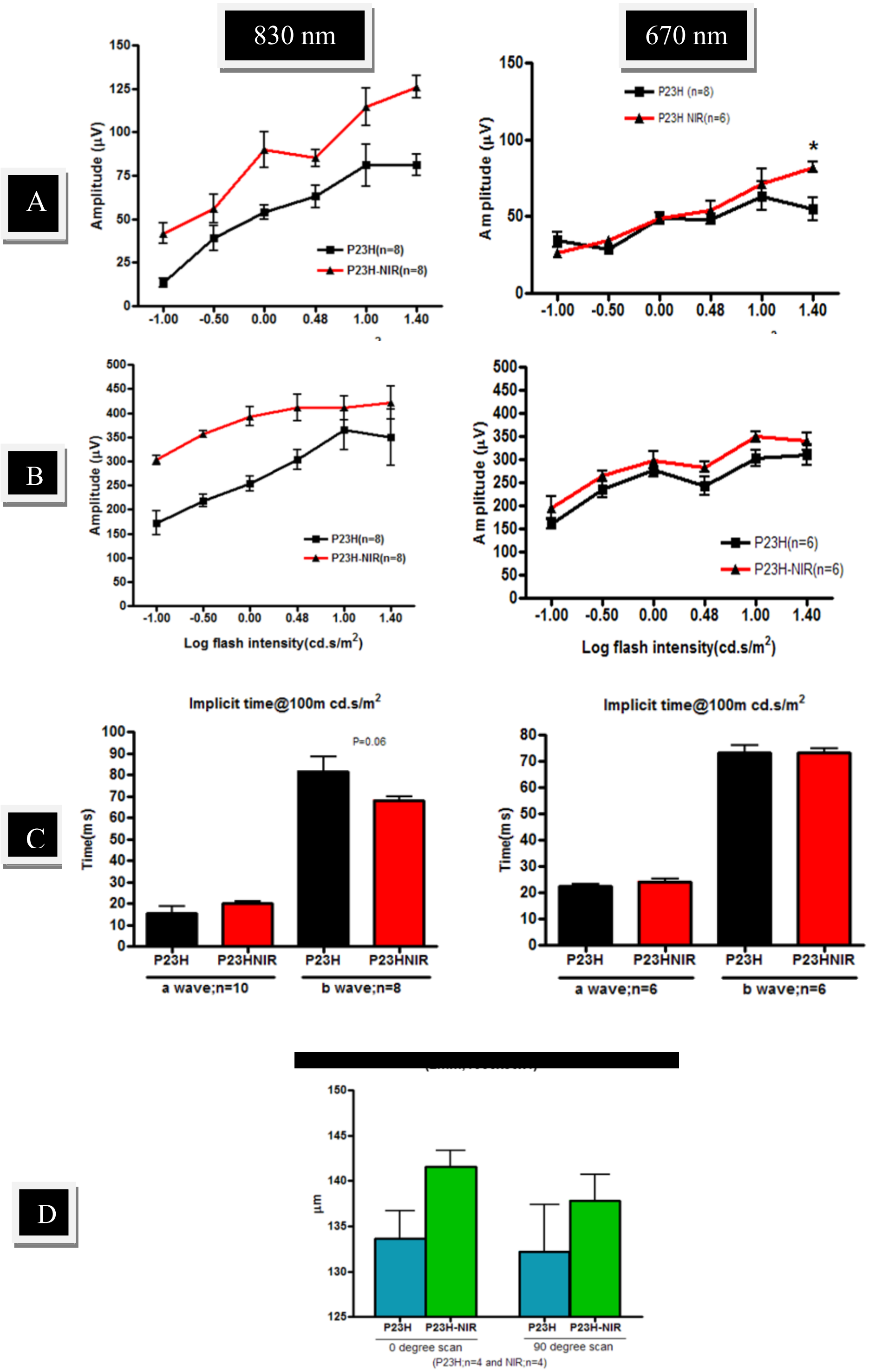
830 nm
670 nm
A
Amplitude (µV)
P23H(n=8)
P23H-NIR(n=8)
P23H (n=8)
P23H NIR(n=6)
*
-1.00
-0.50
0.00
0.48
1.00
1.40
B
Amplitude (µV)
P23H(n=8)
P23H-NIR(n=8)
P23H(n=6)
P23H-NIR(n=6)
Log flash intensity(cd.s/m^2)
C
Implicit time@100m cd.s/m^2
Time(ms)
P=0.06
P23H
P23HNIR
a wave;n=10
b wave;n=8
a wave;n=6
b wave;n=6
[redacted]
D
µm
P23H
P23H-NIR
0 degree scan
90 degree scan
(P23H;n=4 and NIR;n=4)

Figure 49 compares the functional and structural changes in P23H transgenic retina following NIR PBM by 830 and 670 nm photons during the onset of the critical period of photoreceptor cell death to young adulthood (p10-p 40). Panel A compares the a-wave amplitude and panel B compares the b-wave amplitude between P23H (■) and 830 nm treated group (▲, left), P23H (■) and 670 nm treated group (▲, right) respectively. The main effect for a-wave and b-wave between the groups are significantly different [a-wave: ($F_{(1,14)} = 16.63$, $p < .01$); b-wave: ($F_{(1,14)} = 14.6$, $p < .01$)] in 830 nm treated group when compared to that of the 670 nm treated [a-wave: ($F_{(1,10)} = .279$, $p = .609$); b-wave: ($F_{(1,11)} = 2.01$, $p = .172$)]. Panel C compares the implicit time for a-wave and b-wave at 100mcd.s/m^2 and there was no statistically significant difference between P23H and both treatment groups. Panel D shows total retinal thickness measured by SD-OCT linear scans representing retinal structural integrity which was not statistically significant between P23H and 830 nm treated group. Error bars: SEM.

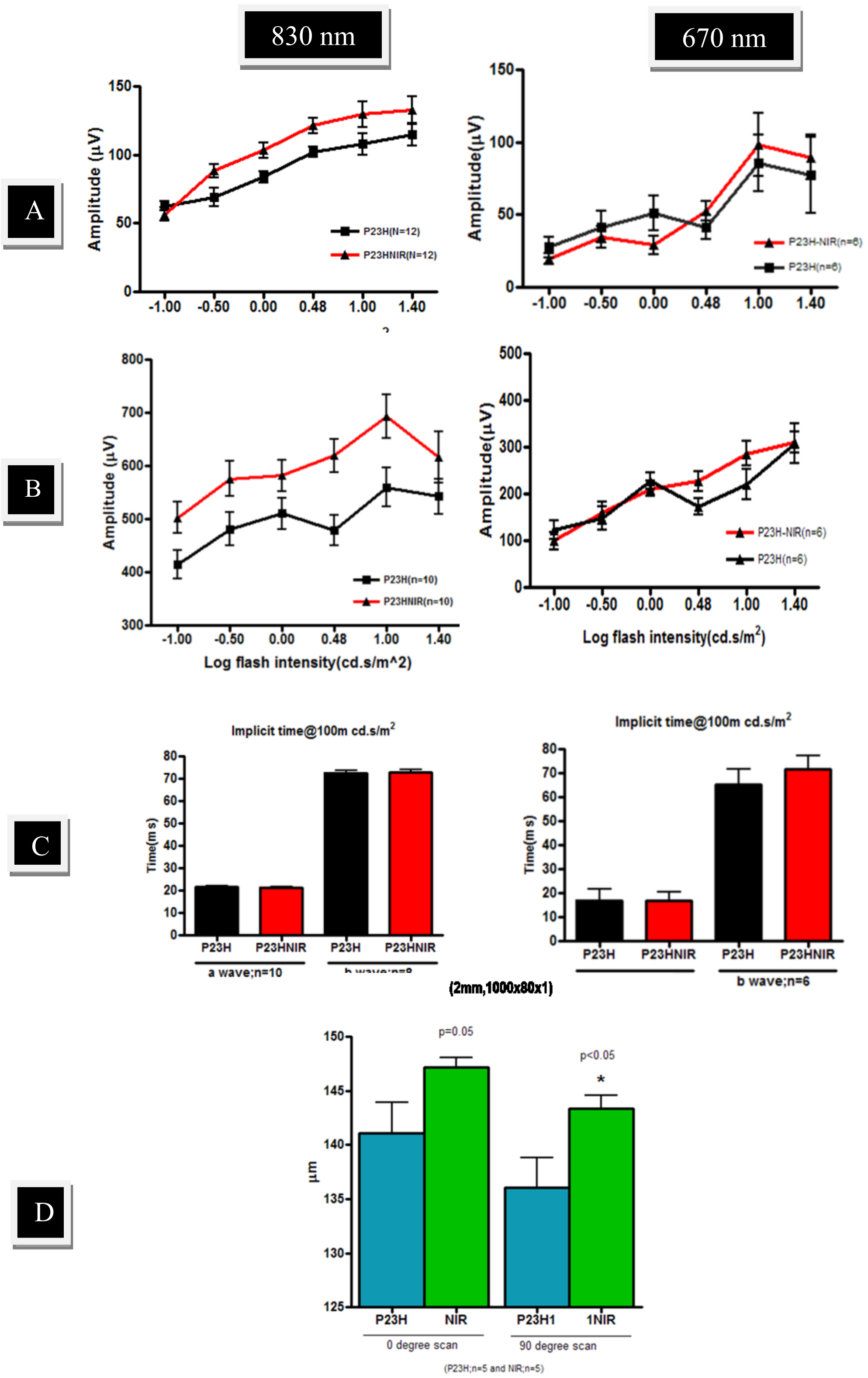
830 nm
670 nm
A
150
100
50
0
Amplitude (µV)
-1.00
-0.50
0.00
0.48
1.00
1.40
P23H(N=12)
P23HNIR(N=12)
Amplitude(µV)
P23H-NIR(n=6)
P23H(n=6)
B
800
700
600
500
400
300
Amplitude (µV)
P23H(n=10)
P23HNIR(n=10)
Log flash intensity(cd.s/m^2)
500
400
300
200
100
0
Amplitude(µV)
P23H-NIR(n=6)
P23H(n=6)
Log flash intensity(cd.s/m^2)
C
Implicit time@100m cd.s/m^2
80
70
60
50
40
30
20
10
0
Time(m s)
P23H
P23HNIR
P23H
P23HNIR
a wave;n=10
Implicit time@100m cd.s/m^2
Time(m s)
P23H
P23HNIR
P23H
P23HNIR
b wave;n=6
(2mm,1000x80x1)
D
150
145
140
135
130
125
µm
p=0.05
p<0.05
*
P23H
NIR
P23H1
1NIR
0 degree scan
90 degree scan
(P23H;n=5 and NIR;n=5)

Figure 50 compares the functional and structural changes in P23H transgenic retina following NIR PBM by 830 and 670 nm photons during the later stage (p20-p 40) to rescue remaining photoreceptors. Panel A compares the a-wave amplitude and panel B compares the b-wave amplitude between P23H (■) and 830 nm treated group (▲, left), P23H (■) and 670 nm treated group (▲, right) respectively. The main effect for a-wave and b-wave between the groups are significantly study [a-wave: ($F_{(1,22)} = 4.60$, $p < .05$); b-wave: ($F_{(1,20)} = 5.85$, $p < .05$)] in 830 nm treated group when compared to that of the 670 nm treated [a-wave: ($F_{(1,10)} = .00$, $p =.99$); b-wave: ($F_{(1,10)} = 0.28$, $p =.608$)]. Panel C compares the implicit time for a-wave and b-wave at 100mcd.s/m^2 and there was no statistically significant difference between P23H and both treatment groups. Panel D shows total retinal thickness measured by SD-OCT linear scans representing retinal structural integrity. 90 degree linear scans were statistically significant between P23H and 830 nm treated group ($p < .05$) but in contrast 0 degree scans were not statistically significant ($p =.05$). Error bars: SEM.

Figure 50 compares the functional and structural changes in P23H transgenic retina following NIR PBM by 830 (left panel) and 670 nm (right panel) photons during the later stage (p20-p 40) to rescue remaining photoreceptors. The main effect of mean ERG amplitudes for a-wave response (panel A) and b-wave response (panel B) was significantly different between P23H and the treated group in the 830nm PBM study [a-wave: ($F_{(1,22)} = 4.60$, $p < .05$); b-wave: ($F_{(1,20)} = 5.85$, $p < .05$)] as seen in previous two treatment paradigms when compared to that of the 670nm study [a-wave: ($F_{(1,10)} = .00$, $p = .99$); b-wave: ($F_{(1,10)} = 0.28$, $p = .608$)]. There was no difference in a-wave or b-wave implicit times between the 670 nm and the 830 nm treatments. (panel C). Interestingly we observed better preservation of retinal structure with 830nm PBM in the 90 degree linear scans ($p<.05$), even though treatment started in young adult rats which has the majority of rods degenerated (paned D). This observation provides new insights into the ability of PBM to preserve the secondary retinal structures and enhance self-renewal and repair of the retinal cells that generally undergo degeneration as rod photoreceptors die.

In summary the results demonstrated in this study shows that 830nm PBM generates more robust cellular and physiological response in P23H transgenic rats when compared to the 670nm PBM in three treatment paradigms.

CHAPTER 7

PHOTOBIOMODUALATION ATTENUATES RETINAL DEGENERATION IN THE P23H RAT MODEL OF RETINITIS PIGMENTOSA

[In preparation for Investigative Ophthalmology & Visual Science]

Introduction

Retinitis pigmentosa (RP) is a hereditary retinal degenerative disorder and the most common cause of inherited blindness in the developed world, with an estimated 1.5 million patients worldwide and a prevalence of one in 5000 individuals worldwide[1,2]. Clinically, RP is characterized by nyctalopia in the initial stages resulting from loss of rod photoreceptors followed by patchy loss of peripheral vision in daylight which progresses towards the center leading to tunnel vision resulting from secondary loss of cone cells. Fundus images of patients with RP reveal attenuation of retinal vessels, waxy palor in the optic disc and pigment deposits in the peripheral retina that resemble bony spicules[3]. Although the majority of RP cases are monogenic, the disease is characterized by its genetic heterogeneity and more than 40 genes have been associated with RP. RP can be inherited in an autosomal dominant, recessive, X-linked or mitochondrial mode[4]. RP is associated with gene defects in proteins involved in the visual transduction cascade, RPE function, photoreceptor structure and RNA splicing[4]. The first gene abnormality reported in RP was a single-base substitution in codon 23 of rhodopsin gene (*RHO*). This mutation [proline 23 histidine] (P23H) accounts for 12% of autosomal dominant RP in US[5].

Rod and cone photoreceptors are the most metabolically active cells in the CNS with a high rate of oxygen consumption. Cones are more metabolically active than rods; however rods greatly outnumber cones in the retina. As rod photoreceptors degenerate in clinical and experimental RP, there is a decrease in oxygen consumption in the retina that results in increased oxygen tension[6]. Choroidal vessels are poorly autoregulated and cannot compensate for this increased oxygen tension, resulting in outer retinal hyperoxia and an altered intracellular redox equilibrium leading to increased oxidative stress[7].

Considerable evidence supports a key role for mitochondrial dysfunction and oxidative damage in the pathogenesis of photoreceptor cell death in RP and other retinal degenerative disorders[8,9]. Despite the degree of genetic heterogeneity, human retinal dystrophies have been associated with profound loss of retinal antioxidant systems and cytoprotective factors thus compromising the ability of retinal neurons and glia to protect against oxidative damage leading to apoptotic cell death[10,11]. Moreover, mitochondrial dysfunction leading to increased oxidative stress and abnormal regulation of apoptosis are characteristic findings of many inner and outer retinal disorders including Leber's hereditary optic neuropathy (LHON), glaucoma, age-related macular degeneration (AMD) and diabetic retinopathy[12,13,14].

Photobiomodulation (PBM) is defined as a process by which cellular signaling pathways are activated when photons interact with cellular photoacceptor molecules leading to physiological changes in the cell. Treatment of tissue with monochromatic photons in the far-red to near-infrared (NIR) region of the spectrum (630-1000 nm) has been shown to attenuate the harmful effects of neuro- and developmental toxins and improve recovery from ischemic reperfusion injury in the heart[15-18]. PBM has also been shown to attenuate degeneration in the injured retina and optic nerve, ameliorate the retinotoxic effects of methanol-derived formic acid in rodents and improve recovery in experimental and clinical stroke[19-23].

Recent studies from our laboratory have demonstrated that NIR photons decreased the concentrations of cytotoxic and pro-apoptotic factors and reduced cell death and inflammation in rodent models of light-induced retinal degeneration and multiple sclerosis[24,25]. Fitzgerald and colleagues demonstrated that NIR photons delivered transcranially to the injury site in an *in vivo* model of partial optic nerve transection resulted in a decrease in secondary oxidative stress in astrocytes, an increase in NG-2 immunopositive oligodendrocyte precursor cells and restored visual function[22].

Increasing evidence indicates that cytochrome c oxidase, the terminal electron acceptor of the electron transport chain, is a key photoacceptor molecule mediating the therapeutic actions of photobiomodulation[26]. The interaction of NIR photons with cytochrome c oxidase increases the mitochondrial membrane potential ($\Delta\Psi$) and proton gradient in the intermembrane space of the mitochondria[27], modifies NADH linked dehydrogenase reactions[28] and alters the rate of ADP/ATP exchange[29] resulting in the activation of intracellular signaling cascades which culminate in improved mitochondrial function, increased synthesis of cytoprotective factors and cell survival[19]. Microarray studies have identified genes and noncoding RNAs involved in the neuroprotective actions of NIR-PBM in light induced retinal degeneration model. These studies demonstrated significant up-regulation of gene expression in pathways involved in mitochondrial energy production and antioxidant cellular protection and down-regulation of gene expression in pathways involved in apoptotic cell death[30].

Mitochondrial dysfunction is a hallmark finding in retinal and neurodegenerative disorders and PBM has been shown to improve cellular mitochondrial energy metabolism in cultured cells and in animal models of disease. The purpose of this investigation was to test the hypothesis that 830nm photobiomodulation would slow disease progression and improve retinal metabolic state in an animal model of retinal dystrophy, the P23H transgenic rat.

Materials and Methods

Animals

All animal experiments were approved by the Institutional Animal Care and Use Committee (IACUC) and were conducted in accordance with the ARVO (The Association for Research in Vision and Ophthalmology) statement for the use of animals in ophthalmic and vision research and with the National Institutes of Health regulations. Heterozygous P23H-1 transgenic rats, the offspring P23H-1 homozygotes (Retinal Degeneration Rat Model Resource, UCSF) and Sprague-Dawley (SD) albino rats (Harlan Sprague Dawley, Madison, WI) were used as the model of RP. All animals were housed and bred in an AAALAC approved animal at the University of Wisconsin-Milwaukee. Rats were fed ad libitum and maintained in a temperature and humidity-controlled environment under dim cyclic light, 12-hour light/12-hour dark cycle, with an average illuminance of 5 to 10 lux inside the cage.

NIR Treatment Protocol

P23H-1 transgenic rat pups were treated with 830 nm LED arrays engineered to eliminate heat (GaAlAs LED arrays, QBMI Photomedicine, Barneveld WI). Rat pups were hand-held by the investigator or placed in a plexiglass restraint device and the 830 nm LED array was positioned directly over the animal's head at a distance of 2 cm exposing both eyes. Treatment protocol consisted of irradiation at 830 nm for 180 seconds at power intensity of 25mW/cm^2 and an energy density of 4.5 joules/cm^2 at the surface of the cornea. Sham-treated P23H-1 transgenic pups were handled in the same way, except that they were not exposed to the LED array. Animals in the NIR-PBM treated group were treated once a day for 5 days per week from p10 to p25.

Electroretinography

Photoreceptor function was assessed by full-field flash-evoked electroretinography (ERG). At p30, animals were dark-adapted overnight and prepared under red dim light. Animals were anesthetized with a ketamine and xylazine cocktail (100 mg/kg and 5 mg/kg respectively, ip) and placed on a heating pad at 37°C during recordings. Pupils were dilated with 0.1% atropine and mild topical anesthesia (proparacaine 0.5%). Full-field ERGs were obtained in a Ganzfeld dome (76 mm diameter Flash Dome with 55 mm aperture) using nylon coated gold thread electrode placed on the corneal surface, overlaid with 1% methylcellulose and a contact lens. A sub dermal needle reference electrode and a ground needle electrode were placed in the cheek and tail respectively. A high-intensity flash unit (HMsERG instrument, Retvet Corp, MO) was used to provide flash intensities (ranging from 10 mcd.s/m^2 to 25000 cd.s/m^2) for scotopic intensity series response measurements. The ISCEV protocol was also employed to examine rod-mediated and rod and cone-mediated responses. Signals were amplified, digitized and averaged using ERG view 2.5 software (RetVet Corp. Inc., Columbia, MO). A custom designed Faraday cage was employed to block 60 cycle electrical noise. The amplitudes and latencies of the a-waves (photoreceptor responses) and b-waves (bipolar cell and Muller cell responses) were fit to a computational model to determine transduction parameters for photoreceptor responses.

Spectral Domain Optical Coherence Tomography (SD-OCT) imaging

High-resolution scans were performed at p30 to assess retinal morphology using SD-OCT (Bioptigen Inc, Research Triangle Park, NC). Animals were anesthetized with a ketamine and xylazine cocktail (i.p., 50:5 mg/kg body weight) and were placed on a custom made six-axis animal alignment system. Both eyes were imaged in a single session after dilation of pupil (1% Atropine sulphate) and hydration of cornea (Systane ultra, polyethylene glycol 400, 0. 4%). The fundus imaging camera in the optical head of the OCT provided initial alignment for the light source during the real time aiming. Final positioning was guided by monitoring and calibrating the real-time OCT image of the retina formed. The optic nerve head (ONH) was used as a landmark (Figure 51a and Figure 51b) and linear (1000 A-scans/B-scan, 80 B-scans) and volume scans (750 A-scans/B-scan, 250 B-scans/volume) per eye were captured and saved using the Bioptigen's InVivoVue^{TM} software. For the linear scans, the B-scans were registered and averaged as previously described[31] using ImageJ [32] (National Institutes of Health, Bethesda, MD) and segmentation of retinal layers for total thickness were determined using an algorithm generated in MatLab (The MathWorks, Inc. , Natick, MA). The difference in reflectivity of retinal layers was used in generating longitudinal reflectivity profile[33] (LRP, Figure 51c) and based on the LRP at fixed locations on either side for the ONH, outer nuclear layer thickness (ONL) was determined as demonstrated in Figure 51d.

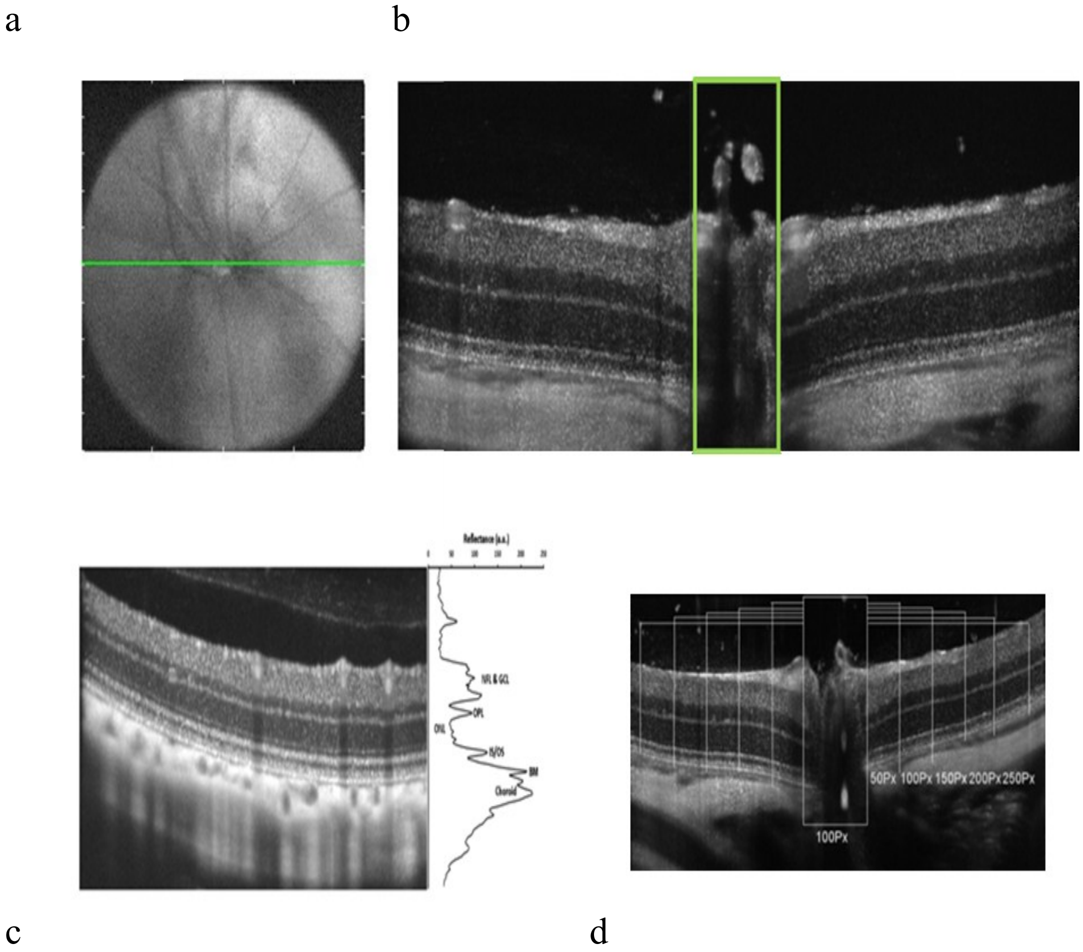

Figure 51 a and 51 b shows the ONH landmark used for SDOCT imaging. Figure 51c shows the difference in the reflectivity of retinal layers from which Longitudinal Reflectivity Profile (LRP) is generated. Low reflecting layers in the linear scan correspond to nuclear layers and high reflecting layers correspond to synaptic layers in the retina[31, 53]. NFL, nerve fibre layer; GCL, ganglion cell layer; OPL, outer plexiform layer; ONL, outer nuclear layer; IS/OS, inner segment/outer segment junction; BM, Bruch's membrane. Figure 51 d represents the LRP lines 50Px apart on either side of the ONH (100Px width) used for characterizing the ONL thickness.

Tissue Collection and Toluidine Blue Staining

Animals were euthanized at p30 by CO_2 inhalation and the eyes were rapidly enuculeated for histological evaluation. The eyes were marked at superior position (in the corneal limbus) using a surgical cautery and immersion-fixed in 4% paraformaldehyde in 0.1 M phosphate-buffered saline (PBS) at pH 7.4 for 2 h. Sections (10 µm) were stained with toluidine blue and examined using an Olympus Axioskop microscope to evaluate structural changes in the retina as described previously[24].

Measurement of ONL thickness

The number of surviving photoreceptors was quantified by counting the rows of photoreceptor nuclei in the ONL in digital images of toluidine blue stained resin sections at three locations (100 µm, 200 µm and 300 µm from the optic nerve head) on the superior pole and inferior pole of the optic nerve as previously described[34].

Freezing and embedding tissue for Optical Cryo Imaging

Retinal metabolic state was assessed using a novel optical redox-sensitive cryoimaging technique. Animals were euthanized at p30, and their eyes were harvested and frozen rapidly for low temperature cryoimaging. The eyes were embedded in a customized black mounting medium (Figure 32) to remove the background fluorescence and scanned by the cryoimager. The cryoimager (Figure 33) is an automated image acquisition and analysis system consisting of software and hardware designed to acquire fluorescence images of tissue sections. The excitation light source is a 200W mercury arc lamp filtered at the excitation wavelength of NADH and FAD, 336 nm and 470 nm, respectively. The emission wavelengths are 450 nm and 520 nm for NADH and FAD and respectively. At each slice, a CCD camera records a fluorescence image of the tissue block. The resolution in the z direction of microtome slices can be as small as 5 μm. For this study, we used a resolution of 10 μm in the z direction, which resulted in ~ 400 z-slices per eye.

FAD and NADH autofluorescence images from each group of eyes were processed using Matlab. The composite images were created using all the image slices for each eye, for both NADH and FAD signals. The ratio of NADH and FAD, known as the NADH redox ratio[35], was calculated voxel by voxel, using Matlab, according to equation (1).

$$\text{Redox Ratio} = \text{RR} = \text{NADH} / \text{FAD} \qquad (1)$$

The 2D representation of each eye was then calculated using the maximum intensities in the z axis of the NADH redox 3D volume *(not included in this dissertation as the figure is in the process of submission for the cover page of Journal of Biomedical Optics*). In the maximum projection method, first a full 3D volume of images was obtained, including RR, and then the maximum projection on the volumetric data was performed and the histograms were plotted for this maximum projection. The maximum projection is used since the entirety of the anatomy has a significant contribution in this representation. A histogram of the max projection of RR values in each group was created, and the mean (or first moment) of this histogram was calculated according to Eq. (2).

$$Mean = \frac{1}{N_x \times N_y} \sum_{i=1}^{N_x} \sum_{j=1}^{N_y} eye\_Maxpro(i,j) \qquad (2)$$

Where Nx and Ny are the number of pixels in the x and y directions and the pixel size in x and y is 10µm and 10µm. The previously mentioned histograms were calculated for quantitative comparison between P23H-sham and P23H-NIR-treated groups.

Data Analysis

Data are presented as mean ± SEM. A mixed model ANOVA (Greenhouse-Geisser correction was performed whenever the assumption of sphericity was violated), MANOVA, 1-way ANOVA (Kruskal-Wallis test) and Student's t-test performed, as appropriate. Statistical analysis was performed using SPSS 19.0 (SPSS Inc, Chicago, IL) and GraphPad Prism 4.0 (GraphPad, La Jolla, CA USA). The level of significance for all statistical tests was set at .05.

Results

830 nm photobiomodulation preserved retinal function in the P23H rat

Figure 52 summarizes the changes in photoreceptor function in P23H transgenic retina following photobiomodulation by 830 nm NIR photons during the critical period (p10-p25) of photoreceptor loss. When the function of the photoreceptors (a-wave amplitude; Figure 52 a) and inner retina (b-wave amplitude; Figure 52 b) was assessed by dark-adapted, full-field flash ERG (scotopic intensity series protocol) at p30, there was a linear increase in the ERG amplitude in both NIR treated P23H and non-treated P23H groups. In agreement with previous studies, the P23H transgene caused a profound decrease in both a-wave and b-wave amplitudes compared to the normal SD controls (data not shown) that was rescued by treatment with 830nm NIR photons.

Figure 52 a summarizes the comparison of mean a-wave ERG amplitude over a range of flash intensities (from 10 mcd.s/m^2 to 25000 cd.s/m^2) between NIR-treated and sham treated P23H-1 transgenic rats. The a-wave amplitude curve in the NIR-treated animals was significantly greater ($F_{(1,\ 14)} = 16.32, p < .001$; Fig. 52a) than that measure in the sham-treated animals indicative of protection of photoreceptor function by 830 nm PBM. The effects of NIR treatment on the functional response post synaptic to photoreceptors was assessed by measuring the b-wave amplitude over the same range of flash intensities in NIR-treated and sham-treated rats. Figure 52 b shows the mean b-wave amplitude in each treatment group. At each intensity the amplitude of the b-wave was 50% greater in the NIR-treated animals compared to the sham-treated animals and was significantly different ($F_{(1,\ 22)} = 23.57, p < .001$; Fig. 52b).

Figure 52 c shows the average a-wave amplitude reflecting the rod-only response in the ISCEV protocol. The rod-only response was significantly greater in the NIR treated retina compared to the sham-treated retina (14.8 ± 2.2 μV vs. 8.8 ± 0.7; $p < .05$ μV, n=4). Figure 52 d shows the average a-wave amplitude reflecting the standard rod and cone response in the ISCEV protocol. The a-wave amplitude of the rod and cone-mediated response was also significantly greater in the NIR-treated compared to the sham-treated animals (69.2 ± 3.2 μV vs. 59.3 ± 0.8 μV; $p < .05$, n=3).

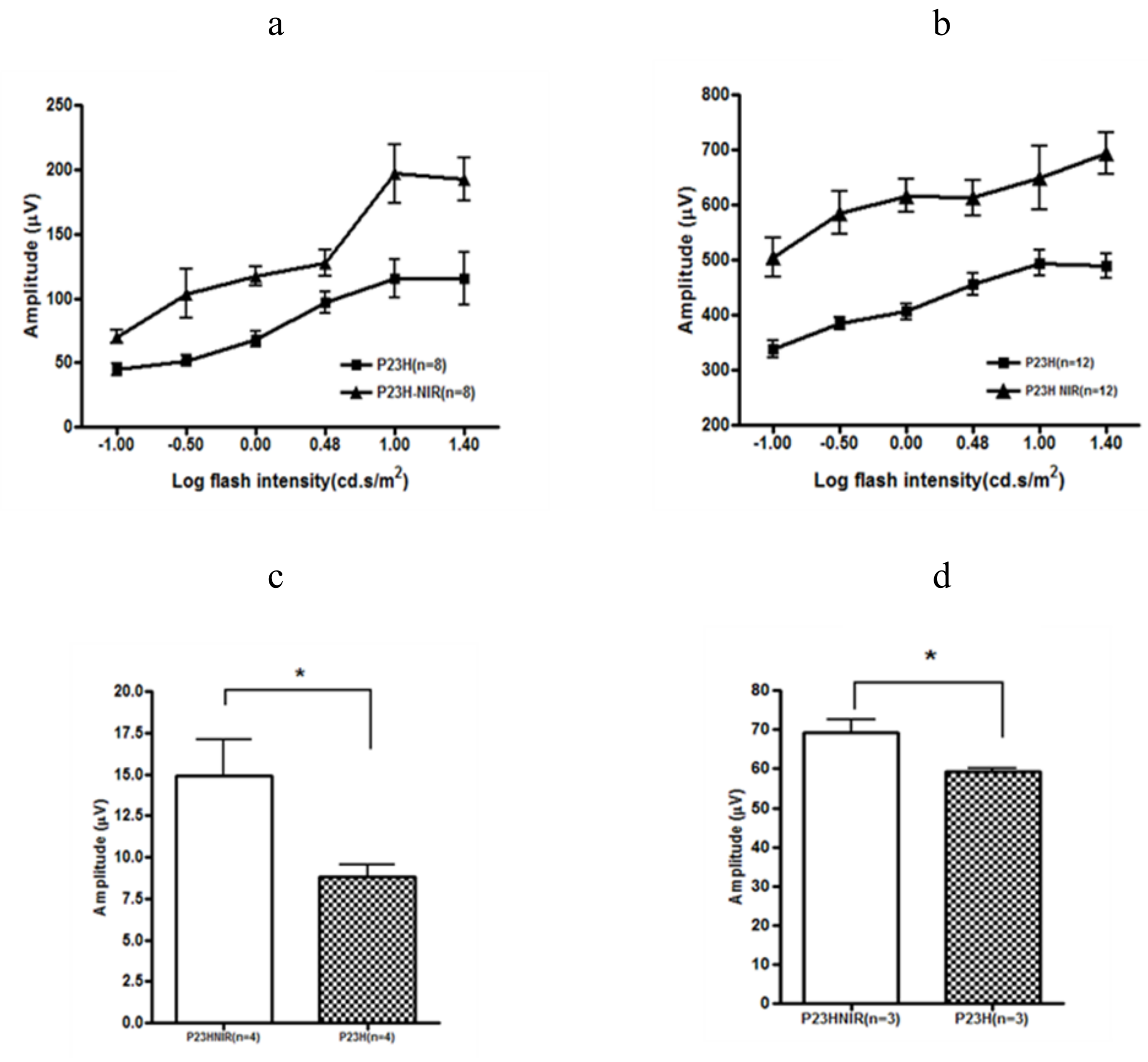

Figure 52a shows the mean a-wave amplitude and figure 52b shows the mean b-wave amplitude assessed by the scotopic intensity series protocol comparing P23H transgenic retina (■) and 830 nm treated P23H retina (▲). 830 nm caused a significant increase in both a-wave ($F_{(1, 14)} = 16.32$, $p < .001$; n=8, Fig. 52a) and b-wave amplitudes ($F_{(1, 22)} = 23.57$, $p < .001$; n=12, Fig. 52b) at all flash intensities compared to the P23H group. Figure 52c shows the ISCEV protocol for Rod only response (a wave; flash strength -10mcds/m^2) which was significantly (p<.05)and Figure 52d shows ISCEV protocol for Standard Rod and Cone response (a wave; flash strength -3000 mcds/m^2). Error bars: SEM.

830 nm photobiomodulation preserved retinal structure in the P23H rat

Figure 53 a shows a comparison of the total retinal thickness of P23H transgenic group with the in NIR-PBM treated group using SD-OCT at p30. In our studies the preservation of total retinal thickness was evident in the in NIR-PBM treated group compared to the non-treated group. The mean total retinal thickness was significantly (*p*<.01) higher in NIR-PBM treated group (171.1 ± 2.0 µm, n=5) when compared to the P23H group (169.2 ± 3.1µm, n=5). Figure 53 b compares the ONL thickness in µm at identical locations on either side of the ONH. The ONL thickness of NIR-PBM treated group was significantly greater ($F_{(1,\ 8)} = 12.23$, $p < .01$; Fig. 53b) compared to the sham-treated group across the entire scan.

Figure 54 shows histologic labeling of plastic sections stained with toluidine blue, which was used to detect surviving photoreceptors in the retina. Histomorphometry demonstrated that the P23H transgene led to structural damage in the outer retina. The ONL was disorganized and there was loss of photoreceptor nuclei and thinning of ONL (Figure 55). The cumulative effect of photoreceptor cell death was assessed by the measurement of the ONL thickness (Figure 55). The number of nuclei in the superior segment of the ONL was significantly greater in the NIR-PBM treated group compared the non-treated group and a similar trend was seen in the inferior segment of the eye.

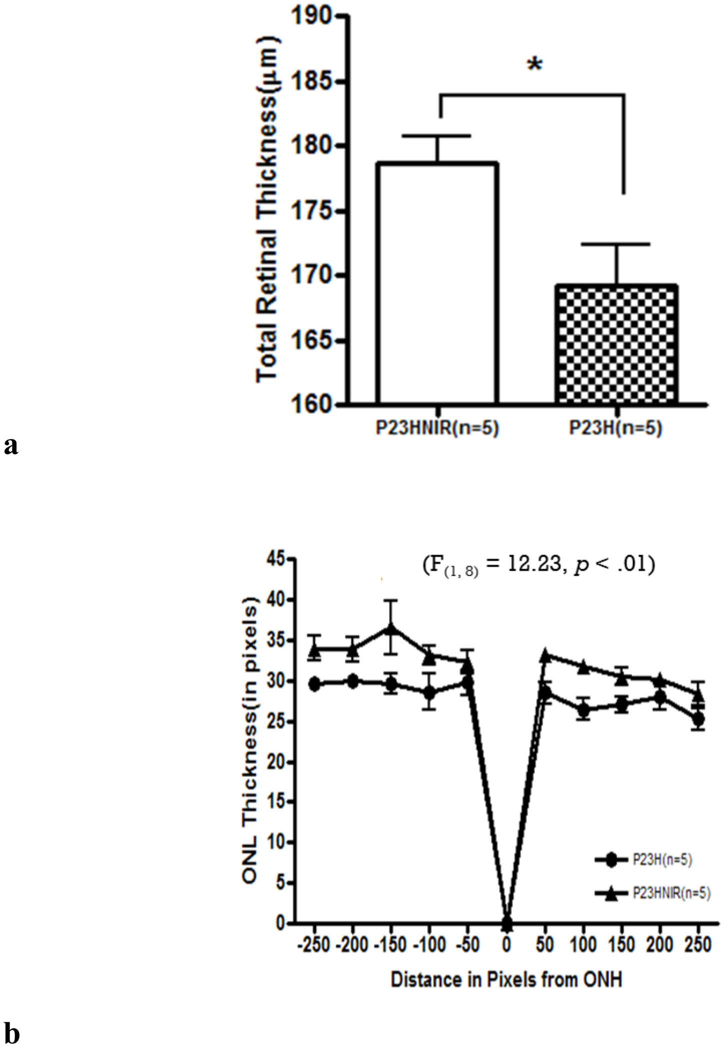

Figure 53a and b compares the total retinal thickness and ONL thickness respectively from SD-OCT linear scans (1000 A-scans/B-scan, 80 B-scans). Total retinal thickness was significantly ($p < .05$; Fig. 53a) higher in NIR-PBM treated group when compared to the P23H group. The ONL thickness of NIR-PBM treated group (▲) derived from Longitudinal Reflectivity Profile (LRP) was significantly greater ($F_{(1,\ 8)} = 12.23$, $p < .01$; Fig.53b) compared to the sham-treated group (●) across the entire scan.

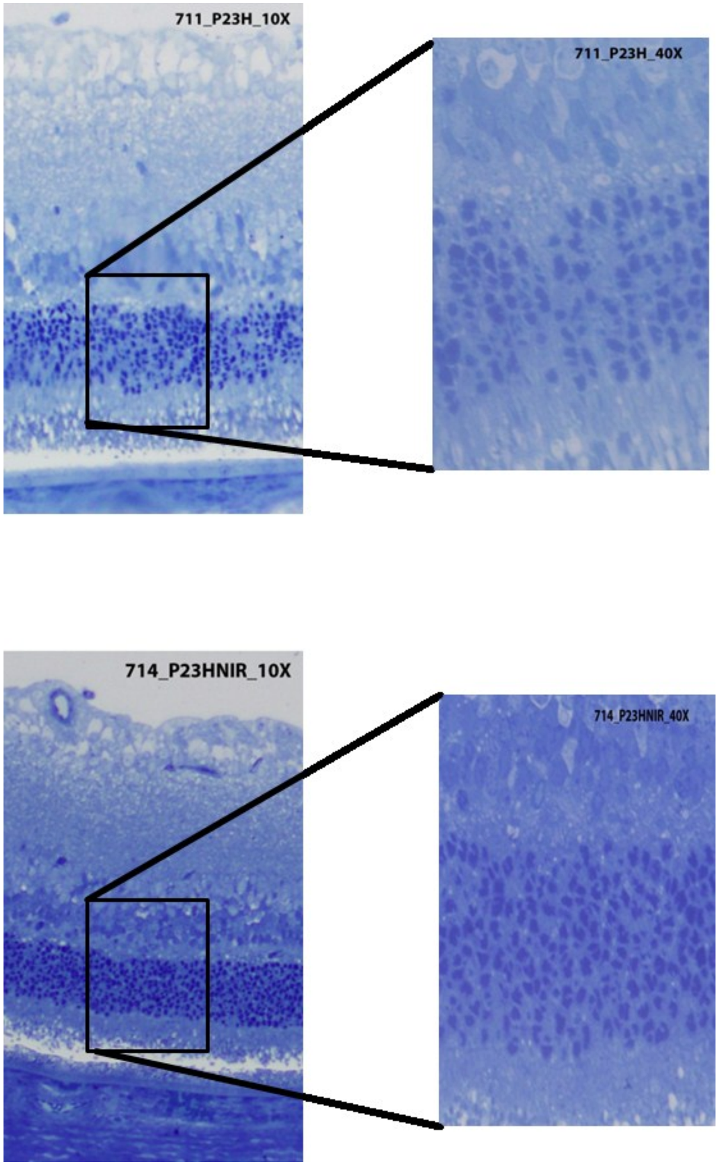

Figure 54 compares the representative images of retinal sections stained with toluidine blue between sham-treated group and the NIR-PBM treated group. The ONL in the NIR-PBM treated group is more organized and symmetrically packed when compared to the sham-treated which was highly disrupted and disorganized.

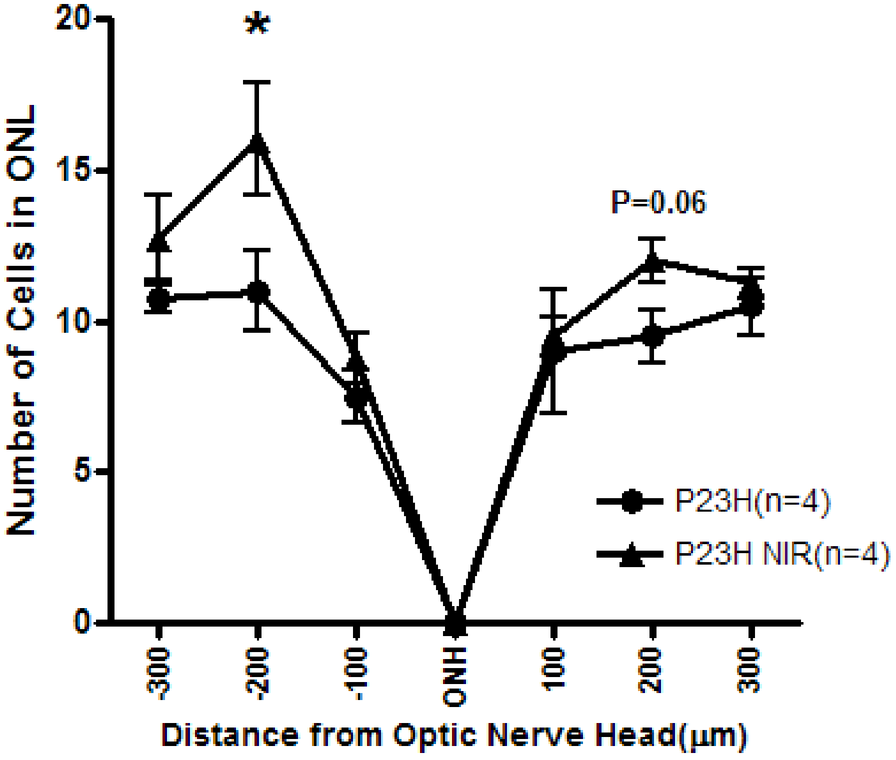

Figure 55 shows quantitative analyses of the ONL thickness sampled across the retina from the superior to inferior edge (n = 4). ONL thickness in NIR-PBM treated group is significantly greater compared to the P23H group. Error bars: SEM.

Efficacy of 830 nm photobiomodulation in P23H transgenic retina monitored by a longitudinal study

Figure 56 and 57 summarize the changes in retinal structure over time following NIR-PBM using SD-OCT. The retinoprotective effects of NIR PBM administered in P23H transgenic rats during the critical period (p10-p25) diminishes as the animal matures and statistically significant difference (*p*<.01) with the non-treated group was found only at the time period, p25. At p25, the average total retinal thickness of P23H-NIR group was 173.7 ± 2.0 µm compared to 159.6 ± 1.89 µm of the non-treated group. However there was an increase trend in the total retinal thickness at p32 (161.6 ± 1.3 µm vs. 155.1 ± 0.57 µm), p39 (156.3 ± 1.3 µm vs. 153.3 ± 1.8 µm) which diminishes at p80.

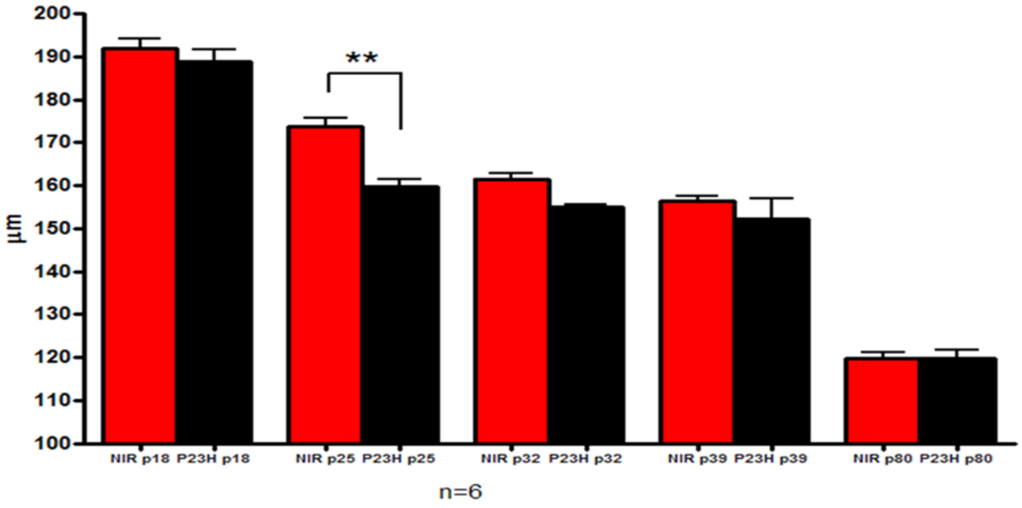

Figure 56 compares the total retinal thickness between NIR-PBM treated group and sham-treated group monitored in a longitudinal study using SD-OCT. The retinoprotective effects of NIR PBM diminishes as the animal matures and statistically significant difference (p<.01) with the non-treated group was found only at the time period, p25. Error bars: SEM.

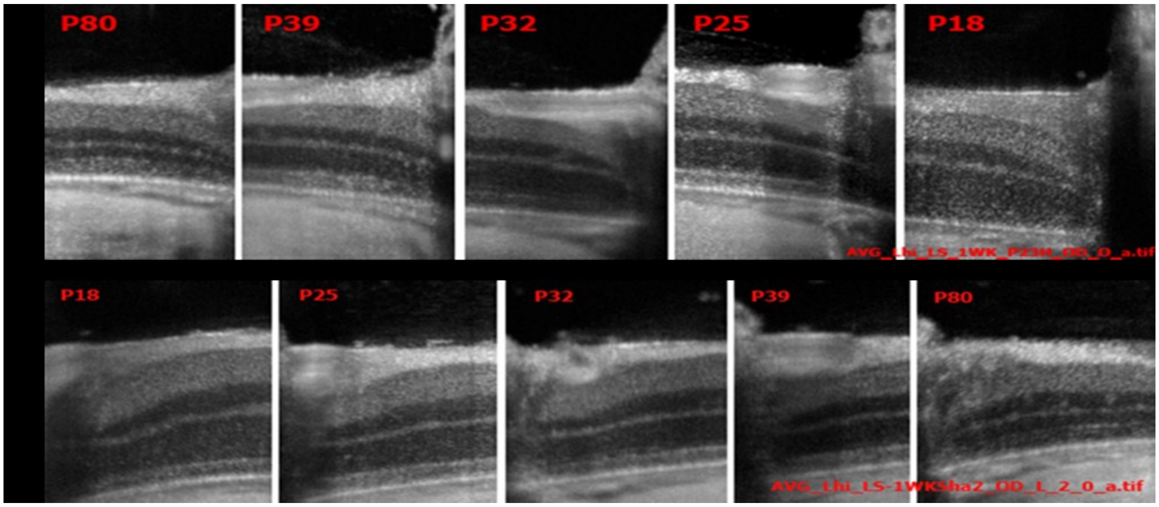

Figure 57 compares representative linear scans at p18, p25, p32, p39 and p80

830 nm photobiomodulation preserved the mitochondrial redox state of the P23H retina.

Figure 58 displays, from left to right, maximum projection images of NADH, FAD, and NADH -RR (NADH/FAD) for a representative retina in normal (SD), transgenic (P23H) and NIR treated (P23H-NIR) groups. The retina in the control group (first column in Figure 58) showed a lower concentration of FAD and a higher concentration of NADH compared to P23H transgenic retina (second column in Figure 58). Thus, the NADH RR is higher (more reduced state) in retina from normal SD eyes compared to the eyes from P23H transgenic rats (more oxidized) suggesting the role of increased oxidative stress and dysfunctional mitochondria in the P23H transgenic retina. Sections from NIR-PBM treated group (third column in Figure 58) consistently demonstrated lower concentrations of FAD, higher concentration of NADH and higher NADH RR compared to P23H transgenic retina demonstrating an altered mitochondrial redox state following NIR-PBM, suggesting decrease in oxidative stress.

Figure 58 (lower panel) shows the NADH redox histograms of a representative eye in each normal, P23H transgenic and NIR-PBM treated groups. In the P23H group the NADH RR indicates a more oxidized mitochondrial redox state with a mean value of 0.80 ± 0.1 compared to a higher mean value of 1.2 ± 0.4 in normal control SD eye[7]. NADH redox histogram for the representative NIR-PBM eye demonstrated a shift to the right with a mean value of 1.02 ± 0.2.

Figure 59 compares the mean values of the NADH RR histograms of max projected images from normal, P23H and NIR-PBM treated groups. The mean NADH RR reveals a significant decrease (p<.001) in P23H transgenic eyes compared to normal SD eyes suggesting an increased accumulation of ROS and mitochondrial dysfunction leading to accumulation of oxidized forms (NAD and FAD) of the mitochondrial coenzymes NADH and FADH as a result of the progressive retinal degeneration in the P23H transgenic retina. 830 nm irradiation of the P23H retina significantly up regulated the NADH RR (p<.01) by increasing the reduced NADH and decreasing FAD. These results support the previous studies suggesting the ability of NIR-PBM to decrease oxidative stress and improve mitochondrial function in progressive retinal and neurodegenerative disorders[22,19]

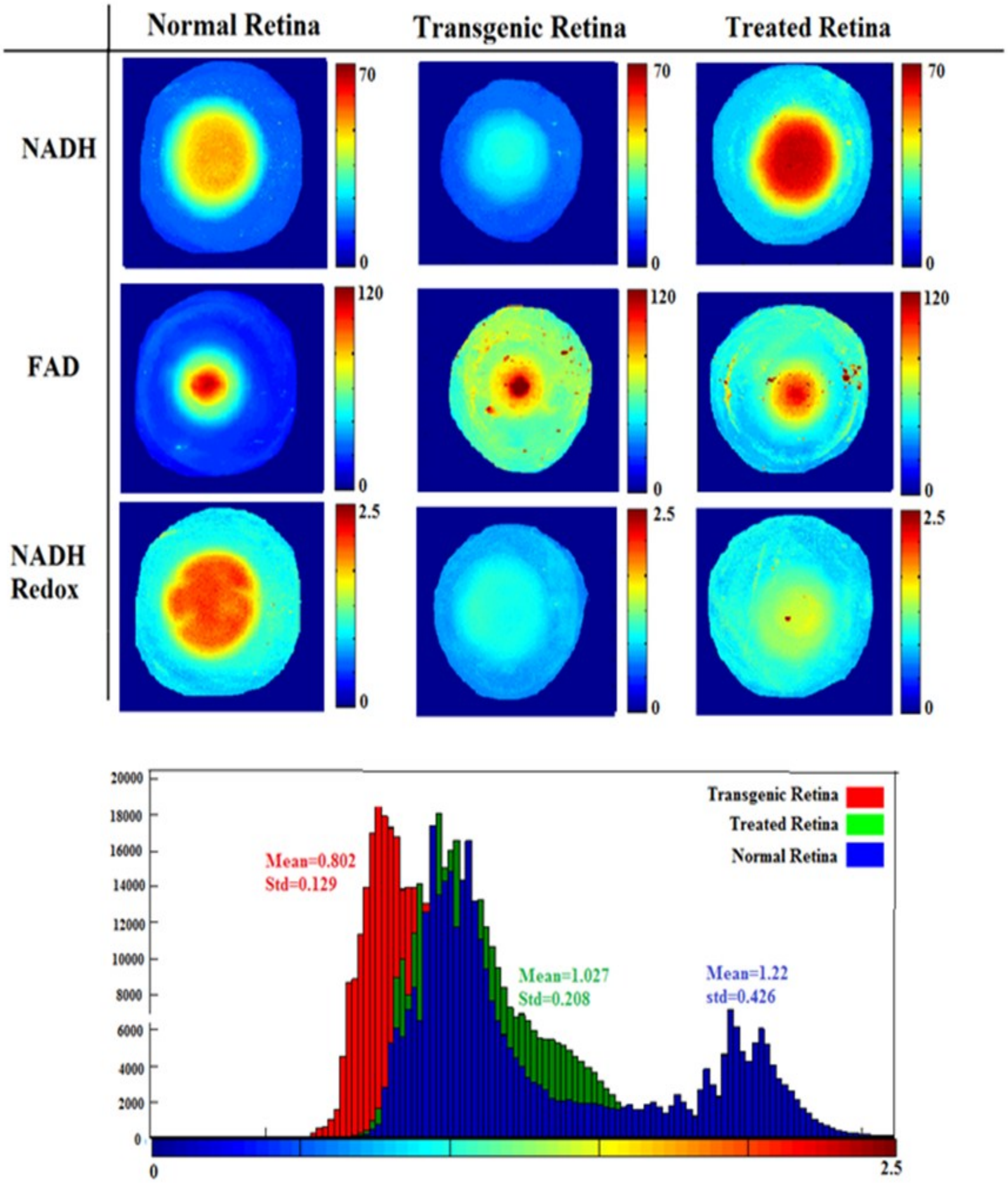

Figure 58 Upper panel shows a representative max projected NADH (upper panel), FAD (middle panel) and RR images (lower panel) for normal (SD), P23H transgenic and 830 nm treated transgenic eyes. Lower panel shows a representative NADH redox histogram for eyes comparing normal (SD), P23H transgenic and 830 nm treated transgenic eyes

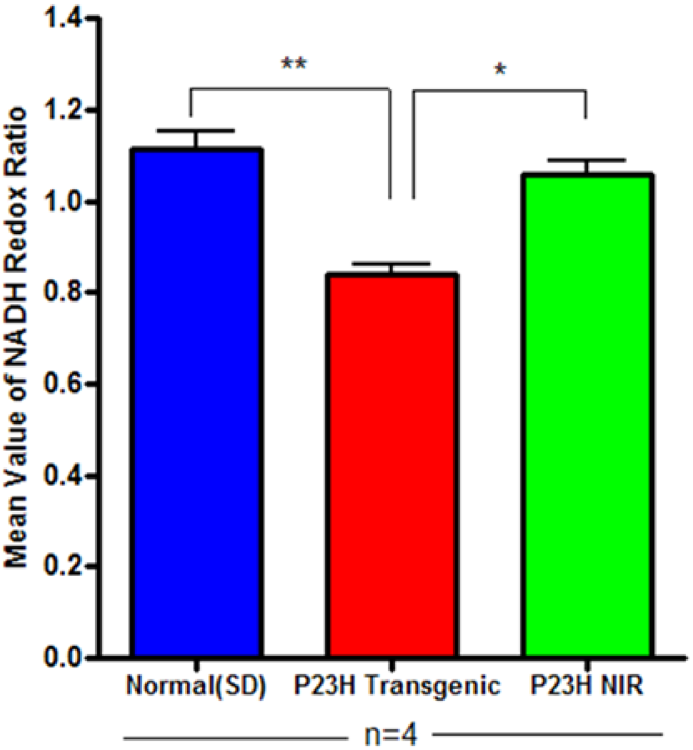

Figure 59 represents bar graph plot comparing the mean values of the histograms of max projected images from SD, P23H transgenic and 830 nm treated P23H transgenic rat eyes. The results show a significant decrease in the ratio between normal and diseased eyes (**p<.01) which is reversed to normal by 830 nm treatment (*p <.01). Error bars: SEM.

Discussion

Even though photobiomodulation by NIR photons are extensively used by researchers to demonstrate preservation and stimulation of cellular events in various clinical and experimental animal models the use of photobiomodulation is still controversial and debated because of the incomplete knowledge of the mechanism of action and the differences in the treatment parameters used by various investigators like range of wavelength, dose, and the nature of light source- Laser vs. non-coherent light ; polarized vs. unpolarized; pulsed vs. continuous wave [36-39]. The altered kinetics of the photoacceptor molecule (cytochrome c oxidase) after NIR photon interaction and how it alters the mitochondrial redox state that triggers secondary signaling cascades which culminate in improved mitochondrial function remains a ‘‘black box’’ and future experiments should emphasize to resolve the above issues.

This report demonstrates that 830 nm PBM can ameliorate the disease progression in the P23H rat model of RP. Recent studies have demonstrated the neuroprotective action of photobiomodulation in several experimental models of progressive degenerative disease including Parkinson’s disease[40,41], Alzheimer's disease[42], multiple sclerosis[25], light-induced retinal degeneration[24,23] and age-related retinal inflammation[40, 43,41]. Clinical studies have confirmed the therapeutic potential of photobiomodulation at doses ranging from 3 to 6 J/cm^2 in radiation and chemotherapy-induced mucositis and stroke[20,44,45,46]. A substantial body of evidence demonstrates that mitochondria are the initial site of action of near-infrared photons leading to mitochondrial repair, increased ATP production, attenuation of oxidative stress and induction of transcription factors[47,22,30,48,43]. *In vitro* studies in our laboratory and by other investigators have shown that near-infrared radiation interacts with the key mitochondrial enzyme of the electron transport chain, cytochrome oxidase, triggering signaling mechanisms that result in improved mitochondrial energy metabolism, antioxidant production and cell survival[18, 19, 49]. Moreover, NIR photon irradiation has been shown to increase electron transfer in purified cytochrome oxidase[50] and up regulate cytochrome oxidase activity in cultured neuronal cells[51]. A similar pattern of thinning of ONL and severely distorted retina was reported in a light-induced retinal degeneration model where NIR-PBM was shown to preserve the retinal structure[24].

Photobiomodulation promotes retinoprotection

Our findings demonstrate that 830 nm photobiomodulation during the critical period (p10-p25) of photoreceptor degeneration in P23H transgenic rats protected against the loss of photoreceptor function and preserved the structural integrity of retina. Both a- and b-wave amplitudes were significantly greater in NIR treated animals indicative of a protection of photorecptor function. The functional protection demonstrated in this manuscript agrees with that reported by Albarracin et al[24] in a light-induced retinal degeneration model. The *in vivo* imaging studies using SD-OCT corroborate the histology data showing that ONL thickness was significnatly preserved in the NIR-treated animals. Morover better nuclear packing and more even arrangement in the ONL was observed in the NIR treated retina compared to that of the sham-treated retina.

The longitudinal study measuring the total retinal thickness demonstrated that the maximum protection is achevied if the photobiomodulation is applied during the critical period. Photobiomodulation treatment parameters used in the study are based on those used effectively by other researchers and the lens transmission spectral studies on albino rat lens demonstrate that the dose delivered on the surface of the lens and cornea will be transmitted between 90 and 100%[52,43]. Importantly, there was no evidence of damage to the normal, nonchallenged retina after NIR PBM.

To the best of our knowledge, there has been no other study that has examined NADH/FAD RR expression in intact eye tissue before and after NIR PBM. This method demonstrates a direct analysis of the cellular metabolic state within the mitochondrial compartment of the retina. The two endogenous fluorophores in tissue that reflect cellular metabolism in the electron transport chain are NADH (transfers electrons to molecular oxygen) and FAD (electron acceptor). Our studies demonstrate that in P23H transgenic retina there is a greater concentration of FAD and lower concentration of NADH compared to normal SD retina indicative of the presence of oxidized mitochondria. In the animals treated with 830nm light, there was a significant reversal in the FAD and NADH signals reflected in the NADH RR and indicative of protection of normal mitochondrial function and a reduction of oxidative stress.

Clinical Significance

The results of this study demonstrate retinoprotection mediated by NIR-PBM in a well-established rodent model of RP. This protection was evident in structural, functional and metabolic studies. Based on these findings, we suggest that NIR-PBM may represent an innovative therapeutic approach for the treatment of retinal injury and the treatment of retinal diseases, including AMD, glaucoma, diabetic retinopathy, and LHON where mitochondrial dysfunction and oxidative stress play a central role in the pathology.

References

1. Berson EL. Retinitis pigmentosa. The Friedenwald Lecture. *Invest Ophthalmol Vis Sci* 1993;34:1659-1676.

2. Hartong DT, Berson EL, Dryja TP. Retinitis pigmentosa. *Lancet* 2006;368:1795-1809.

3. Hamel C. Retinitis pigmentosa. *Orphanet J Rare Dis* 2006;1:40.

4. Berger W, Kloeckener-Gruissem B, Neidhardt J. The molecular basis of human retinal and vitreoretinal diseases. *Prog Retin Eye Res* 2010;29:335-375.

5. Dryja TP, McGee TL, Reichel E, et al. A point mutation of the rhodopsin gene in one form of retinitis pigmentosa. *Nature* 1990;343:364-366.

6. Yu DY, Cringle S, Valter K, Walsh N, Lee D, Stone J. Photoreceptor death, trophic factor expression, retinal oxygen status, and photoreceptor function in the P23H rat. *Invest Ophthalmol Vis Sci* 2004;45:2013-2019.

7. Yu DY, Cringle SJ. Oxygen distribution and consumption within the retina in vascularised and avascular retinas and in animal models of retinal disease. *Prog Retin Eye Res* 2001;20:175-208.

8. Campian JL, Qian M, Gao X, Eaton JW. Oxygen tolerance and coupling of mitochondrial electron transport. *J Biol Chem* 2004;279:46580-46587.

9. Vlachantoni D, Bramall AN, Murphy MP, et al. Evidence of severe mitochondrial oxidative stress and a protective effect of low oxygen in mouse models of inherited photoreceptor degeneration. *Hum Mol Genet* 2011;20:322-335.

10. Carmody RJ, Cotter TG. Oxidative stress induces caspase-independent retinal apoptosis in vitro. *Cell Death Differ* 2000;7:282-291.

11. Portera-Cailliau C, Sung CH, Nathans J, Adler R. Apoptotic photoreceptor cell death in mouse models of retinitis pigmentosa. *Proc Natl Acad Sci U S A* 1994;91:974-978.

12. Kong GY, Van Bergen NJ, Trounce IA, Crowston JG. Mitochondrial dysfunction and glaucoma. *J Glaucoma* 2009;18:93-100.

13. Pieczenik SR, Neustadt J. Mitochondrial dysfunction and molecular pathways of disease. *Exp Mol Pathol* 2007;83:84-92.

14. Karunadharma PP, Nordgaard CL, Olsen TW, Ferrington DA. Mitochondrial DNA damage as a potential mechanism for age-related macular degeneration. *Invest Ophthalmol Vis Sci* 2010;51:5470-5479.

15. de Sousa AP, Santos JN, Dos Reis JA, Jr., et al. Effect of LED phototherapy of three distinct wavelengths on fibroblasts on wound healing: a histological study in a rodent model. *Photomed Laser Surg* 2010;28:547-552.

16. Lim J, Sanders RA, Snyder AC, Eells JT, Henshel DS, Watkins JB, 3rd. Effects of low-level light therapy on streptozotocin-induced diabetic kidney. *J Photochem Photobiol B* 2010;99:105-110.

17. Whelan HT, Buchmann EV, Dhokalia A, et al. Effect of NASA light-emitting diode irradiation on molecular changes for wound healing in diabetic mice. *J Clin Laser Med Surg* 2003;21:67-74.

18. Wong-Riley MT, Liang HL, Eells JT, et al. Photobiomodulation directly benefits primary neurons functionally inactivated by toxins: role of cytochrome c oxidase. *J Biol Chem* 2005;280:4761-4771.

19. Eells JT, Henry MM, Summerfelt P, et al. Therapeutic photobiomodulation for methanol-induced retinal toxicity. *Proc Natl Acad Sci U S A* 2003;100:3439-3444.

20. Lampl Y, Zivin JA, Fisher M, et al. Infrared laser therapy for ischemic stroke: a new treatment strategy: results of the NeuroThera Effectiveness and Safety Trial-1 (NEST-1). *Stroke* 2007;38:1843-1849.

21. Stemer AB, Huisa BN, Zivin JA. The evolution of transcranial laser therapy for acute ischemic stroke, including a pooled analysis of NEST-1 and NEST-2. *Curr Cardiol Rep* 2010;12:29-33.

22. Fitzgerald M, Bartlett CA, Payne SC, et al. Near infrared light reduces oxidative stress and preserves function in CNS tissue vulnerable to secondary degeneration following partial transection of the optic nerve. *J Neurotrauma* 2010;27:2107-2119.

23. Qu C, Cao W, Fan Y, Lin Y. Near-infrared light protect the photoreceptor from light-induced damage in rats. *Adv Exp Med Biol* 2010;664:365-374.

24. Albarracin R, Eells J, Valter K. Photobiomodulation protects the retina from light-induced photoreceptor degeneration. *Invest Ophthalmol Vis Sci* 2011;52:3582-3592.

25. Muili KA, Gopalakrishnan S, Meyer SL, Eells JT, Lyons JA. Amelioration of Experimental Autoimmune Encephalomyelitis in C57BL/6 Mice by Photobiomodulation Induced by 670 nm Light. *PLoS One* 2012;7:e30655.

26. Karu TI. Mitochondrial signaling in mammalian cells activated by red and near-IR radiation. *Photochem Photobiol* 2008;84:1091-1099.

27. Karu T. Primary and secondary mechanisms of action of visible to near-IR radiation on cells. *J Photochem Photobiol B* 1999;49:1-17.

28. Passarella S, Casamassima E, Molinari S, et al. Increase of proton electrochemical potential and ATP synthesis in rat liver mitochondria irradiated in vitro by helium-neon laser. *FEBS Lett* 1984;175:95-99.

29. Passarella S, Ostuni A, Atlante A, Quagliariello E. Increase in the ADP/ATP exchange in rat liver mitochondria irradiated in vitro by helium-neon laser. *Biochem Biophys Res Commun* 1988;156:978-986.

30. Natoli R, Zhu Y, Valter K, Bisti S, Eells J, Stone J. Gene and noncoding RNA regulation underlying photoreceptor protection: microarray study of dietary antioxidant saffron and photobiomodulation in rat retina. *Mol Vis* 2010;16:1801-1822.

31. Tanna H, Dubis AM, Ayub N, et al. Retinal imaging using commercial broadband optical coherence tomography. *Br J Ophthalmol* 2010;94:372-376.

32. Abramoff MD MP, Ram SJ. Image processing with ImageJ. *J Biophotonics International* 2004;11:36-42.

33. Huang Y, Cideciyan AV, Papastergiou GI, et al. Relation of optical coherence tomography to microanatomy in normal and rd chickens. *Invest Ophthalmol Vis Sci* 1998;39:2405-2416.

34. Usui S, Komeima K, Lee SY, et al. Increased expression of catalase and superoxide dismutase 2 reduces cone cell death in retinitis pigmentosa. *Mol Ther* 2009;17:778-786.

35. Maleki S, Sepehr R, Staniszewski K, Sheibani N, Sorenson CM, Ranji M. Mitochondrial redox studies of oxidative stress in kidneys from diabetic mice. *Biomed Opt Express* 2012;3:273-281.

36. Chung H, Dai T, Sharma SK, Huang YY, Carroll JD, Hamblin MR. The nuts and bolts of low-level laser (light) therapy. *Ann Biomed Eng* 2012;40:516-533.

37. Posten W, Wrone DA, Dover JS, Arndt KA, Silapunt S, Alam M. Low-level laser therapy for wound healing: mechanism and efficacy. *Dermatol Surg* 2005;31:334-340.

38. Quirk BJ, Desmet KD, Henry M, et al. Therapeutic effect of near infrared (NIR) light on Parkinson's disease models. *Front Biosci (Elite Ed)* 2012;4:818-823.

39. Wu Q, Xuan W, Ando T, et al. Low-level laser therapy for closed-head traumatic brain injury in mice: effect of different wavelengths. *Lasers Surg Med* 2012;44:218-226.

40. Peoples C, Spana S, Ashkan K, et al. Photobiomodulation enhances nigral dopaminergic cell survival in a chronic MPTP mouse model of Parkinson's disease. *Parkinsonism Relat Disord* 2012;18:469-476.

41. Shaw VE, Peoples C, Spana S, et al. Patterns of Cell Activity in the Subthalamic Region Associated with the Neuroprotective Action of Near-Infrared Light Treatment in MPTP-Treated Mice. *Parkinsons Dis* 2012;2012:296875.

42. Sommer AP, Bieschke J, Friedrich RP, et al. 670 nm laser light and EGCG complementarily reduce amyloid-beta aggregates in human neuroblastoma cells: basis for treatment of Alzheimer's disease? *Photomed Laser Surg* 2012;30:54-60.

43. Kokkinopoulos I, Colman A, Hogg C, Heckenlively J, Jeffery G. Age-related retinal inflammation is reduced by 670 nm light via increased mitochondrial membrane potential. *Neurobiol Aging* 2012.

44. Cauwels RG, Martens LC. Low level laser therapy in oral mucositis: a pilot study. *Eur Arch Paediatr Dent* 2011;12:118-123.

45. Bensadoun RJ, Nair RG. Low-level laser therapy in the prevention and treatment of cancer therapy-induced mucositis: 2012 state of the art based on literature review and meta-analysis. *Curr Opin Oncol* 2012;24:363-370.

46. Hodgson BD, Margolis DM, Salzman DE, et al. Amelioration of oral mucositis pain by NASA near-infrared light-emitting diodes in bone marrow transplant patients. *Support Care Cancer* 2012;20:1405-1415.

47. Liang HL, Whelan HT, Eells JT, et al. Photobiomodulation partially rescues visual cortical neurons from cyanide-induced apoptosis. *Neuroscience* 2006;139:639-649.

48. Whelan HT, Connelly JF, Hodgson BD, et al. NASA light-emitting diodes for the prevention of oral mucositis in pediatric bone marrow transplant patients. *J Clin Laser Med Surg* 2002;20:319-324.

49. Rojas JC, Lee J, John JM, Gonzalez-Lima F. Neuroprotective effects of near-infrared light in an in vivo model of mitochondrial optic neuropathy. *J Neurosci* 2008;28:13511-13521.

50. Pastore D, Greco M, Passarella S. Specific helium-neon laser sensitivity of the purified cytochrome c oxidase. *Int J Radiat Biol* 2000;76:863-870.

51. Wong-Riley MT, Bai X, Buchmann E, Whelan HT. Light-emitting diode treatment reverses the effect of TTX on cytochrome oxidase in neurons. *Neuroreport* 2001;12:3033-3037.

52. Lei B, Yao G. Spectral attenuation of the mouse, rat, pig and human lenses from wavelengths 360 nm to 1020 nm. *Exp Eye Res* 2006;83:610-614.

53. Srinivasan VJ, Monson BK, Wojtkowski M, et al. Characterization of outer retinal morphology with high-speed, ultrahigh-resolution optical coherence tomography. *Invest Ophthalmol Vis Sci* 2008;49:1571-1579.

CHAPTER 8

DISCUSSION AND CONCLUSIONS

Taken as a whole, the When taken together the studies presented in this thesis provides novel insights into the putative mechanism for NIR PBM involving mitochondria which leads to retinoprotective effects and emphasize the importance of harnessing the capacity of damaged cells to self-repair for the treatment of inherited retinal degenerations like RP, for which no current treatment strategies are available.

The current study was designed based on the growing body of evidence that exposure of tissue to low energy photon irradiation in the far-red (FR) to near-infrared (NIR) range of the spectrum (630-1000 nm) interacts with the mitochondrial enzyme cytochrome oxidase inducing a cascade of signaling events that culminate in improved cell survival. FR/NIR light has been shown to restore the function of damaged mitochondria, up-regulate the production of cytoprotective factors and prevent apoptotic cell death in clinical and experimental models of neurodegenerative diseases (Eells, Wong-Riley et al. 2004; Wong-Riley, Liang et al. 2005; Desmet, Paz et al. 2006; Fitzgerald, Bartlett et al. 2010).

The current studies have assessed the use of NIR PBM in non-dystrophic animal model. These studies showed that PBM did not alter the functional and structural integrity of the retina and support the safety of PBM which is essential to advance the therapy to clinical use. In a non-dystrophic animal model there was no significant difference in structural integrity and the functional response of the retina between active treatment group and the sham control group. This result is of significant clinical importance and similar results are reported in clinical trials in the treatment of radiation-induced mucositis and stroke

(Lampl, Zivin et al. 2007) (Whelan, Connelly et al. 2002). Studies on the efficacy of NIR PBM in non-dystrophic animal model support the hypothesis by our collaborators and other investigators that preconditioning events may be triggered in healthy non challenged retina at the cellular level by NIR PBM that leads to altered regulation of damaging genes that respond differently in the presence of any cellular stress events. Lack of any apparent effect was demonstrated in the sham control group after exposure to NIR photons in light-induced retinal degeneration and methanol-induced retinal cytotoxicity models (Eells, Henry et al. 2003) (Albarracin, Eells et al. 2011).

Mitochondria is shown to selectively absorb wavelengths 670 nm and 830 nm of the far-red to near-infrared range of the electromagnetic spectrum (Greco, Guida et al. 1989). Using action spectrum studies, Wong-Riley et al. demonstrated that 670-nm and 810-nm photon irradiation rescued visual cortical neurons from cyanide-mediated cytotoxicity (Wong-Riley, Liang et al. 2005). Karu et al. reported that the mitochondrial photoacceptor molecule, cytochrome c oxidase has distinct absorption bands in the red (~665 nm) and in the NIR (~810 nm) region of the electromagnetic spectrum (Karu, Pyatibrat et al. 2005). The work presented has shown that the effect of 830nm PBM is more robust than 670 nm PBM in preserving retinal function and structural integrity in P23H transgenic model of RP. Recently Albarracin et al. demonstrated that 670nm PBM attenuated bright-light induced retinal degeneration in albino rats (Albarracin, Eells et al. 2011). In our studies using the P23H model of retinal degeneration we did not see protection with 670 nm PBM. An important difference in the two studies is the dose of the light. In our study, rats were treated for 90 sec at 60 mW/cm^2 resulting in a dose of 5.4 J/cm^2. In the Abarracin study, rats were pre-treated for 180 sec at 60 mW/cm^2 resulting in a dose of 10.8 J/cm^2.

Comparing the efficacy of 830nm photobiomodulation using three different treatment paradigms- photobiomodulation during the critical period of photoreceptor degeneration (p10-p25), photobiomodulation during the onset of the critical period of photoreceptor cell death to young adulthood (p10-p 40) and photobiomodulation during the later stage (p20-p 40) to rescue remaining photoreceptors was essential to characterize the most effective treatment window using 830 nm photons and with the current P23H transgenic model used in this study we report that the effective time period to perform 830nm PBM to attenuate disease progression is the 'critical period' of photoreceptor degeneration. Studies' demonstrating the prolonged effect of brief photobiomodulation treatment implies interaction of NIR photons at the cellular level induces a cascade of events leading to the stimulation of gene expression, protein synthesis, and oxidative metabolism (Eells, Henry et al. 2003). The functional rescue of photoreceptors in p10-p 40 paradigm demonstrates the ability to use 830 nm photons from onset of the disease extending to adulthood. Future experiments will be designed to validate the efficacy of extended treatment protocols. Variability in the onset and presentation of clinical symptoms in RP with individuals having same mutation is challenging. The structural and functional preservation of photoreceptors in p20-p40 paradigm by 830nm photobiomodulation holds promise for the use of NIR PBM during the later stages of degeneration process.

Oxidative stress associated with mitochondrial dysfunction play a key role in the pathogenesis of RP and in other retinal degenerative disorders including glaucoma, age related macular degeneration (AMD) and diabetic retinopathy (Kong, Tanito et al. 2007; Kong, Van Bergen et al. 2009; Karunadharma, Nordgaard et al. 2010). To the best of our knowledge, this thesis demonstrate the first attempts to provide a direct analysis of the cellular metabolic state within the mitochondrial compartment of the retina of P23H transgenic rat model of RP by imaging endogenous fluorophores using novel optical cryofluorescence imaging technique that has very high sensitivity and specificity (Chapter 5). NADH redox ratio, acts as a quantitative marker of the mitochondrial redox and metabolic state of tissue *ex vivo* and *in vivo* (Ranji, Jaggard et al. 2006; Ranji, Kanemoto et al. 2006; Sepehr, Staniszewski et al. 2012). Our findings showed that P23H transgene caused a significant increase in the oxidized forms (NAD and FAD) of the coenzymes NADH and $FADH_2$ and NIR PBM by 830 nm reduced the NAD and FAD in the degenerating retina significantly there by altering the NADH redox ratio. The redox alterations observed in mitochondria results in the activation of intracellular signaling cascades which culminate in improved mitochondrial function, increased synthesis of cytoprotective factors and cell survival. We observed an increase in signal intensity in the eye samples from the vitreous in both NADH and FAD channels that needs to be further investigated and explained.

Use of NIR PBM may be a challenge in individuals having inherited or induced retinal degeneration with anterior segment anomalies (e.g. primary defects in lens) of the eye which will interfere with the delivery of photons to the retina and it should be addressed while recruiting people in clinical trials.

The functional, structural and metabolic insights obtained from the current study provides crucial information needed for clinical trials and FDA approval for the use of NIR-LED devices in the treatment of retinal degenerative diseases. By harnessing the potential of damaged cells to self-repair, photobiomodulation may provide an innovative and non-invasive therapeutic approach for the prevention and treatment of retinal degenerative disease.

Future Directions

Although photobiomodulation by NIR photons is extensively used by researchers to demonstrate preservation and stimulation of cellular events in various clinical and experimental animal models the use of photobiomodulation is still controversial and debated because of the incomplete knowledge of the mechanism of action and the differences in the treatment parameters used by various investigators like range of wavelength, dose, and the nature of light source- Laser vs. non-coherent light ; polarized vs. unpolarized; pulsed vs. continuous wave (Posten, Wrone et al. 2005; Quirk and Whelan 2011; Wu, Xuan et al. 2012) (Chung, Dai et al. 2012). The altered kinetics of the photoacceptor molecule (cytochrome c oxidase) after NIR photon interaction and the how it alters the mitochondrial redox state that triggers secondary signaling cascades which culminate in improved mitochondrial function remains a ‘‘black box’’ and future experiments should emphasize to resolve the above issues.

This thesis validated the safety of using NIR photobiomodulation in non-dystrophic rats in which animals are treated from p10-p25, which is the critical period of photoreceptor development, however, it is crucial to demonstrate that photobiomodulation does not adversely affect retinal function, metabolism and retinal architecture during prolonged treatment paradigms. So far there are no reported adverse effects of PBM in experimental and clinical studies (Whelan, Buchmann et al. 2003; Lampl, Zivin et al. 2007; Oron, Oron et al. 2012). Recent studies from our collaborators in alpha-synuclein transgenic mice model of Parkinson's disease showed no evidence of adverse effects in which animals were treated daily with 670 nm PBM for more than a year (Quirk, Desmet et al. 2012).

BIBLIOGRAPHY

Albarracin, R., J. Eells, et al. (2011). "Photobiomodulation protects the retina from light-induced photoreceptor degeneration." Invest Ophthalmol Vis Sci **52**(6): 3582-3592.

Alexandratou, E., D. Yova, et al. (2002). "Human fibroblast alterations induced by low power laser irradiation at the single cell level using confocal microscopy." Photochem Photobiol Sci **1**(8): 547-552.

Ali, R. R., M. B. Reichel, et al. (1998). "Absence of p53 delays apoptotic photoreceptor cell death in the rds mouse." Curr Eye Res **17**(9): 917-923.

Ames, A., 3rd, Y. Y. Li, et al. (1992). "Energy metabolism of rabbit retina as related to function: high cost of Na+ transport." J Neurosci **12**(3): 840-853.

Arendt, D. (2003). "Evolution of eyes and photoreceptor cell types." Int J Dev Biol **47**(7-8): 563-571.

Barron, M. J., M. A. Johnson, et al. (2001). "Mitochondrial abnormalities in ageing macular photoreceptors." Invest Ophthalmol Vis Sci **42**(12): 3016-3022.

Beauvoit, B., T. Kitai, et al. (1994). "Contribution of the mitochondrial compartment to the optical properties of the rat liver: a theoretical and practical approach." Biophys J **67**(6): 2501-2510.

Bennett, J., T. Tanabe, et al. (1996). "Photoreceptor cell rescue in retinal degeneration (rd) mice by in vivo gene therapy." Nat Med **2**(6): 649-654.

Berger, W., B. Kloeckener-Gruissem, et al. (2010). "The molecular basis of human retinal and vitreoretinal diseases." Prog Retin Eye Res **29**(5): 335-375.

Bernard, S. L., J. R. Ewen, et al. (2000). "High spatial resolution measurements of organ blood flow in small laboratory animals." Am J Physiol Heart Circ Physiol **279**(5): H2043-2052.

Berson, E. L., B. Rosner, et al. (1991). "Ocular findings in patients with autosomal dominant retinitis pigmentosa and a rhodopsin gene defect (Pro-23-His)." Arch Ophthalmol **109**(1): 92-101.

Berson, E. L., M. A. Sandberg, et al. (1985). "Natural course of retinitis pigmentosa over a three-year interval." Am J Ophthalmol **99**(3): 240-251.

Besch, D., H. Jagle, et al. (2003). "Inherited multifocal RPE-diseases: mechanisms for local dysfunction in global retinoid cycle gene defects." Vision Res **43**(28): 3095-3108.

Bhattacharya, S. S., A. F. Wright, et al. (1984). "Close genetic linkage between X-linked retinitis pigmentosa and a restriction fragment length polymorphism identified by recombinant DNA probe L1.28." Nature **309**(5965): 253-255.

Bourne, H. R. and E. C. Meng (2000). "Structure. Rhodopsin sees the light." Science **289**(5480): 733-734.

Bramall, A. N., A. F. Wright, et al. (2010). "The genomic, biochemical, and cellular responses of the retina in inherited photoreceptor degenerations and prospects for the treatment of these disorders." Annu Rev Neurosci **33**: 441-472.

Braun, R. D., R. A. Linsenmeier, et al. (1995). "Oxygen consumption in the inner and outer retina of the cat." Invest Ophthalmol Vis Sci **36**(3): 542-554.

Brookes, P. S., A. L. Levonen, et al. (2002). "Mitochondria: regulators of signal transduction by reactive oxygen and nitrogen species." Free Radic Biol Med **33**(6): 755-764.

Burns, M. E. and V. Y. Arshavsky (2005). "Beyond counting photons: trials and trends in vertebrate visual transduction." Neuron **48**(3): 387-401.

Burnstock, G. (2009). "Purines and sensory nerves." Handb Exp Pharmacol(194): 333-392.

Butow, R. A. and N. G. Avadhani (2004). "Mitochondrial signaling: the retrograde response." Mol Cell **14**(1): 1-15.

Butterfield, D. A., T. Reed, et al. (2007). "Roles of amyloid beta-peptide-associated oxidative stress and brain protein modifications in the pathogenesis of Alzheimer's disease and mild cognitive impairment." Free Radic Biol Med **43**(5): 658-677.

Campian, J. L., M. Qian, et al. (2004). "Oxygen tolerance and coupling of mitochondrial electron transport." J Biol Chem **279**(45): 46580-46587.

Carmody, R. J. and T. G. Cotter (2000). "Oxidative stress induces caspase-independent retinal apoptosis in vitro." Cell Death Differ **7**(3): 282-291.

Cashman, S. M., E. A. Binkley, et al. (2005). "Towards mutation-independent silencing of genes involved in retinal degeneration by RNA interference." Gene Ther **12**(15): 1223-1228.

Cassarino, D. S., R. H. Swerdlow, et al. (1998). "Cyclosporin A increases resting mitochondrial membrane potential in SY5Y cells and reverses the depressed mitochondrial membrane potential of Alzheimer's disease cybrids." Biochem Biophys Res Commun **248**(1): 168-173.

Ceriello, A. and E. Motz (2004). "Is oxidative stress the pathogenic mechanism underlying insulin resistance, diabetes, and cardiovascular disease? The common soil hypothesis revisited." Arterioscler Thromb Vasc Biol **24**(5): 816-823.

Chen, B. and C. L. Cepko (2009). "HDAC4 regulates neuronal survival in normal and diseased retinas." Science **323**(5911): 256-259.

Chertov, A. O., L. Holzhausen, et al. (2011). "Roles of glucose in photoreceptor survival." J Biol Chem **286**(40): 34700-34711.

Chung, H., T. Dai, et al. (2012). "The nuts and bolts of low-level laser (light) therapy." Ann Biomed Eng **40**(2): 516-533.

Clemson, C. M., R. Tzekov, et al. (2011). "Therapeutic potential of valproic acid for retinitis pigmentosa." Br J Ophthalmol **95**(1): 89-93.

Collin, S. P., W. L. Davies, et al. (2009). "The evolution of early vertebrate photoreceptors." Philos Trans R Soc Lond B Biol Sci **364**(1531): 2925-2940.

Cooper, C. E. (2002). "Nitric oxide and cytochrome oxidase: substrate, inhibitor or effector?" Trends Biochem Sci **27**(1): 33-39.

de Sousa, A. P., J. N. Santos, et al. (2010). "Effect of LED phototherapy of three distinct wavelengths on fibroblasts on wound healing: a histological study in a rodent model." Photomed Laser Surg **28**(4): 547-552.

Desmet, K. D., D. A. Paz, et al. (2006). "Clinical and experimental applications of NIR-LED photobiomodulation." Photomed Laser Surg **24**(2): 121-128.

Donovan, M., R. J. Carmody, et al. (2001). "Light-induced photoreceptor apoptosis in vivo requires neuronal nitric-oxide synthase and guanylate cyclase activity and is caspase-3-independent." J Biol Chem **276**(25): 23000-23008.

Drexler, W., U. Morgner, et al. (2001). "Ultrahigh-resolution ophthalmic optical coherence tomography." Nat Med **7**(4): 502-507.

Dryja, T. P., T. L. McGee, et al. (1990). "Mutations within the rhodopsin gene in patients with autosomal dominant retinitis pigmentosa." N Engl J Med **323**(19): 1302-1307.

Dryja, T. P., T. L. McGee, et al. (1990). "A point mutation of the rhodopsin gene in one form of retinitis pigmentosa." Nature **343**(6256): 364-366.

Dykens, J. A., A. K. Carroll, et al. (2004). "Photoreceptor preservation in the S334ter model of retinitis pigmentosa by a novel estradiol analog." Biochem Pharmacol **68**(10): 1971-1984.

Eells, J. T., M. M. Henry, et al. (2003). "Therapeutic photobiomodulation for methanol-induced retinal toxicity." Proc Natl Acad Sci U S A **100**(6): 3439-3444.

Eells, J. T., M. T. Wong-Riley, et al. (2004). "Mitochondrial signal transduction in accelerated wound and retinal healing by near-infrared light therapy." Mitochondrion **4**(5-6): 559-567.

Farrar, G. J., P. F. Kenna, et al. (2002). "On the genetics of retinitis pigmentosa and on mutation-independent approaches to therapeutic intervention." EMBO J **21**(5): 857-864.

Fishman, G. A., L. D. Gilbert, et al. (1989). "Acetazolamide for treatment of chronic macular edema in retinitis pigmentosa." Arch Ophthalmol **107**(10): 1445-1452.

Fitzgerald, M., C. A. Bartlett, et al. (2010). "Near infrared light reduces oxidative stress and preserves function in CNS tissue vulnerable to secondary degeneration following partial transection of the optic nerve." J Neurotrauma **27**(11): 2107-2119.

Frohman, E. M., J. G. Fujimoto, et al. (2008). "Optical coherence tomography: a window into the mechanisms of multiple sclerosis." Nat Clin Pract Neurol **4**(12): 664-675.

Geller, S., R. Krowka, et al. (2006). "Toxicity of hyperoxia to the retina: evidence from the mouse." Adv Exp Med Biol **572**: 425-437.

Giuliani, A., L. Lorenzini, et al. (2009). "Low infra red laser light irradiation on cultured neural cells: effects on mitochondria and cell viability after oxidative stress." BMC Complement Altern Med **9**: 8.

Goldman, A. I., P. S. Teirstein, et al. (1980). "The role of ambient lighting in circadian disc shedding in the rod outer segment of the rat retina." Invest Ophthalmol Vis Sci **19**(11): 1257-1267.

Gospe, S. M., 3rd, S. A. Baker, et al. (2010). "Facilitative glucose transporter Glut1 is actively excluded from rod outer segments." J Cell Sci **123**(Pt 21): 3639-3644.

Greco, M., G. Guida, et al. (1989). "Increase in RNA and protein synthesis by mitochondria irradiated with helium-neon laser." Biochem Biophys Res Commun **163**(3): 1428-1434.

Green, D. R. and G. I. Evan (2002). "A matter of life and death." Cancer Cell **1**(1): 19-30.

Green, K., M. D. Brand, et al. (2004). "Prevention of mitochondrial oxidative damage as a therapeutic strategy in diabetes." Diabetes **53 Suppl 1**: S110-118.

Hartong, D. T., E. L. Berson, et al. (2006). "Retinitis pigmentosa." Lancet **368**(9549): 1795-1809.

He, L., A. T. Poblenz, et al. (2000). "Lead and calcium produce rod photoreceptor cell apoptosis by opening the mitochondrial permeability transition pore." J Biol Chem **275**(16): 12175-12184.

Hoang, Q. V., R. A. Linsenmeier, et al. (2002). "Photoreceptor inner segments in monkey and human retina: mitochondrial density, optics, and regional variation." Vis Neurosci **19**(4): 395-407.

Hoffman, D. R., K. G. Locke, et al. (2004). "A randomized, placebo-controlled clinical trial of docosahexaenoic acid supplementation for X-linked retinitis pigmentosa." Am J Ophthalmol **137**(4): 704-718.

Hu, W. P., J. J. Wang, et al. (2007). "Helium-neon laser irradiation stimulates cell proliferation through photostimulatory effects in mitochondria." J Invest Dermatol **127**(8): 2048-2057.

Huang, Y. Y., A. C. Chen, et al. (2009). "Biphasic dose response in low level light therapy." Dose Response **7**(4): 358-383.

Janssen-Heininger, Y. M., B. T. Mossman, et al. (2008). "Redox-based regulation of signal transduction: principles, pitfalls, and promises." Free Radic Biol Med **45**(1): 1-17.

Joseph, L. R. (2006). "*Principles of Fluorescence Spectroscopy*." Springer.

Kajiwara, K., E. L. Berson, et al. (1994). "Digenic retinitis pigmentosa due to mutations at the unlinked peripherin/RDS and ROM1 loci." Science **264**(5165): 1604-1608.

Kanwar, M., P. S. Chan, et al. (2007). "Oxidative damage in the retinal mitochondria of diabetic mice: possible protection by superoxide dismutase." Invest Ophthalmol Vis Sci **48**(8): 3805-3811.

Karu, T. (1999). "Primary and secondary mechanisms of action of visible to near-IR radiation on cells." J Photochem Photobiol B **49**(1): 1-17.

Karu, T. (2010). "Mitochondrial mechanisms of photobiomodulation in context of new data about multiple roles of ATP." Photomed Laser Surg **28**(2): 159-160.

Karu, T. I. (2008). "Mitochondrial signaling in mammalian cells activated by red and near-IR radiation." Photochem Photobiol **84**(5): 1091-1099.

Karu, T. I., L. V. Pyatibrat, et al. (2004). "Photobiological modulation of cell attachment via cytochrome c oxidase." Photochem Photobiol Sci **3**(2): 211-216.

Karu, T. I., L. V. Pyatibrat, et al. (2005). "Absorption measurements of a cell monolayer relevant to phototherapy: reduction of cytochrome c oxidase under near IR radiation." J Photochem Photobiol B **81**(2): 98-106.

Karunadharma, P. P., C. L. Nordgaard, et al. (2010). "Mitochondrial DNA damage as a potential mechanism for age-related macular degeneration." Invest Ophthalmol Vis Sci **51**(11): 5470-5479.

Keeler, C. E. (1924). "The Inheritance of a Retinal Abnormality in White Mice." Proc Natl Acad Sci U S A **10**(7): 329-333.

Kim, T., S. J. Kim, et al. (2007). "Profiling of vitreous proteomes from proliferative diabetic retinopathy and nondiabetic patients." Proteomics **7**(22): 4203-4215.

Komeima, K., B. S. Rogers, et al. (2007). "Antioxidants slow photoreceptor cell death in mouse models of retinitis pigmentosa." J Cell Physiol **213**(3): 809-815.

Kong, G. Y., N. J. Van Bergen, et al. (2009). "Mitochondrial dysfunction and glaucoma." J Glaucoma **18**(2): 93-100.

Kong, L., M. Tanito, et al. (2007). "Delay of photoreceptor degeneration in tubby mouse by sulforaphane." J Neurochem **101**(4): 1041-1052.

Lagnado, L. (2000). "The Wellcome Prize Lecture. Visual signals in the retina: from photons to synapses." Exp Physiol **85**(1): 1-16.

Lamb, T. D., D. A. Baylor, et al. (1979). "The membrane current of single rod outer segments." Vision Res **19**(4): 385.

Lampl, Y., J. A. Zivin, et al. (2007). "Infrared laser therapy for ischemic stroke: a new treatment strategy: results of the NeuroThera Effectiveness and Safety Trial-1 (NEST-1)." Stroke **38**(6): 1843-1849.

Lapchak, P. A. and L. De Taboada (2010). "Transcranial near infrared laser treatment (NILT) increases cortical adenosine-5'-triphosphate (ATP) content following embolic strokes in rabbits." Brain Res **1306**: 100-105.

LaVail, M. M., D. Yasumura, et al. (2000). "Ribozyme rescue of photoreceptor cells in P23H transgenic rats: long-term survival and late-stage therapy." Proc Natl Acad Sci U S A **97**(21): 11488-11493.

Leonard, K. C., D. Petrin, et al. (2007). "XIAP protection of photoreceptors in animal models of retinitis pigmentosa." PLoS One **2**(3): e314.

Liang, H. L., H. T. Whelan, et al. (2006). "Photobiomodulation partially rescues visual cortical neurons from cyanide-induced apoptosis." Neuroscience **139**(2): 639-649.

Lim, J., R. A. Sanders, et al. (2010). "Effects of low-level light therapy on streptozotocin-induced diabetic kidney." J Photochem Photobiol B **99**(2): 105-110.

Lin, M. T. and M. F. Beal (2006). "Mitochondrial dysfunction and oxidative stress in neurodegenerative diseases." Nature **443**(7113): 787-795.

Linsenmeier, R. A. (1990). "Electrophysiological consequences of retinal hypoxia." Graefes Arch Clin Exp Ophthalmol **228**(2): 143-150.

Lowry, O. H., N. R. Roberts, et al. (1956). "The quantitative histochemistry of the retina." J Biol Chem **220**(2): 879-892.

Machida, S., M. Kondo, et al. (2000). "P23H rhodopsin transgenic rat: correlation of retinal function with histopathology." Invest Ophthalmol Vis Sci **41**(10): 3200-3209.

Maleki, S., R. Sepehr, et al. (2012). "Mitochondrial redox studies of oxidative stress in kidneys from diabetic mice." Biomed Opt Express **3**(2): 273-281.

Matsubara, M., M. Ranji, et al. (2010). "In vivo fluorometric assessment of cyclosporine on mitochondrial function during myocardial ischemia and reperfusion." Ann Thorac Surg **89**(5): 1532-1537.

McBee, J. K., K. Palczewski, et al. (2001). "Confronting complexity: the interlink of phototransduction and retinoid metabolism in the vertebrate retina." Prog Retin Eye Res **20**(4): 469-529.

Menon, S. T., M. Han, et al. (2001). "Rhodopsin: structural basis of molecular physiology." Physiol Rev **81**(4): 1659-1688.

Miller, R. F. and J. E. Dowling (1970). "Intracellular responses of the Muller (glial) cells of mudpuppy retina: their relation to b-wave of the electroretinogram." J Neurophysiol **33**(3): 323-341.

Naash, M. L., N. S. Peachey, et al. (1996). "Light-induced acceleration of photoreceptor degeneration in transgenic mice expressing mutant rhodopsin." Invest Ophthalmol Vis Sci **37**(5): 775-782.

Nambu, H., K. Yuge, et al. (1997). "Morphologic characteristics of N-methyl-N-nitrosourea-induced retinal degeneration in C57BL mice." Pathol Int **47**(6): 377-383.

Natoli, R., Y. Zhu, et al. (2010). "Gene and noncoding RNA regulation underlying photoreceptor protection: microarray study of dietary antioxidant saffron and photobiomodulation in rat retina." Mol Vis **16**: 1801-1822.

Neveling, K., R. W. Collin, et al. (2012). "Next-generation genetic testing for retinitis pigmentosa." Hum Mutat.

Noell, W. K., V. S. Walker, et al. (1966). "Retinal damage by light in rats." Invest Ophthalmol **5**(5): 450-473.

Okada, T. and K. Palczewski (2001). "Crystal structure of rhodopsin: implications for vision and beyond." Curr Opin Struct Biol **11**(4): 420-426.

Oron, A., U. Oron, et al. (2012). "Near Infrared Transcranial Laser Therapy Applied at Various Modes to Mice following Traumatic Brain Injury Significantly Reduces Long-Term Neurological Deficits." J Neurotrauma **29**(2): 401-407.

Otani, A., M. I. Dorrell, et al. (2004). "Rescue of retinal degeneration by intravitreally injected adult bone marrow-derived lineage-negative hematopoietic stem cells." J Clin Invest **114**(6): 765-774.

Padnick-Silver, L., J. J. Kang Derwent, et al. (2006). "Retinal oxygenation and oxygen metabolism in Abyssinian cats with a hereditary retinal degeneration." Invest Ophthalmol Vis Sci **47**(8): 3683-3689.

Papermaster, D. S., B. G. Schneider, et al. (1985). "Vesicular transport of newly synthesized opsin from the Golgi apparatus toward the rod outer segment. Ultrastructural immunocytochemical and autoradiographic evidence in Xenopus retinas." Invest Ophthalmol Vis Sci **26**(10): 1386-1404.

Penn, J. S., B. L. Tolman, et al. (1992). "Effect of light history on the rat retina: timecourse of morphological adaptation and readaptation." Neurochem Res **17**(1): 91-99.

Phelan, J. K. and D. Bok (2000). "A brief review of retinitis pigmentosa and the identified retinitis pigmentosa genes." Mol Vis **6**: 116-124.

Phillips, M. J., T. A. Walker, et al. (2008). "Tauroursodeoxycholic acid preservation of photoreceptor structure and function in the rd10 mouse through postnatal day 30." Invest Ophthalmol Vis Sci **49**(5): 2148-2155.

Piccolino, M., E. Strettoi, et al. (1989). "Santiago Ramon y Cajal, the retina and the neuron theory." Doc Ophthalmol **71**(2): 123-141.

Pieczenik, S. R. and J. Neustadt (2007). "Mitochondrial dysfunction and molecular pathways of disease." Exp Mol Pathol **83**(1): 84-92.

Posten, W., D. A. Wrone, et al. (2005). "Low-level laser therapy for wound healing: mechanism and efficacy." Dermatol Surg **31**(3): 334-340.

Punzo, C., W. Xiong, et al. (2012). "Loss of daylight vision in retinal degeneration: are oxidative stress and metabolic dysregulation to blame?" J Biol Chem **287**(3): 1642-1648.

Quirk, B. J., K. D. Desmet, et al. (2012). "Therapeutic effect of near infrared (NIR) light on Parkinson's disease models." Front Biosci (Elite Ed) **4**: 818-823.

Quirk, B. J. and H. T. Whelan (2011). "Near-infrared irradiation photobiomodulation: the need for basic science." Photomed Laser Surg **29**(3): 143-144.

Ramanujam, N., R. Richards-Kortum, et al. (2001). "Low Temperature Fluorescence Imaging of Freeze-trapped Human Cervical Tissues." Opt Express **8**(6): 335-343.

Rando, R. R. (1996). "Polyenes and vision." Chem Biol **3**(4): 255-262.

Ranji, M., D. L. Jaggard, et al. (2006). "Simultaneous fluorometry and phosphorometry of Langendorff perfused rat heart: ex vivo animal studies." Opt Lett **31**(20): 2995-2997.

Ranji, M., S. Kanemoto, et al. (2006). "Fluorescence spectroscopy and imaging of myocardial apoptosis." J Biomed Opt **11**(6): 064036.

Ranji, M., M. Matsubara, et al. (2009). "Quantifying acute myocardial injury using ratiometric fluorometry." IEEE Trans Biomed Eng **56**(5): 1556-1563.

Richards-Kortum, R., M. F. Mitchell, et al. (1994). "In vivo fluorescence spectroscopy: potential for non-invasive, automated diagnosis of cervical intraepithelial neoplasia and use as a surrogate endpoint biomarker." J Cell Biochem Suppl **19**: 111-119.

Ridge, K. D. and K. Palczewski (2007). "Visual rhodopsin sees the light: structure and mechanism of G protein signaling." J Biol Chem **282**(13): 9297-9301.

Rizzo, J. F., 3rd, J. Wyatt, et al. (2003). "Perceptual efficacy of electrical stimulation of human retina with a microelectrode array during short-term surgical trials." Invest Ophthalmol Vis Sci **44**(12): 5362-5369.

Roessler, G., T. Laube, et al. (2009). "Implantation and explantation of a wireless epiretinal retina implant device: observations during the EPIRET3 prospective clinical trial." Invest Ophthalmol Vis Sci **50**(6): 3003-3008.

Rojas, J. C., J. Lee, et al. (2008). "Neuroprotective effects of near-infrared light in an in vivo model of mitochondrial optic neuropathy." J Neurosci **28**(50): 13511-13521.

Ryan, M. T. and N. J. Hoogenraad (2007). "Mitochondrial-nuclear communications." Annu Rev Biochem **76**: 701-722.

Saliba, R. S., P. M. Munro, et al. (2002). "The cellular fate of mutant rhodopsin: quality control, degradation and aggresome formation." J Cell Sci **115**(Pt 14): 2907-2918.

Sancho-Pelluz, J., B. Arango-Gonzalez, et al. (2008). "Photoreceptor cell death mechanisms in inherited retinal degeneration." Mol Neurobiol **38**(3): 253-269.

Sanvicens, N., V. Gomez-Vicente, et al. (2004). "Oxidative stress-induced apoptosis in retinal photoreceptor cells is mediated by calpains and caspases and blocked by the oxygen radical scavenger CR-6." J Biol Chem **279**(38): 39268-39278.

Sanz, M. M., L. E. Johnson, et al. (2007). "Significant photoreceptor rescue by treatment with a combination of antioxidants in an animal model for retinal degeneration." Neuroscience **145**(3): 1120-1129.

Sarti, P., A. Giuffre, et al. (2003). "Nitric oxide and cytochrome oxidase: reaction mechanisms from the enzyme to the cell." Free Radic Biol Med **34**(5): 509-520.

Schremser, J. L. and T. P. Williams (1995). "Rod outer segment (ROS) renewal as a mechanism for adaptation to a new intensity environment. I. Rhodopsin levels and ROS length." Exp Eye Res **61**(1): 17-23.

Schroeder, P., C. Pohl, et al. (2007). "Cellular response to infrared radiation involves retrograde mitochondrial signaling." Free Radic Biol Med **43**(1): 128-135.

Seme, M. T., P. Summerfelt, et al. (1999). "Formate-induced inhibition of photoreceptor function in methanol intoxication." J Pharmacol Exp Ther **289**(1): 361-370.

Sepehr, R., K. Staniszewski, et al. (2012). "Optical imaging of tissue mitochondrial redox state in intact rat lungs in two models of pulmonary oxidative stress." J Biomed Opt **17**(4): 046010.

Shen, J., X. Yang, et al. (2005). "Oxidative damage is a potential cause of cone cell death in retinitis pigmentosa." J Cell Physiol **203**(3): 457-464.

Shigenaga, M. K., T. M. Hagen, et al. (1994). "Oxidative damage and mitochondrial decay in aging." Proc Natl Acad Sci U S A **91**(23): 10771-10778.

Steinberg, R. H., S. K. Fisher, et al. (1980). "Disc morphogenesis in vertebrate photoreceptors." J Comp Neurol **190**(3): 501-508.

Stone, J., J. Maslim, et al. (1999). "Mechanisms of photoreceptor death and survival in mammalian retina." Prog Retin Eye Res **18**(6): 689-735.

Takahashi, M., H. Miyoshi, et al. (1999). "Rescue from photoreceptor degeneration in the rd mouse by human immunodeficiency virus vector-mediated gene transfer." J Virol **73**(9): 7812-7816.

Todaro, M., A. Zeuner, et al. (2004). "Role of apoptosis in autoimmunity." J Clin Immunol **24**(1): 1-11.

Umino, Y., D. Everhart, et al. (2006). "Hypoglycemia leads to age-related loss of vision." Proc Natl Acad Sci U S A **103**(51): 19541-19545.

Usui, S., K. Komeima, et al. (2009). "Increased expression of catalase and superoxide dismutase 2 reduces cone cell death in retinitis pigmentosa." Mol Ther **17**(5): 778-786.

Vander Heiden, M. G., L. C. Cantley, et al. (2009). "Understanding the Warburg effect: the metabolic requirements of cell proliferation." Science **324**(5930): 1029-1033.

Vlachantoni, D., A. N. Bramall, et al. (2011). "Evidence of severe mitochondrial oxidative stress and a protective effect of low oxygen in mouse models of inherited photoreceptor degeneration." Hum Mol Genet **20**(2): 322-335.

Wagnieres, G. A., W. M. Star, et al. (1998). "In vivo fluorescence spectroscopy and imaging for oncological applications." Photochem Photobiol **68**(5): 603-632.

Wald, G., J. Durell, et al. (1950). "The light reaction in the bleaching of rhodopsin." Science **111**(2877): 179-181.

Wallace, D. C. (2005). "A mitochondrial paradigm of metabolic and degenerative diseases, aging, and cancer: a dawn for evolutionary medicine." Annu Rev Genet **39**: 359-407.

Walsh, N., Van Driel D, et al. (2004). "Multiple vulnerability of photoreceptors to mesopic ambient light in the P23H transgenic rat." Brain Res **1013**(2): 197-203.

Walsh, N., D. van Driel, et al. (2004). "Multiple vulnerability of photoreceptors to mesopic ambient light in the P23H transgenic rat." Brain Res **1013**(2): 194-203.

Wellard, J., D. Lee, et al. (2005). "Photoreceptors in the rat retina are specifically vulnerable to both hypoxia and hyperoxia." Vis Neurosci **22**(4): 501-507.

Whelan, H. T., E. V. Buchmann, et al. (2003). "Effect of NASA light-emitting diode irradiation on molecular changes for wound healing in diabetic mice." J Clin Laser Med Surg **21**(2): 67-74.

Whelan, H. T., J. F. Connelly, et al. (2002). "NASA light-emitting diodes for the prevention of oral mucositis in pediatric bone marrow transplant patients." J Clin Laser Med Surg **20**(6): 319-324.

Whiteley, S. J., T. M. Litchfield, et al. (1996). "Improvement of the pupillary light reflex of Royal College of Surgeons rats following RPE cell grafts." Exp Neurol **140**(1): 100-104.

Winkler, B. S. (1981). "Glycolytic and oxidative metabolism in relation to retinal function." J Gen Physiol **77**(6): 667-692.

Wong-Riley, M. T., H. L. Liang, et al. (2005). "Photobiomodulation directly benefits primary neurons functionally inactivated by toxins: role of cytochrome c oxidase." J Biol Chem **280**(6): 4761-4771.

Wu, Q., W. Xuan, et al. (2012). "Low-level laser therapy for closed-head traumatic brain injury in mice: effect of different wavelengths." Lasers Surg Med **44**(3): 218-226.

Yamada, H., E. Yamada, et al. (2001). "Fibroblast growth factor-2 decreases hyperoxia-induced photoreceptor cell death in mice." Am J Pathol **159**(3): 1113-1120.

Yang, L., J. H. Kim, et al. (2009). "Minocycline inhibition of photoreceptor degeneration." Arch Ophthalmol **127**(11): 1475-1480.

Yau, K. W. and K. Nakatani (1984). "Cation selectivity of light-sensitive conductance in retinal rods." Nature **309**(5966): 352-354.

Ying, R., H. L. Liang, et al. (2008). "Pretreatment with near-infrared light via light-emitting diode provides added benefit against rotenone- and MPP+-induced neurotoxicity." Brain Res **1243**: 167-173.

Young, R. W. and D. Bok (1969). "Participation of the retinal pigment epithelium in the rod outer segment renewal process." J Cell Biol **42**(2): 392-403.

Yu, D. Y., S. Cringle, et al. (2004). "Photoreceptor death, trophic factor expression, retinal oxygen status, and photoreceptor function in the P23H rat." Invest Ophthalmol Vis Sci **45**(6): 2013-2019.

Yu, D. Y. and S. J. Cringle (2001). "Oxygen distribution and consumption within the retina in vascularised and avascular retinas and in animal models of retinal disease." Prog Retin Eye Res **20**(2): 175-208.

Yuge, K., H. Nambu, et al. (1996). "N-methyl-N-nitrosourea-induced photoreceptor apoptosis in the mouse retina." In Vivo **10**(5): 483-488.

Zhang, Y., S. Song, et al. (2003). "cDNA microarray analysis of gene expression profiles in human fibroblast cells irradiated with red light." J Invest Dermatol **120**(5): 849-857.

Zivin, J. A., G. W. Albers, et al. (2009). "Effectiveness and safety of transcranial laser therapy for acute ischemic stroke." Stroke **40**(4): 1359-1364.

APPENDIX

Conference Proceedings

ARVO 2011

830 nm Photobiomodulation Attenuates Retinal Degeneration in a Rodent Model of Retinitis Pigmentosa

S.Gopalakrishnan[1], B.Abroe[1], H.Schmitt[1], A.Dubis[2], P.Summerfelt[2], J.Caroll[2] and J.T. Eells[1]. University of Wisconsin-Milwaukee, WI[1], Medical College of Wisconsin, Milwaukee, WI[2]

Purpose: Irradiation by light in the far-red to near-infrared (NIR) region of the spectrum (photobiomodualtion, PBM) has been demonstrated to attenuate the severity of neurodegenerative disease in experimental and clinical studies. The purpose of this study was to test the hypothesis that a brief course of 830 nm PBM would protect against the loss of retinal function and improve photoreceptor survival in a rodent model of retinitis pigmentosa.

Methods: P23H-1 pups were treated once per day for 180 seconds with 830 nm light (25 mW/cm^2; fluence 4 J/cm^2) using a light-emitting diode array (Quantum Devices, Barneveld WI) from postnatal day p10 to p25. Sham-treated rats were restrained for 180 seconds, but not exposed to NIR light. The status of the retina was determined at p30 by measuring indices of photoreceptor function by ERG (scotopic series from 100mcd.s/m^2 to 25000mcd.s/m^2) and retinal morphology by Spectral Domain Optical Coherence Tomography (SD-OCT; line scans centered on the ONH, 1000x80x1samplings; Bioptigen, Inc). Following SD-OCT analysis, animals were euthanized and the eyes harvested and prepared for histological and molecular analysis.

Results: 830 nm PBM protected against retinal degeneration in the P23H rat as assessed by ERG and SD-OCT. In NIR treated animals the a-wave amplitude at 1000 mcd.s/m^2

was 117 ± 10 µV compared to 77 ± 7 µV in sham treated animals (p=0.007). The b-wave amplitude in NIR treated rats was 643 ± 49 µV compared to 415 ± 27 µV in sham treated animals (p=0.002). Total retinal thickness measured by SD-OCT linear scans was 179 ± 8 µm in NIR treated animals compared to 147± 8 µm for sham treated animals (p=0.04). **Conclusions:** Studies from our laboratory have documented preservation of retinal function and attenuation of photoreceptor loss by PBM in animal models of mitochondrial injury and light-induced retinal degeneration. Results from this study demonstrate the retinoprotective effects of 830nm PBM in a transgenic animal model of retinitis pigmentosa and support the use of PBM as an innovative, non-invasive therapeutic approach for the treatment of retinal degenerative disease.

ARVO 2010

670 nm Photobiomodulation Attenuates Light-Induced Retinal Degeneration

J.T. Eells[1], S. Gopalakrishnan[1], B. Abroe[1], R. Albarracin[2], K. Valter-Kocsi[2].

[1]Health Sciences, University of Wisconsin - Milwaukee, Milwaukee, WI; [2]ARC Center for Excellence in Vision Science, Australian National University, Canberra, Australia.

Purpose: Irradiation by light in the far-red to near-infrared (NIR) region of the spectrum (photobiomodulation; PBM) has been demonstrated to attenuate the severity of degenerative retinal diseases in experimental and clinical studies. The cytoprotective actions of NIR-PBM have been attributed to improved mitochondrial energy production and the up regulation of cytoprotective factors. The purpose of this study was to test the hypothesis that a brief course of 670 nm photobiomodulation would protect against the loss of retinal function, prevent mitochondrial dysfunction and attenuate photoreceptor loss in the light damaged retina. **Methods:** The eyes of adult female Sprague Dawley rats

(250 g) were treated with 670 nm light for 90 sec at 50 mW/cm2 (fluence = 4.5 joules/cm2) using a light emitting diode array (Quantum Devices, Inc). Rats were treated once per day for 5 days prior to light damage [LD] (1500 lux for 24 h). Sham treated LD rats were restrained for 90 sec, but not exposed to 670 nm PBM. At day 7 following LD, retinal function was examined by ERG. At day 14, eyes were enucleated. One eye was prepared for histological evaluation and the retina from the other eye was removed, snap frozen and stored at -80 C for future analysis of mitochondrial function and antioxidant concentrations. **Results:** 670 nm photobiomodulation protected against LD-induced loss of rod and cone function. In sham-treated LD animals rod-mediated b-wave amplitude was 320 ± 78 mV compared to 450 ± 65 mV in NIR-treated LD rats. The rod-mediated b/a ratio was 14 ± 4 in sham-treated LD animals and 22 ± 6 in NIR-treated LD animals ($p < 0.05$). The cone-mediated b-wave in LD rats was 103 ± 9 mV compared to 165 ± 25 mV ($p < 0.05$) in NIR-treated LD rats.**Conclusions:** Previous studies in our laboratory have demonstrated neuroprotective and retinoprotective actions of 670 nm PBM light treatment *in vitro* and *in vivo.* The present study extends these findings to include protection against light-damage induced photoreceptor dysfunction. Given the reliance of photoreceptors on mitochondrial oxidative metabolism and the evidence for LD-induced mitochondrial injury, we speculate that the observed retinoprotective actions of NIR PBM are due, in part, to the prevention of photoreceptor mitochondrial dysfunction and the induction of mitochondrial repair in retinal light damage.

670 nm Photobiomodulation Attenuates Light-Induced Retinal Degeneration

Janis.T. Eells[1], S. Gopalakrishnan[1], B. Abroe[1],R. Albarracin[2], K. Valter-Kocsi[2].
[1]Health Sciences, University of Wisconsin - Milwaukee, Milwaukee, WI; [2]ARC Center for Excellence in Vision Science,
Australian National University, Canberra, Australia.

Introduction

- Retinal diseases, including retinitis pigmentosa (RP) and age-related macular degeneration (AMD), are major causes of blindness due to photoreceptor degeneration. There is no effective treatment or prevention for these diseases.

- Mitochondrial dysfunction and oxidative stress play key roles in the pathogenesis of RP, AMD and other retinal degenerative diseases.

- Therapeutic strategies directed towards improving mitochondrial function and reducing oxidative stress have considerable potential for the treatment of retinal disease.

- Low-intensity near-infrared (NIR) light has been shown to act on mitochondria-mediated signaling pathways to preserve mitochondrial function, attenuate oxidative stress, stimulate the production of cytoprotective factors and prevent neuronal death in cultured neurons and in animal models of retinal injury and disease.

- NIR photons penetrate the brain, retina and optic nerve and NIR photon treatment, commonly known as NIR-photobiomodulation [NIR-PBM], has documented efficacy in experimental models of degenerative diseases including Parkinson's disease, multiple sclerosis, and diabetes. Clinical studies have confirmed the therapeutic potential of NIR-PBM in radiation-induced mucositis and stroke.

PURPOSE: To test the hypothesis that NIR-PBM will act in the retina to promote mitochondrial integrity and function, stimulate antioxidant pathways, prevent photoreceptor cell death and preserve retinal function in two established models of retinal degeneration, light damage (LD) and the P23H rat model of retinitis pigmentosa.

Light Damage Protocol

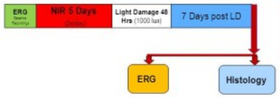

ERG Baseline Recordings

NIR 5 Days (2x/day)

Light Damage 48 Hrs (1000 lux)

7 Days post LD

ERG

Histology

The eyes of adult female Sprague Dawley rats (250 g) were treated with 670 nm light for 90 sec at 50 mW/cm² (fluence = 4.5 joules/cm²) using a light emitting diode array (Quantum Devices, Inc). Rats were treated twice per day for 5 days prior to light damage [LD] (1000 lux for 48 h). Sham-treated LD rats were restrained for 90 sec, but not exposed to 670 nm PBM. Retinal function was assessed by ERG at day 0 (Baseline) and 7 days after LD. The eyes were enucleated. One eye was prepared for histological evaluation and the retina from the other eye was removed, snap frozen and stored at -80 C for biochemical analysis (mitochondrial function, oxidative damage and antioxidant capacity).

Hypothesized Mechanism of Photobiomodulation

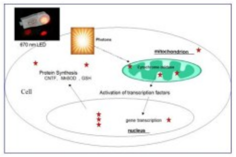

Light Damage

Baseline and Post-LD ERG Recordings Sham vs. NIR-Treated

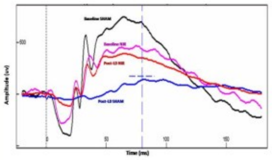

Data Summary

ERG Recording	a-wave Amplitude (uv)	b-wave Amplitude (uv)
Baseline Sham	408.5	1155.4
Post-LD Sham	26.3	194.0
Baseline NIR	313.4	750.6
Post-LD NIR	126.0	512.4

a-wave Amplitude Following LD in NIR-Treated and Sham rats

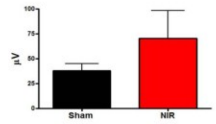

b-wave Amplitude Following LD in NIR-Treated and Sham rats

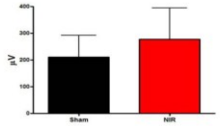

P23H Model of Retinitis Pigmentosa

Photobiomodulation Decreases Photoreceptor Cell Death in the P23H Rat

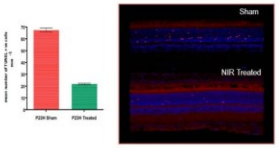

ERG Recordings from NIR-Treated and Sham-Treated P23H Rats

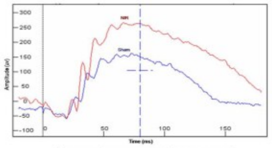

Treatment	a-wave Amplitude (uv)	b-wave Amplitude (uv)
Sham	37	229
NIR	105	439

Spectral Domain Optical Coherence Tomography (SD-OCT) Imaging

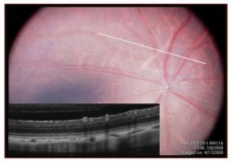

In Collaboration with Dr. Joe Carroll and Dr. Thomas B.Connor, Jr., Department of Ophthalmology, Medical College of Wisconsin, Milwaukee, WI

Photobiomodulation Increases Cytochome oxidase and MnSOD in the P23H Rat

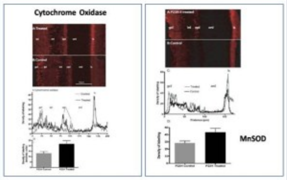

Photobiomodulation Attenuates the Reduction in a-wave Amplitude in the P23H rat

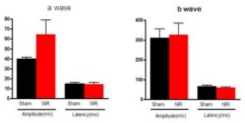

Photobiomodulation Attenuates Photoreceptor Cell Loss in P23H Rats- SD-OCT Imaging

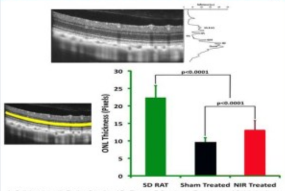

In Collaboration with Dr. Joe Carroll and Dr. Thomas B.Connor, Jr., Department of Ophthalmology, Medical College of Wisconsin. Milwaukee,WI

Summary and Conclusions

- These data support our hypothesis that 670 nm photobiomodulation protects against retinal dysfunction and degeneration in light-induced retinal injury and in the P23H rat model of retinitis pigmentosa.

- Photobiomodulation increases retinal mitochondrial cytochrome oxidase activity, upregulates the production of antioxidant protective enzymes in the retina, and protects against retinal dysfunction and apoptotic photoreceptor cell death.

- These findings have profound implications for the use of photobiomodulation in the treatment of retinal degenerative diseases. They support the therapeutic potential of 670 nm photobiomodulation in well-established models of retinal injury and retinal degeneration, thus setting the stage for clinical trials of photobiomodulation in human disease.

Protocol for P23H Studies

Experiment 1

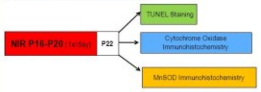

NIR P16-P20 (1x/day)

P22

TUNEL Staining

Cytochrome Oxidase Immunohistochemistry

MnSOD Immunohistochemistry

Experiment 1: P23H rat pups were exposed to 4.5 joules cm² of 670 nm light from a light emitting diode (LED) array or received sham treatment once per day for 5 days from postnatal day (P) 16 to P20. At P22, retinae were collected. Mitochondrial energy metabolism was assessed by measurement of cytochrome oxidase activity and MnSOD was measured as an index of mitochondrial antioxidant capacity. The other eye of each animal was immersion fixed in 4% paraformaldehyde, washed, cryoprotected in 15% sucrose and sectioned at 14um. TUNEL labeling was performed to detect apoptotic cells.

Experiment 2

NIR P10-P30 (1 x/day)

P60

ERG

SD-OCT

HISTOLOGY

Experiment 2: P23H rat pups were exposed to to 4.5 joules cm² of 670 nm photobiomodulation using a light emitting diode (LED) array or received sham treatment. Animals were treated once per day from postnatal day (P) 10 to P30. ERG assessment of retinal function and SD-OCT assessment of ONL thickness were performed at P60. Following ERG and OCT assesements, eyes were enucleated. One eye was prepared for histological evaluation and the retina from the other eye was removed, snap frozen and stored at -80 C for biochemical analysis (mitochondrial function, oxidative damage and antioxidant capacity).

References

- Yu, D., et al., Photoreceptor Death, Trophic Factor Expression, Retinal Oxygen Status, and Photoreceptor Function in the P23H Rat. Invest Ophthalmol Vis Sci, 2004. 45(6).
- Desmet, K.D., et al., Clinical and experimental applications of NIR-LED photobiomodulation. Photomed Laser Surg, 2006. 24(2): p. 121-8.
- Wong-Riley, M.T., et al., Photobiomodulation directly benefits primary neurons functionally inactivated by toxins: role of cytochrome c oxidase. J Biol Chem, 2005. 280(6): p. 4761-71.
- Eells, J., et al., Therapeutic photobiomodulation for methanol-induced retinal toxicity. PNAS, 2003. 100(6).
- Lampl Y., et al. Infrared Laser Therapy for Ischemic Stroke: A New Treatment Strategy: Results of the NeuroThera Effectiveness and Safety Trial-1 (NEST-1). Stroke 2007; 38:1843-9.
- Stone, J., et al., Mechanisms of photoreceptor death and survival in mammalian retina. Prog Ret Eye Res, 1999. 18: p. 689-735.
- Eells, J.T., et al., Mitochondrial signal transduction in accelerated wound and retinal healing by near-infrared light therapy. Mitochondrion, 2004. 4(5-6): p. 559-67.
- Eells, J., et al., Near-infrared light therapy for retinitis pigmentosa. Invest Ophthalmol Vis Sci, 2006. 47 p. ARVO Abstract 1022.
- Oron, U. et al. Low-Level Laser Therapy Applied Transcranially to Rats After Induction of Stroke Significantly Reduces Long-Term Neurological Deficits. Stroke 2006; 37:2620-4.
- Eells, J.T. et al. Photobiomodulation for the Treatment of Retinal Injury and Retinal Degenerative Diseases. In Proceedings of Light Activated Tissue Regeneration and Therapy Conference ed. R.W. Waynant and D.B. Tata pp 39-51, Springer, New York, 2008.
- Shen, J., et al., Oxidative Damage is a Potential Cause of Cone Cell Death in Retinitis Pigmentosa. Journal of Cellular Physiology, 2005. 203: p. 457-464.
- Whelan, H. T. et al. (2002). NASA light-emitting diodes for the prevention of oral mucositis in pediatric bone marrow transplant patients. J Clin Laser Med Surg 20(6): 319-24.
- Whelan, H., et al. Harnessing the cell's own ability to repair and prevent neurodegenerative disease. SPIE 10.1117. 1-4, 2008.

Support

Foundation Fighting Blindness
Grants
TA-NE-0606-0348-UWI
TA-NP-1107-0435-UWI
TA-NP-0709-0465-UWI
And
Australian Research Council through the ARC Centre of Excellence in Vision Science (CE0561903)
Save Sight

Photobiomodulation Attenuates Retinal Degeneration in a Rodent Model of Retinitis Pigmentosa (Program Number:5465)

Sandeep Gopalakrishnan[1], Betsy Abroe[1], Heather Schmitt[1], Adam Dubis[2], Phyllis Summerfelt[2], Joseph Carroll[2] and Janis Eells[1]
[1]Health Sciences, University of Wisconsin –Milwaukee ,WI . [2] Eye Institute ,Medical College of Wisconsin, Milwaukee,WI

INTRODUCTION

Retinitis pigmentosa (RP) is the most common cause of inherited blindness in the developed world. RP is caused by the progressive degeneration of photoreceptor cells with rod degeneration preceding cone degeneration. Considerable evidence supports a key role for photoreceptor mitochondrial dysfunction and oxidative damage in the pathogenesis of photoreceptor death in RP and other retinal degenerative conditions. Low energy photon irradiation (photobiomodulation) in the far-red to near-infrared (NIR) range of the spectrum (630-1000 nm) has been shown to act on mitochondria-mediated signaling pathways to preserve mitochondrial function, attenuate oxidative stress, stimulate the production of cytoprotective factors and prevent cell death in cultured neurons and in animal models of retinal injury and neurodegenerative disease. The purpose of this study was to test the hypothesis that photobiomodulation would protect against retinal degeneration in a rodent model of RP .

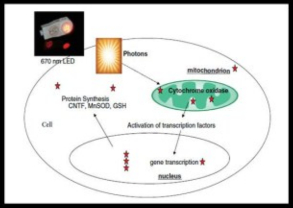

Hypothesized mechanism of Photobiomodulation

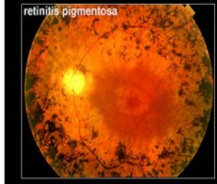

Fundus image in RP

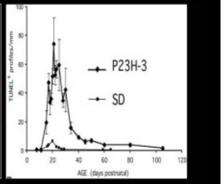

Time course of photoreceptor cell death in the P23H-3 rat. Yu et al. IOVS (2004) 45:2013-2019

PURPOSE: To test the hypothesis that 830 nm photon irradiation will act in the retina to preserve retinal function and attenuate photoreceptor death in a rodent model of retinitis pigmentosa, the P23H-1 rat.

RESULTS

Photobiomodulation Preserves Retinal Function

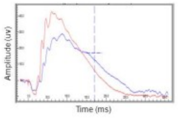

Treatment	a-wave Amplitude (uv)	a-wave Implicit Time (ms)	b-wave Amplitude (uv)	b-wave Implicit Time (ms)
Sham	63.6	20.3	380.2	72.8
NIR	96.9	19.5	548.1	61.3

a-wave amplitude

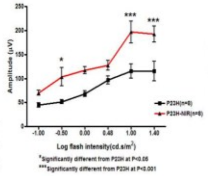

*Significantly different from P23H at P<0.05
***Significantly different from P23H at P<0.001

b-wave amplitude

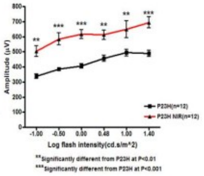

**Significantly different from P23H at P<0.01
***Significantly different from P23H at P<0.001

Photobiomodulation Attenuates Photoreceptor Cell Loss

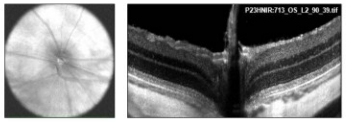

Representative volume intensity projection and linear SDOCT scans of NIR treated P23H-1 retina centered around ONH

Total Retinal Thickness in SD-OCT linear scans (2mm,1000x80x1),p10-p25

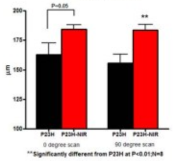

**Significantly different from P23H at P<0.01;N=8

Average ONL Thickness calculated from LRP

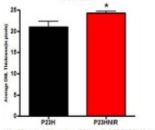

*Significantly different from P23H at P<0.05;P=0.04;N=4

CONCLUSIONS

- Studies from our laboratory and those of our collaborators have documented preservation of retinal function and attenuation of photoreceptor loss by photobiomodulation in animal models of mitochondrial injury and light-induced retinal degeneration.
- Results from this study demonstrate the retinoprotective effects of 830nm photobiomodulation in a transgenic animal model of retinitis pigmentosa and support the use of photobiomodulation as an innovative, non-invasive therapeutic approach for the treatment of retinal degenerative disease.

METHODOLOGY

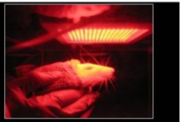

Treatment Protocol: P23H-1 pups were treated once per day for 180 seconds with 830 nm light (25 mW/cm2; fluence 4 joules/cm2) using a light-emitting diode array (Quantum Devices, Barneveld WI) from postnatal day (P) 10 to P25. Sham-treated rats were restrained for 180 seconds, but not exposed to NIR light .

Retinal function was assessed at P30 by full-field, flash-evoked electroretinogram (ERG). Animals were dark-adapted overnight and prepared for recording under dim red illumination. Scotopic log intensity responses from 100mcd.s/m² to 25000mcd.s/m² were recorded. Signals were amplified digitized and averaged. The amplitudes of the a-wave (photoreceptor function) and the b-wave (bipolar and Müller cell function) were determined.

Retinal Morphology was assessed by measuring Total Retinal Thickness and ONL Thickness at P30 by **high resolution SDOCT** suited to image the retina in rodents (Bioptigen Inc.). The images were captured and saved using the Bioptigen's InVivoVue™ software. The images were registered, averaged and segmented using image J and an algorithm generated in Matlab

Instrumentation for SDOCT imaging

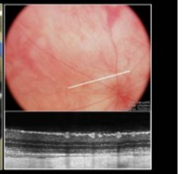

Fundus image and the corresponding OCT layer

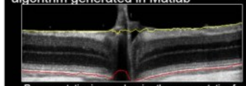

Representative image showing the segmentation for Total Retinal Thickness

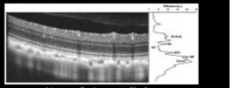

Linear reflectance profile for individual retinal layers

REFERENCES

- Yu, D., et al., Photoreceptor Death, Trophic Factor Expression, Retinal Oxygen Status, and Photoreceptor Function in the P23H Rat. *Invest Ophthalmol Vis Sci*, 2004; 45:2013-2019.
- Hafezi, F., C. Grimm, et al. (2000).Molecular ophthalmology: an update on animal models for retinal degenerations and dystrophies. *Br J Ophthalmol* 84: 922-927.
- Kim, Ki Hean et al. (2008).Monitoring mouse retinal degeneration with high-resolution spectral-domain optical coherence tomography. *Journal of Vision* 8(1)17:1-11
- Wong-Riley, M.T., et al., Photobiomodulation directly benefits primary neurons functionally inactivated by toxins: role of cytochrome c oxidase. *J Biol Chem*, 2005; 280: 4761-71.
- Eells, J., et al., Therapeutic photobiomodulation for methanol-induced retinal toxicity. *PNAS*, 2003; 100: 3439-3444
- Lampl Y., et al. Infrared Laser Therapy for Ischemic Stroke: A New Treatment Strategy: Results of the NeuroThera Effectiveness and Safety Trial-1 (NEST-1). *Stroke* 2007; 38:1843 -9
- Eells, J.T., et al., Mitochondrial signal transduction in accelerated wound and retinal healing by near-infrared light therapy. *Mitochondrion*, 2004; 4: 559-67.
- Eells, J., et al., Near-infrared light therapy for retinitis pigmentosa. Invest Ophthalmol Vis Sci, 2006. *ARVO Abstract* 1022.
- Oron, U. et al. Low-Level Laser Therapy Applied Transcranially to Rats After Induction of Stroke Significantly Reduces Long-Term Neurological Deficits. *Stroke* 2006; 37:2620-4.
- Shen, J., et al., Oxidative Damage is a Potential Cause of Cone Cell Death in Retinitis Pigmentosa. *J Cell Physiol*, 2005. 203. 457-464.
- Abarracin, R, Eells, J and Valter, K. Photobiomodulation protects the retina from light-induced photoreceptor damage. *Invest. Ophthalmol. Vis. Sci.* 2011; (iovs.10-6664)

SUPPORT

SG: UWM College of Health Sciences Graduate Student Research Grant Award; Fight for Sight Graduate Summer Fellowship.JE: Foundation Fighting Blindness (TA-NP-0709-0465-UWI), International Retinal Research Foundation, NIH (EY001931). JC: NIH (EY017607, EY001931, EY014537), MCW Research Affairs Committee, RBP Career Development Award.

Photobiomodulation by 830nm near-infrared light attenuates disease progression in P23H transgenic rats

Sandeep Gopalakrishnan[1], Heather Schmitt[1], Sepideh Maleki[2], Adam Dubis[3], Joseph Carroll[3], Mahsa Ranji[2] and Janis Eells[1] (Faculty Sponsor)
[1]Department of Health Sciences, University of Wisconsin-Milwaukee, Milwaukee, WI. [2]Department of Electrical Engineering and Computer Science, University of Wisconsin-Milwaukee, Milwaukee, WI.
[3]Ophthalmology; Cell Biology, Neurobiology and Anatomy, Medical College of Wisconsin, Milwaukee, WI.

Abstract

PURPOSE: Irradiation by light in the far-red to near-infrared (NIR) region of the spectrum (photobiomodulation, PBM) has been demonstrated to attenuate the severity of neurodegenerative disease in experimental and clinical studies. The purpose of this study was to test the hypothesis that a brief course of 830 nm PBM would protect against the loss of retinal function, and improve photoreceptor survival in the P23H-1 rhodopsin transgenic rat. **METHODS:** P23H-1 pups were treated once per day for 180 second (25 mW/cm2) with 830 nm light (25 mW/cm2; fluence 4 joules/cm2)using a light-emitting diode array (Quantum Devices, Barneveld WI) from postnatal day (p) 10 to p25. Sham-treated rats were restrained for 180 seconds, but not exposed to NIR light. The status of the retina was determined at p30 by measuring indices of photoreceptor function by ERG (scotopic series from 10 mcd.s/m2 to 25000 cd.s/m2, ISCEV protocol for rod only and standard rod and cone response) and retinal morphology *in vivo* by Spectral Domain Optical Coherence Tomography (SD-OCT). Following SD-OCT analysis, animals were euthanized and the eyes harvested and prepared for histological analysis to correlate the retinal architecture in *in vivo* imaging studies. The metabolic state of the retina was evaluated at p30 by a novel cryo fluorescence imaging technique which calculates Redox Ratio (RR) according to the equation, RR=NADH/FAD. **RESULTS:** PBM by 830 nm profoundly attenuated retinal degeneration in the P23H transgenic rat. NIR treatment preserved retinal function and retinal morphology in treated animals in comparison to the sham-treated group. The RR of the NIR treated retina (Mean=1.9 ± 0.5)was significantly higher than the P23H retina (Mean=1.0 ± 0.1) and supports the use of NIR PBM during the critical period (p10-p25) of photoreceptor degeneration in P23H transgenic rats, to preserve the surviving photoreceptors. **CONCLUSIONS:** Previous studies from our laboratory have documented preservation of retinal function and attenuation of photoreceptor loss in animal models of mitochondrial injury and light-induced retinal degeneration. Results from this study demonstrate the retinoprotective effects of 830nm PBM in a transgenic animal model of retinal degeneration and supports the use of PBM as an innovative, non-invasive therapeutic approach for the treatment of retinal degenerative disease.

Background and Literature Review

Retinitis pigmentosa (RP) is the most common cause of inherited blindness in the developed world. RP is caused by the progressive degeneration of photoreceptor cells with rod degeneration preceding cone degeneration (1,2). Considerable evidence supports a key role for photoreceptor mitochondrial dysfunction and oxidative damage in the pathogenesis of photoreceptor death in RP and other retinal degenerative conditions (3). Low energy photon irradiation (photobiomodulation) in the far-red to near-infrared (NIR) range of the spectrum (630-1000 nm) has been shown to restore the function of damaged mitochondria, up-regulate the production of cytoprotective factors and prevent apoptotic cell death (4). The purpose of this study was to test the hypothesis that photobiomodulation would protect against retinal degeneration in a rodent model of RP

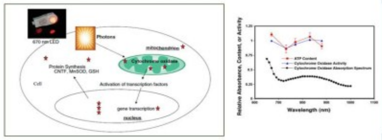

Hypothesized Mechanism of Near-Infrared Photobiomodulation (NIR-PBM)

A majority of RP cases result from a mutation in the rhodopsin gene leading to misfolding opsin which increases oxidative stress and mitochondrial dysfunction leading to photoreceptor apoptosis.

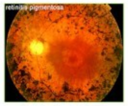

Fundus image in RP

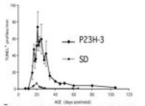

Pattern of photoreceptor cell death during the critical period

Methodology

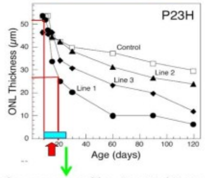

Retinal Morphology assessed by Spectral Domain Optical Coherence Tomography (SD-OCT) imaging and Histology

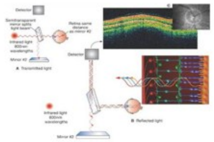

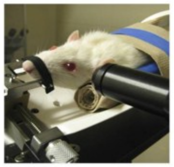

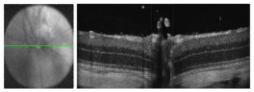

Photoreceptor function assessed by Full-Field Flash Electroretinography

Retinal Metabolic state assessed by Cryo Fluorescence Redox Imaging

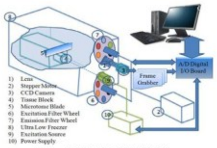

Redox Ratio=RR=NADH/FAD

Conclusions

Results from this study demonstrate the retinoprotective effects of 830nm PBM in a transgenic animal model of retinal degeneration and supports the use of PBM as an innovative, non-invasive therapeutic approach for the treatment of retinal degenerative disease.

Results

Full-Field Flash Electroretinography

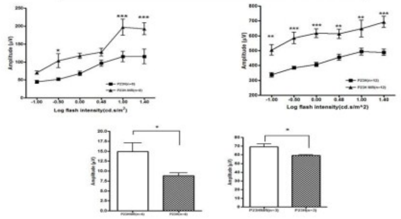

Spectral Domain Optical Coherence Tomography (SD-OCT) imaging and Histology

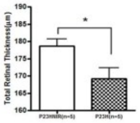

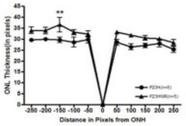

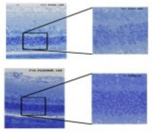

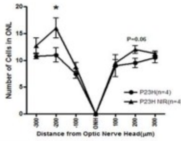

Cryo Fluorescence Redox Imaging

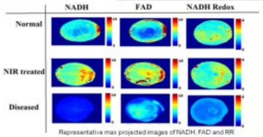

Representative max projected images of NADH, FAD and RR

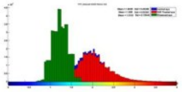

References

1. Berson, E. L. , B. Rosner, et al. (1991). "Ocular findings in patients with autosomal dominant retinitis pigmentosa and a rhodopsin gene defect (Pro-23-His). " Arch Ophthalmol 109(1): 92-101.
2. Bramall, A. N. , A. F. Wright, et al. (2010). "The genomic, biochemical, and cellular responses of the retina in inherited photoreceptor degenerations and prospects for the treatment of these disorders. " Annu Rev Neurosci 33: 441-472.
3. Carmody, R. J. and T. G. Cotter (2000). "Oxidative stress induces caspase-independent retinal apoptosis in vitro. " Cell Death Differ 7(3): 282-291.
4. Desmet, K. D. , D. A. Paz, et al. (2006). "Clinical and experimental applications of NIR-LED photobiomodulation. " Photomed Laser Surg 24(2): 121-126.

Acknowledgements

Sight for Sight
Foundation Fighting Blindness
UW-Milwaukee College of Health Sciences
Medical College of Wisconsin
ANU
QBMI

Curriculum Vitae

Sandeep Gopalakrishnan

Place of birth: Palakkad, Kerala, India

Education:

2008-2012: Ph.D. in Health Sciences /Biomedical Sciences, University of Wisconsin-Milwaukee.

Dissertation Title: Photobiomodulation in Inherited Retinal Degenerations.

2005-2008: M.S. in Clinical Laboratory Science (GPA: 3.8/4), University of Wisconsin-Milwaukee

1997-2002: B.Sc. (Hons.) in Medical Lab Technology; Faculty of Medicine, (GPA: 3.9/4), University of Kerala, India.

Honors and Awards:

- UWM College of Health Sciences Research Grant Award-2011.
- Graduate School Travel Award-2010, 2011.
- Fight for Sight Summer Fellowship-2010.
- Research Excellence Assistantship, UWM, 2009-2010
- Molly Yeffeth Krain and Irwin Amrani Memorial Award, 2009, 2011.
- Best research Presentation Award-CHS symposium, UWM, Fall 2009, Fall 2010.
- Quantum Devices Scholar-2008.
- Victor A. Drill Award for the Best Student Poster-26th Society of Toxicology-Midwest Regional Chapter Meeting, 2008.
- UWM Chancellors Fellowship-Spring 2008, Summer 2010, Fall 2010, Summer 2012
- UWM-Thesis Proposal Grant Award, UWM, 2007.
- Bajpai-Saha Award for the best research paper presented at XV National Conference of Society for Biomaterials and Artificial Organs – India, January 2005
- Top 1% in the graduating class of 2002 in Medical Laboratory Technology, University of Kerala, India.

Membership:

Association for Research in Vision and Ophthalmology
American Association of Clinical Chemistry
American Physiological Society

Professional /Research Experience:

07/2012-07/2012 **Research Associate**
Mentor: Janis Eells, Ph.D.
Department of Health Sciences: BioMedical Sciences
College of Health Sciences, University of Wisconsin-Milwaukee
Milwaukee, WI 53201

08/2008-06/2012 **Doctoral Research Assistant/Dissertator**
Mentor: Janis Eells, Ph.D.
Department of Health Sciences: BioMedical Sciences
College of Health Sciences, University of Wisconsin-Milwaukee
Milwaukee, WI 53201

08/2011-06/2012 **Project Assistant/Research Assistant**
Mentor: Mary Pat Kunert, Ph.D., RN
Biobehavioral Research Laboratory
College of Nursing, University of Wisconsin-Milwaukee
Milwaukee, WI 53201

10/2010-07/2011 **Research Technologist-Internship**
Mentor: Joseph Carroll, Ph.D.
Department of Ophthalmology, Eye Institute
Medical College of Wisconsin, Milwaukee, WI 53226

08/2005-07/2008 **Graduate Teaching Assistant-Clinical Laboratory Science**
Mentor: Robert Burlage, Ph.D. / Janis Eells, Ph.D.
Department of Health Sciences: BioMedical Sciences
College of Health Sciences, University of Wisconsin-Milwaukee
Milwaukee, WI 53201

03/2004-07/2005 **Research Assistant**
Mentor: Annie John, Ph.D.
Transmission Electron Microscope Laboratory, Division of Histopathology
Sree Chitra Tirunal Institute for Medical Sciences & Technology, India

02/2003-02/2004 **Medical Laboratory Technologist**
Mentor: C. C. Kartha, M.D., Professor of Eminence
Division of Cellular and Molecular Cardiology/Pathology
Sree Chitra Tirunal Institute for Medical Sciences & Technology, India.

06/2002-01/2003 **Faculty of Medical Laboratory Technology Program**
Directorate of Vocational Higher Secondary Education
Government of Kerala, India.

Peer-reviewed Publications:

1. **Sandeep Gopalakrishnan**, Suresh Babu S, H. K. Varma, Annie John. "Characterization of novel bioactive glass coated hydroxyapatite granules in correlation with in vitro and in vivo studies". Trends *in Biomaterials & Artificial Organs.* Volume 19, Number 2, January 2006.
2. Annie John, Susan Mani, **Sandeep Gopalakrishnan**, S. Suresh Babu, Arthur V. Lal, H.K.Varma. "Osteogenesis of a bioactive ceramic - calcium phospho silicate composite system in goat femur defect". *Journal of Applied Ceramic Technology,* Volume 8, Issue 3, pages 491–500, May/June 2011
3. Kamaldeen Muili, **Sandeep Gopalakrishnan**, Stacy L. Meyer, Janis Eells, Jeri-Anne Lyons. "Amelioration of Experimental Autoimmune Encephalomyelitis in C57BL/6 Mice by Photobiomodulation Induced by 670 nm Light". *PLoS ONE;* 7(1): e30655. Epub 2012 Jan 24. PMID:22292010
4. Sepideh Maleki*, **Sandeep Gopalakrishnan*,** Zahra Ghanian, Reyhaneh Sepehr, Heather Schmitt, Janis Eells, Mahsa Ranji "Optical Imaging of Mitochondrial Redox State in Rodent Model of Retinitis Pigmentosa". *(Submitted to Journal of Biomedical Optics)**: Contributed equally
5. **Sandeep Gopalakrishnan**, Sepideh Maleki, Heather Schmitt, Phyllis Summerfelt, Adam Dubis, Betsy Abroe, Mahsa Ranji, Joseph Carroll and Janis T. Eells "Photobiomodulation attenuates retinal degeneration in the P23H rat model of retinitis pigmentosa". *(In preparation for Invest. Ophthalmol. Vis. Sci).*
6. Kamaldeen Muili, **Sandeep Gopalakrishnan**, Janis Eells, Jeri-Anne Lyons. "670nm NIR-LED irradiation ameliorates MOG35-55 induced EAE in female C57BL/6 mice is dependent on oxidative and nitrosative stress remediation". *(In Preparation for PLoS ONE).*
7. **Sandeep Gopalakrishnan**, Robert Wilson III, Dan S Lark, Ann Snyder, Diane S. Henshel and Janis T. Eells. "670 nm photobiomodulation protects against oxidative damage to the heart in a rodent model of diabetes mellitus". *(In Preparation for Photomedicine and Laser Surgery).*

Published Abstracts:

1. Lisa L Anderson- Antle, David J Bauer, **Sandeep Gopalakrishnan**, Daniel S Lark, Christopher L Sandoval, Janis T Eells, and Ann C Snyder. *"*Streptozotocin-Induced Diabetic Animal Model Recapitulates Many Features of Frailty in Older Adults with Diabetes". *FASEB J, Mar 2008; 22: 1163.10*
2. **Sandeep Gopalakrishnan**, Daniel S Lark, Chris L Sandoval, Ann C Snyder, and Janis T Eells. *"*Hyperglycemia induced oxidative stress is attenuated in cardiac tissue by 670nm photobiomodulation in an experimental model of diabetes". *FASEB J, Mar 2008; 22: 751.5*

3. Christopher L Sandoval, Robert W Wilson, **Sandeep Gopalakrishnan**, Daniel S Lark, Janis T Eells, and Ann C Snyder. "670 nm LED Treatment Affects Hyperglycemia-Induced Oxidative Stress in Skeletal Muscle in Diabetic Rats". *FASEB J, Mar 2008; 22: 758.34.*
4. J.T. Eells, **S. Gopalakrishnan**, B. Abroe, R. Albarracin and K. Valter-Kocsi. "670 nm Photobiomodulation Attenuates Light-Induced Retinal Degeneration". *Invest. Ophthalmol. Vis. Sci., Apr 2009; 50: 680.*
5. **Sandeep Gopalakrishnan**, Robert Wilson, Jason Rakita, Sarah Antoniewski, Betsy Abroe, Ann Snyder and Janis Eells. "Near-Infrared LED Photobiomodulation Attenuates Hyperglycemia-Induced Cardiotoxicity in a Rodent Model of Diabetes Mellitus". *FASEB J, Apr 2010; 24: 1001.18*
6. Robert William Wilson, II, **Sandeep Gopalakrishnan**, Janis T Eells, and Ann C Snyder**. "**Near-Infrared Photobiomodulation Protects Against Diabetes-Induced Glutathione Oxidation in White Gastrocnemius Muscle" *FASEB J, Apr 2010; 24: 783.11*
7. **Gopalakrishnan, S**., Abroe, B., Schmitt, H. Dubis, A. M., Summerfelt, P., **Carroll, J.**, Eells, J. T. "Photobiomodulation attenuates retinal degeneration in a rodent model of retinitis pigmentosa". *Invest. Ophthalmol. Vis. Sci. Suppl.* 52: E-Abstract 5465 (2011).

Conference Presentation:

1. David J. Bauer, Chris Sandoval, Dan Lark, Robert W. Wilson II, **Sandeep Gopalakrishnan**, Janis T. Eells and Ann C. Snyder. "Photobiomodulation-induced attenuation of CNS oxidative stress in an animal model of diabetes". *The 37th annual meeting of the Society for Neuroscience 2007, San Diego, California, USA.*
2. Jinhwan Lim, Ruth Sanders, Robert Wilson, Ann C. Snyder, **Sandeep Gopalakrishnan**, Janis T. Eells, Diane Henshel, John Watkins . "Attenuation of oxidative stress by 670 nm photobiomodulation in a rodent model of diabetes mellitus". *The Society of Environmental Toxicology and Chemistry (SETAC), 28th Annual Conference-2007, Milwaukee, USA.*
3. C. L. Sandoval, R. W. Wilson, **Sandeep Gopalakrishnan**, D. S. Lark, J. T. Eells and A.C. Snyder. "Near infrared radiation attenuates diabetes induced oxidative damage in the rectus femoris muscle". *(ACSM) 55th Annual Meeting 2008.Indianapolis, Indiana, USA*
4. Kamaldeen Muili, **Sandeep Gopalakrishnan**, Janis T Eells, Jeri-Anne Lyons. "Amelioration of Experimental Autoimmune Encephalomyelitis (EAE) by near-infrared light therapy". *Autumn Immunology Conference (AIC-2007),Chicago,USA.*
5. Jinhwan Lim, Ruth Sanders, Robert Wilson, Ann C. Snyder, **Sandeep Gopalakrishnan**, Janis T. Eells, Diane Henshel, John Watkins. "670 nm photobiomodulation normalizes antioxidant enzyme activities suppressed in streptozotocin-induced diabetic rat". *The Society of Toxicology (SOT) Annual Meeting 2007, Charlotte, North Carolina, USA.*
6. **Sandeep Gopalakrishnan**, Daniel S Lark, Chris L Sandoval, Ann C Snyder, and Janis T Eells. "Hyperglycemia induced oxidative stress is attenuated in cardiac tissue

by 670nm photobiomodulation in an experimental model of diabetes". *26th Annual MRC/SOT Meeting;2008 and Experimental Biology 2008,San Diego, USA*. (Best Poster Award)

7. Jeri Anne Lyons, Kamaldeen Muili, **Sandeep Gopalakrishnan**, Betsy Abroe, Janis Eells "The Therapeutic Potential of Near Infrared Light Therapy for the Treatment of Multiple Sclerosis". *American Society of photobiology.June 14, 2010***.** *Providence, RI,USA*